الجمهورية الجزائرية الديمقراطية الشعبية
République Algérienne Démocratique Et Populaire
وزارة التعليم العالي والبحث العلمي
Ministère de l'Enseignement Supérieur
et de la Recherche Scientifique
جامعة الشهيد الشيخ العربي التبسي – تبسة
Université Echahid Cheikh Larbi Tebessi – Tébessa
معـــــــهد المـــــناجم
Institut des Mines
قسم المناجم و الجيو-تكنولوجيا
Département des Mines Et Géo-technologie

MEMOIRE

Présenté en vue de l'obtention du diplôme de Master:

Characterization and Optimization of Iron Ore Beneficiation Parameters: El-Ouenza Mine Case

Filière : Génie Minier
Option : Valorisation des Ressources Minérales

Par

AYAD HADJER

Devant le jury:

KRIM Mansour	Président	MAA	Université Echahid Cheikh Larbi Tebessi – Tébessa
LARABA Mohammed	Encadreur	MCA	Université Echahid Cheikh Larbi Tebessi – Tébessa
BOUZENZANA Abdellali	Examinateur	MCA	Université Echahid Cheikh Larbi Tebessi – Tébessa

Année universitaire 2024/2025

Dedication

I dedicate this work to my beloved family, whose unwavering support and encouragement have been my source of strength, to my parents who always believed in me, to my sisters Dhouha, Kaouther, and Aya , V , and to everyone inspired and motivated me throughout this journey,

This achievement is also yours.

Acknowledgments

First and foremost, I would like to express my heartfelt gratitude to my supervisor Dr. Mohammed Laraba for his continuous support, valuable advice, and guidance throughout this work.

I am also thankful to all the professors and stuff of the mining institution at the Sheikh Larbi Tébessa University for providing me with the necessary knowledge that helped me to accomplish this study.

Special thanks to Ms.Boukhamla Yousra for her continuous help, great support and role in completing this research.to my family and friends for their constant encouragement and moral support during every stage of this journey.

Abstract

This thesis focuses on the characterization and optimization of iron ore concentration parameters from the El Ouenza deposit. The study aims to improve the quality of the concentrate by increasing the iron content and reducing impurities, using an experimental approach based on a factorial design. Samples were collected from the Chagoura El-Ouenza site, and then subjected to crushing, grinding, screening and magnetic separation operations. The methodology is based on the combination of several factors, including grain-size (GS), ball dimensions of matrix (DB) and magnetic field intensity (I), according to a factorial design, in order to determine their influences on the separation efficiency. The results show that an optimal adjustment of these parameters can significantly improve the iron concentration. For this purpose; The values proposed by the model indicate that a maximum Fe_2O_3 content and a very good yield (respectively 63.18% and 91.25%) of the product can be obtained by optimizing the variable factors as follows: matrix ball size (DB) at 12m, particle size (GS) at 0.24mm and finally an Intensity (I) at 2 T. This work constitutes a solid basis for the development of processes adapted to the valorization of iron ore from El-Ouenza.

Key words: El-Ouenza mine, Fe_2O_3, HIMS, Box-Behnken design, RSM.

Résumé

Ce mémoire de master porte sur la caractérisation et l'optimisation des paramètres de concentration du minerai de fer du gisement d'El Ouenza. L'étude vise à améliorer la qualité du concentré en augmentant la teneur en fer et en réduisant les impuretés, grâce à une approche expérimentale basée sur un plan factoriel. Des échantillons ont été prélevés sur le site de Chagoura El-Ouenza, puis soumis à des opérations de concassage, de broyage, de tamisage et de séparation magnétique. La méthodologie repose sur la combinaison de plusieurs facteurs, dont la granulométrie, les dimensions des billes de la matrice et l'intensité du champ magnétique, selon un plan factoriel de Box-Behneken, afin de déterminer leurs influences sur l'efficacité de la séparation. Les résultats montrent qu'un ajustement optimal de ces paramètres permet d'améliorer significativement la concentration en fer. Pour cet effet; les valeurs proposées par le modèle indique qu'une teneur maximale en Fe_2O_3 et un très bon rendement (respectivement à 63,18 % et à 91,25 %) du produit peuvent être obtenus en optimisant les facteurs variables comme suit: Dimension des billes de la matrice (DB) à 12m, dimension des particules (GS) à 0.24mm et finalement une Intensité (I) à 2 T.

Mots clés : El-Ouneza mine, Fe_2O_3, SMHI, Box-Behnken design, RSM**.**

ملخص:

تركز هذه الرسالة على توصيف وتحسين معايير تركيز خام الحديد من رواسب الونزة. تهدف الدراسة إلى تحسين جودة المركز من خلال زيادة محتوى الحديد وتقليل الشوائب، باستخدام نهج تجريبي قائم على تصميم عاملي. جُمعت عينات من موقع شاغورة الونزة، ثم خضعت لعمليات التكسير والطحن والغربلة والفصل المغناطيسي. تعتمد المنهجية على الجمع بين عدة عوامل، بما في ذلك حجم الحبيبات *(GS)* وأبعاد كرات المصفوفة *(DB)* وشدة المجال المغناطيسي*(I)* ، وفقًا لتصميم عاملي، من أجل تحديد تأثيرها على كفاءة الفصل. تُظهر النتائج أن التعديل الأمثل لهذه المعايير يمكن أن يحسن تركيز الحديد بشكل كبير. ولهذا الغرض؛ تشير القيم المقترحة في النموذج إلى إمكانية الحصول على أقصى محتوى من أكسيد الحديد *(Fe2O3)* وعائد جيد جدًا (63.18% و91.25% على التوالي) من المنتج عن طريق تحسين العوامل المتغيرة التالية: حجم كرة المصفوفة *(DB)* عند عمق 12 مترًا، وحجم الجسيمات *(GS)* عند 0.24 مم، وأخيرًا الكثافة *(I)* عند 2 تيسلا. يُشكل هذا العمل أساسًا متينًا لتطوير عمليات مُصممة لتثمين خام الحديد من الونزة.

الكلمات المفتاحية: منجم الونزة، أكسيد الحديد*(Fe2O3)* ، *HIMS* ، تصميم بوكس-بهينكن.RSM ,

Contents Table

Dedication	
Acknowledgement	
Abstract	
Résume	
ملخص	
Contents Table	
List of figures	
List of Tables	
General Introduction	
Chapter I Bibliographic Review	**Page**
I.1 Iron Ores	**2**
I.1.1 Introduction	**2**
I.1.2 Definition of Iron (metal)	**2**
I.1.3 Definition of Iron (Ores)	**2**
I.1.4 Different Types of Iron Ore	**3**
I.1.5 Composition of Iron Ore	**4**
I.1.6 Properties of Iron	**5**
I.1.6.1 Physical Properties	**5**
I.1.6.2 Chemical properties	**5**
I.1.6.3 Magnetic Properties	**6**
I.1.7 Beneficiation Technique	**6**
I.1.7.1 History of Iron Ore Beneficiation methods	**7**
I.1.7.2 Beneficiation Techniques of Iron Ore: A Comprehensive Analysis	**7**
I.1.7.3 Modern Beneficiation Techniques: Future Directions and Challenges	**9**
I.1.8 Industrial Applications of Iron Ore	**10**
I.1.9 Industrial Advancement in Iron Production	**10**
I.1.10 Economic Importance of Iron Ores	**11**
I.1.11 World Iron Ore Trade	**11**
I.1.11.1 World Iron Ore Reserves and Resources	**11**
I.1.12 Challenges in Algeria's Iron Ore Sector	**13**
I.2 The El-Ouenza Iron Mine: A Comprehensive Study on Geology, Operation and Sustainable Development	**14**
I.2.1 Geographic Location in Algeria	**14**
I.2.2 Transportation Infrastructure and Economic Connectivity	**15**
I.2.3 Structural Evolution and Stratigraphic Architecture of Geomorphology	**15**
I.2.4 Mineralization and Ore Characteristics	**17**
I.2.5 Mining and Processing Methods: Integrated Extraction to Concentration Technology	**18**
I.2.5.1 Sector-Adapted Extraction Methodologies	**18**
I.2.5.2 Beneficiation Challenges and Titration Dependency Crisis	**19**
I.2.5.3 Agglomeration Technologies and Modernization Roadmap	**20**
I.2.6 Reuse and Recycling of Valuables	**20**
I.2.6.1 Legacy Environmental Liabilities, and Remediation Initiatives	**20**
I.2.6.2 Circular Economy Material Repurposing Pathways	**21**
I.2.6.3 Socioeconomic Integration and Community Health Initiatives	**22**
I.2.7 Previous Studies	**22**
I.2.8 Integrating Geological Heritage and Sustainable Futures	**23**
Conclusion	

Chapter II Materials and Methods of Experiment	
II.1 Introduction	**28**
II.2 Sampling	**28**
II.3 Comminution and valorization of iron ore	**29**
II.3.1 Crushing	**30**
II.3.2 Grinding	**30**
II.3.3 Quartering	**31**
II.4 Analytical Methods	**32**
II.4.1 Particle Size Distribution	**32**
II.5 Chemical Composition	**33**
II.6 Complementary Analyses	**36**
II.6.1 X-Ray Fluorescence (XRF)	**36**
II.6.2 X-Ray Diffraction (XRD)	**37**
II.6.3 Scanning Electron Microscopy (SEM-EDS)	**38**
II.7 Magnetic Separation Testing	**38**
II.7.1 Principal of Operation (LIMS,HIMS,Wet-Dry magnetic Separation)	**38**
II.7.2 Used Equipment Description	**39**
II.7.3 Operating principal of the magnetic separation	**39**
II.8 Statistical approach	**42**
II.8.1 Design of experiment (DOE)	**42**
II.8.2 Response surface methodology	**43**
II.8.3 Calculation of technological indices	**44**
Conclusion	
Chapter III Results and Discussion	
III.1 Introduction	**47**
III.2 Results of iron ore characterization	**47**
III.2.1 Grain-size analysis	**47**
III.2.2 Grain-size chemical analysis	**48**
III.2.3 Mineralogical analysis (XRD)	**49**
III.2.4 SEM-EDS Microanalysis	**50**
III.2.5 Technological indices results	**51**
III.3 Results of the statically approach	**52**
III.3.1 Experimental design for the magnetic separation tests	**52**
III.3.2 ANOVA and Pareto Diagram	**54**
III.3.3 Observed and predicted responses of the Fe_2O_3 in magnetic products(concentrates)	**57**
III.3.3 Observed and predicted responses of Fe_2O_3 in magnetic products (concentrates)	**59**
III.3.4 Effect of process variables on grade of concentrate	**60**
III.3.6 Main effects of parameters on Fe_2O_3	**61**
III.3.7 Optimization of magnetic separation variables on Responses	**62**
General Conclusion	
References	
ANNEXES	

List of figures

N°	Title	P
I .1	Distribution of world seaborne iron ore trade by destination in 2023 (RoW: rest of the world).	14
I .2	View of El-Ouenza mine Open pit (Google Maps;2025)	21
II.1	The proposed flowsheet of El- Ouenza iron ore	29
II.2	El-Ouenza mine laboratory crusher	30
II.3	El-Ouenza mine laboratory grinder	31
II.4	Sampling quartering method	32
II.5	The Samples and the sieve stack	33
II.6	Measuring and heating procedure	34
II.7	Titration procedure	35
II.8	The end point of the titration	36
II.9	The used XRF machine (laboratory of GICA, Skikda, 2025)	37
II.10	The used XRD machine (laboratory of GICA, Skikda, 2025)	37
II.11	The used SEM-EDS (Laboratory of NHSTE, Annaba)	38
II12	Used magnetic separator (Manufactured by Dr. Laraba M.)	39
II.13	The used Matrix Balls with different sizes	40
III.1	Samples of grain-size distribution	48
III.2	Grain-size curve of the iron ore from El-Ouenza mine	49
III.3	SEM-EDS analysis of El-Ouenza iron ore	51
III.4	XRD pattern of the magnetic product (Test 12)	54
III.5	Relation between Observed and predicted values of grade	56
III.6	Relation between Observed and predicted values of yield	56

List of Table

N°	Title	P
I .1	Common iron ore and gangue mineral definitions.	6
I .2	World iron ore trade	14
I.1	Estimated iron ore reserves in 2013 in the main iron ore-producing countries	15
II.1	Filling factors of different matrices (Jan Drzymala, 2007).	41
II.2	Variables factors and their levels	42
II.3	Encoded and coded variables of each test.	44
III.1	Grain-size analysis of El- Ouenza iron ore	47
III.2	Results of Grain-size chemical analysis of low-grade iron ore from El-Ouenza mine (%)	49
III.3	Elemental analysis of iron ore according to EDS pattern	52
III.4	Technological indices of magnetic separation tests	52
III.5	Results of factorial designed of experiments (DOE)	53
III.6	Observed and predicted values of grade, recovery and yield.	55

General Introduction

This study aimed to characterize the mineralogical and chemical composition of iron ore extracted from the Chagoura sector of the El-Ouenza mine and to optimize the key parameters influencing its recovery by magnetic separation. A comprehensive methodological approach was used, including particle size analysis, SEM-EDS microanalysis, X-ray fluorescence, X-ray diffraction, and magnetic separation tests supported by titrimetric validation.

The results revealed that the ore is predominantly fine-grained and composed primarily of hematite and goethite, with significant amounts of quartz and calcite as gangue minerals. SEM-EDS analysis confirmed the presence of complex mineral associations, while X-ray fluorescence provided a consistent overall chemical profile across all particle size classes. The particle size distribution suggested that over 80% of the material lies below 0.250 mm, a size range conducive to effective mineral liberation. Magnetic separation tests demonstrated the feasibility of improving iron concentration in specific particle size classes. Optimization tests confirmed that particle size and magnetic intensity significantly influence enrichment results.

In conclusion, the El-Ouenza iron ore shows promising potential for industrial enrichment by magnetic separation, particularly when particle size and operational parameters are carefully controlled. These results contribute to current efforts to valorize low-grade iron ores in Algeria and support the implementation of cost-effective and sustainable enrichment strategies tailored to local ore characteristics.

This thesis is divided into three chapters:

Chapter I: is devoted to a detailed literature review on iron and its ores, as well as to conventional and innovative processes for the beneficiation of low-grade iron ores. This chapter also presents the geological and mineralogical context of the El Ouenza deposit.

Chapter II describes the materials studied and the methods implemented for mineralogical and chemical characterization, as well as for magnetic separation tests. It presents in detail the analytical techniques used and the experimental conditions applied.

Chapter III presents and analyses the results obtained. It discusses the performance of the various enrichment parameters tested and offers recommendations for optimizing the concentration process for the ore studied.

Chapter I

Bibliographic review

I.1 Iron Ores

I.1.1 Introduction

Iron is the most material to be used in the steelmaking all over the world. In fact, more than 50% of steelmaking raw materials consist of “iron ore” (World Steel Association, 2023). It is a vital resource that has supported human progress from basic tools to its infrastructure. This chapter starts by introducing the iron as an element then as an ore, and then it discusses its composition. After that, it identifies some of the impurities that degrade the ore and lower iron’s quality. Thereafter, we present iron's physical, chemical, and magnetic properties and how they make it useful for mankind. Beneficiation methods have evolved from primitive to state-of-the-art processes; recent developments in the industry have also been highlighted. A look at global trends and regionally-focused case studies will bring out the economic importance of iron ore, followed by a comprehensive look at its industrial uses. Finally, the review focuses on Algeria’s El-Ouenza mine. Despite its great potential, ongoing technical impediments hold back its growth and development. However, some studies indicate that controlling the beneficiation parameters could help improve the ore’s grade and reduce waste.

I.1.2 Definition of Iron (metal):

The metal iron (Fe) with atomic number 26 is a transition element in the periodic table. It is the fourth most abundant metal in the Earth's crust, making up around 5%. This chemically active element rarely reduces naturally to its metallic state and mostly occurs in mineral form as it can easily oxidize.

The physical properties of pure iron include high ductility and malleability; it also has a very high melting point of 1,538 °C. The chemical reactivity of iron is evident from the formation of iron oxide hydrates due to its reaction with oxygen and moisture (both water vapor and liquid) present in the air. Rust is the common name for these hydrates. Iron is also an important biological molecule, serving as the central atom of the hemoglobin molecule that transports oxygen in the blood of vertebrates (Frausto da Silva & Williams, 2001). The dual importance of iron in biological systems and industrial applications places it uniquely among metals.

I.1.3 Definition of Iron (Ores):

- Iron ores are naturally found rocks from which metallic iron can be economically extracted. Iron ore is made primarily of iron oxide. These ores are the main ores used for making steel. The iron ore deposit refers to iron ores that have become sufficiently concentrated in metal content over geological time. It generally gives rise to rich deposits; the deposits are mostly oxides of iron such as hematite, Fe_2O_3, and magnetite, Fe_3O_4, intergrown with various amounts of gangue minerals that are impurities. Many factors determine whether an iron ore deposit is feasible or not. The iron grade of the ore deposit is an important factor. The iron grade of ore deposits usually ranges between 30%

and 70% by weight. Apart from this, the mineralogy of both valuable and gangue minerals, along with the geographic accessibility of the deposit, play important roles. Whether a mineral deposit is considered “ore” or just iron mineralization fundamentally depends on market conditions and extraction technologies available at a particular time. Thus, it is both economically and time-dependent. The mineralogical complexity of iron ores often necessitates extensive beneficiation to achieve the chemical and physical specifications required for industrial use, particularly in steel production where strict limits on certain impurities apply.

I.1.4 Different Types of Iron Ores:

-Types and Characteristics of Iron Ores:

The mineral components, origin and geochemistry of iron ore deposits are highly varied. Notable forms are banded iron formations (BIFS), oolitic iron ores, and goethite-rich ores. Banded iron formations are important sources of iron ore composed of alternating layers of iron minerals and silica. Regions with ancient geological settings mainly host these formations, an example being the Singhbhum-Orissa Craton of eastern India (Prasad et al., 2017) and globally distributed Meso- to Neo-Archean terrains. Oolitic iron ores are analyzed and found to host hematite and goethite minerals (Quast, 2018). These ores are often of complicated mineralogy (LOUIS, 1920).

Iron ores are divided into different types on the basis of mineralogical and geological formations.

Hematite is a widely known iron ore, reddish-brown in color. It could be said that it includes about 70% iron and is commonly located as supergene ores, which result from the weathering and oxidation of iron-rich minerals, namely magnetite (Clout & Manuel, 2022) (Oshchepkova et al., 2020)

This iron ore, black or brownish-black in color, contains 72% iron, along with 11% oxygen and lesser amounts of other minerals. Magnetite is a principal source of iron due to its magnetic nature making processing easier (Clout & Manuel, 2022) (Oshchepkova et al., 2020) (Mao et al., 2014).

Siderite is an iron carbonate ore containing around 48% iron. To convert to more economically viable forms of iron, such as magnetite, requires more specific processing techniques (e.g. roasting, magnetic separation) during their extraction (Chun et al., 2014).

Limonite is a hydrated iron oxide ($FeO(OH)\cdot nH_2O$) closely associated with the mineral goethite. Hematite is considered a higher-grade ore than limonite as it has a more uniform composition. Limonite plays an important role in iron making because although it has a varied composition, it is abundant (Mao et al., 2014).

Other than hematite, goethite is also a common iron ore found in the same deposits. It is an important source of iron, especially when hematite is less available. (Quast, 2018), (Teutsong et al., 2020)

Banded iron formation (BIF) is a sedimentary rock consisting of alternating layers of iron-rich minerals (hematite and magnetite) and quartz. Banded iron formations (BIFs), due to their large reserves, make a significant contribution to the global iron market (Hassanzadeh et al., 2023) (Bolonin et al., 2019) (Ebotehouna et al., 2019).

Table I.1: Common iron ore and gangue mineral definitions.

Ore mineral	**Chemical formula**	**Description**
Hematite	Fe_2O_3	Iron oxide
Magnetite	Fe_3O_4	Primary iron oxide
Goethite	FeOOH	Most abundant iron oxyhydroxide with three subtypes: yellow ochreous has excess water and chemical impurities; brown, the most common variant, is stoichiometric; while vitreous is glassy and contains 2–9% $SiO_2 + Al_2O_3$, either as an impurity or as submicron inclusions of quartz
Maghemite[a] "Keno-magnetite"[b]	$Fe^{3+}[_{Fe^{3+}1.67}]\ [_{0.93}]\ O_4$	Intermediate iron oxide Intermediate metal-deficient phase between magnetite and maghemite Hematite that has replaced primary magnetite
	$Fe_{3-x}([])_xO_4$	A defect solid solution where OH^- ions replace oxygen
"Martite"	Fe_2O_3	
"Hydro-hematite"[c]	$Fe_{(2-x)/3}(OH)_xO_{3-x}$	
Gangue mineral		
Quartz	SiO_2	Common oxide of silicon
Kaolinite	$Al_4(Si_4O_{10})(OH)_8$	Clay
Gibbsite	$Al(OH)_3$	Clay
Minnesotaite[d]	$(Mg,Fe)_3Si4O_{10}(OH)_2$	Common Fe-Mg silicate in iron formations
Stilpnomelane	$(K,Na,Ca)_{0.6}$ $(Mg,Fe^{2+},Fe^{3+})_6$ $Si_8Al(O,OH)_{27}$ $2–4H_2O$	Common silicate in iron formations
"Chlorite"[e]	$(Fe,Al,Mg)_3(Si,Al)_2\ O_5(OH)_4$	Silicate
Pyrite	FeS_2	Iron sulfide
Pyrolusite	MnO_2	Manganese dioxide
Siderite	$FeCO_2$	Fe-carbonate
Ankerite	$Ca(Fe, Mg, Mn)(CO_3)_2$	Ca-Fe-Mg-Mn carbonate

I.1.5 Composition of Iron Ores:

Iron ores are composed of iron alone but also contain certain impurities or gangue minerals. Key components include:

- Iron Oxides: Mainly found in most iron ores such as hematite and magnetite. Extractable iron mainly comes from these oxides (Clout & Manuel, 2022) (, 1978).
- Silicon Dioxide (SiO_2), commonly found in banded iron formations and other ores, is prevalent as quartz or silicate minerals (Teutsong et al., 2020).
- Calcium carbonate ore also contributes towards sintering in steelmaking processes (Tserenkhand et al., 2014) (Chun et al., 2014).
- Some geological formations contain sulfides such as pyrite and chalcopyrite, sulfide content of iron ores (Wang et al. 2020).
- Phosphorus and Other Trace Elements: Present in varying amounts, these elements can affect the quality of steel produced from the ore. Their distribution is often uneven among different ore types (Parak, 1985).

A steel-making industry relies on understanding iron ore's definition, types and composition as it governs mining strategy, processing techniques and pricing. The variety of iron ores calls for distinct approaches to their extraction and refining to achieve the best economic results and meet consumer demand for high-quality iron. As a result, many ongoing researches on these ores aim to improve beneficiation processes and identify new deposits and to develop material efficiency in industrial applications (Krishna et al., 2013) (Cho et al., 2021) (Obara et al., 2021).

I.1.6 Properties of Iron:

I.1.6.1 Physical Properties:

Iron has a range of properties, which make it useful in industry. Iron is classified as a heavy metal, with a density of 7.87 g/cm³. It is commonly used in structures such as buildings and machinery. The metal melts at 1,538°C and boils at 2,862°C. Thus, it is well-suited for high-temperature applications such as engine parts and industrial furnaces. The pure form of iron is very ductile and malleable, allowing it to be shaped into wires without breaking under normal conditions. This flexibility and adaptability are largely due to an important transformation that iron undergoes at around 912°C.At this temperature, its crystal structure changes from a body-centered cubic (BCC) form, called alpha iron (α-Fe), to face-centered cubic (FCC) form, known as gamma iron (γ-Fe). This transformation plays a vital role in enhancing iron's mechanical properties, such as its hardness and ductility, and is fundamental to heat treatment processes that help improve the metal's overall performance.

I.1.6.2 Chemical Properties:

The chemical nature of iron suggests that it is a transition metal as it has several oxidation states and shows redox activity. The process of rusting begins when metallic iron readily oxidizes in moist air to form rust. Rust is a characteristic layer of hydrated iron oxides. The rusting of iron is also galvanic in nature. The process is accelerated if there are salts and acids present. Due to its susceptibility to corrosion, it should be galvanized or alloyed with chromium to produce stainless steel. Iron can be found primarily in two states in compounds, that is, ferrous (Fe^{2+}) and ferric (Fe^{3+}). Ferric state is more thermodynamically stable under oxidizing conditions. The metal is violently treated with dilute acid to give ferrous salts and hydrogen gas, and it will be passivated by concentrated nitric acid. When heated, iron forms inner compounds with carbon, which in turn affect the properties of steel. These include cementite which is Fe_3C and carbide phases. Iron can be used for many different purposes industrially because of the chemical properties that it possesses. However, it must be managed well in the environment when it is processed or used in order to not degrade.

I.1.6.3 Magnetic Properties:

Iron possesses strong magnetic properties. These properties have been taken advantage of since ancient times. They remain highly useful in modern technology. At room temperature, the metal is ferromagnetic, which means it has strong spontaneous magnetization and high magnetic permeability; as a result, the metal concentrates magnetic flux. This ferromagnetism persists up to the Curie temperature of 770 °C, above which ferromagnetic iron becomes paramagnetic, exhibiting a much weaker magnetic response. The magnetic properties are very sensitive to microstructure and impurities, for example carbon content affects the coercivity and remanence of steel alloys. These characteristics have led to iron's dominance in electromagnetic applications ranging from electric motors and generators to transformer cores and magnetic shielding. Modern high-performance magnetic materials often combine iron with rare earth elements to enhance properties, though pure iron and low-carbon steels remain indispensable for many conventional applications due to their favorable magnetic saturation and cost-effectiveness (Cullity & Graham, 2008).

I.1.7 Beneficiation Techniques:

As high-grade iron ore resources are quickly dwindling, the beneficiation of low-grade iron ores has become necessary. Magnetic separation, gravity separation steel on basis, froth flotation and other physical separation methodologies Yet, these methods are often not sufficient for more complex ores, which require advanced processes like reduction roasting followed by magnetic separation (Roy et al, 2020).

While beneficiation techniques continue to evolve, the production side of the industry is also undergoing major changes to reduce environmental impact. The use of hydrogen-based reduction

technologies is becoming more popular for manufacturing low-carbon steel instead of traditional carbon-based technologies (Sun et al., 2021). Electrochemical ironmaking is another interesting opportunity to reduce carbon dioxide emissions in iron production (Wallace et al., 2024).

Sintering and pelletizing remain critical processes in preparing iron ores for blast furnaces. Recent studies focus on optimizing these processes to improve energy efficiency and reduce emissions. For instance, the introduction of biomass in sintering as a partial substitute for coke shows potential in reducing the carbon footprint of iron ore processing (Legemza et al., 2020).

I.1.7.1 History of Iron Ore Beneficiation Methods:

The iron ore beneficiation process has existed for a long time, and as human demand for iron products has grown, our technology is getting better. The Hittites and the Egyptians were among the first to experiment with beneficiation techniques around 1500 BCE. This mainly included handpicking rich iron ore bearing rocks from worthless gangue. This was followed by crushing using stone hammers and grinding with querns. The subsequent smelting occurred in furnaces, where layers of ore and charcoal were alternately heated to about 1200°C. These produced iron blooms of low density that required extensive subsequent forging to remove slag inclusions. In the Middle Ages, a water-powered trip hammer improved all-metal production methods, while bellows increased furnace temperatures. And yet, ore preparation remained largely manual and selective mining of high-grade deposits predominated. The changes that led to what we now call mechanical crushing began with the Industrial Revolution. The first gravity separation devices, such as buddles and jigs, evolved during this period. The 19th century saw the arrival of electromagnetic separators for magnetite ores. In the early 20th century, the process of froth flotation was used for the extraction of base metal ores. Shortly afterward, this process was adapted for the beneficiation of iron. The process was able to economically treat finer particles and more complex types of ores. The history shows that beneficiation technologies have continuously grown to satisfy changing resource availability and industrial needs (Smith et al, 2021).

I.1.7.2 Beneficiation Techniques of Iron Ores: A Comprehensive Analysis

Iron ore beneficiation is essential for upgrading low-grade ores into commercially viable concentrates. The choice of methods relies on the mineralogical composition, freedom features and the gangue mineral nature. We take a look at the basic methods and their mechanisms and innovations below.

1. ***Physical Separation Techniques:***

a) Gravity Separation:

Gravity methods exploit density differences between iron oxides (hematite, magnetite) and gangue (quartz, alumina). The density differences (4.5-5.3 g/cm³ for iron minerals and 2.6-2.8 g/cm³ for gangue minerals) enable the use of gravity separation methods (spiral concentrators

and centrifugal separators) to separate particles in the size range of 0.1 mm -2 mm. and they do not involve addition of any chemical reagents, key approaches include:

Spiral concentrators and jigs: Effective for coarse-grained ores. For example, Specularite ores achieved 37.62% Fe grade using spiral separators (Wang et al., 2011) (Pandiri et al., 2022).

Shaking tables: Used for fine particles (−74 μm), achieving up to 61.54% Fe recovery in magnetite ores (Ali et al., 2021) (You & Liu, 2023).

b) Magnetic Separation:

Low-intensity magnetic separation (LIMS): Targets magnetite (Fe_3O_4) with magnetic susceptibility >1.26×10^{-5} m^3/kg. Modern LIMS circuits recover >90% magnetite from crushed ore (Pelevin, 2022) (Chokin et al., 2022).

High-gradient magnetic separation (HGMS): can treat weakly magnetic hematite or goethite; after reduction roasting. There are also superconducting magnets that cut down energy consumption by quite an extent.

A study recovered 74.04% Fe from ultrafine hematite (−30 μm) using HGMS at 47.76 kA/m (Su et al., 2016).

2. Chemical and Surface-Based Techniques:

a) Froth Flotation:

Reverse flotation: Silica/alumina gangue is floated using cationic collectors (e.g., ether amines), leaving iron in the sink. A Brazilian itabirite ore achieved 67% Fe concentrate by replacing reverse flotation with magnetic separation (Rodrigues et al., 2023). The use of new chemical collector such as hydroxamates for iron oxides minerals and starch derivatives as depressants of silica now enables effective froth flotation of high-value minerals at sizes below 150 μm.

-Selective flocculation: Polymers like starch selectively aggregate iron particles. Sodium humate increased Fe recovery by 12% in slimes by dispersing gangue (Sarma et al., 2022).

b) Leaching:

Acid or alkali leaching removes impurities like phosphorus. For high-phosphorus oolite hematite, HCl leaching reduced P content from 0.89% to 0.12% while retaining 95% Fe (Gong et al., 2024).

3. Thermal and Phase-Transformation Methods

a) Magnetizing Roasting:

Hematite (Fe_2O_3) is reduced to magnetite (Fe_3O_4) or metallic iron using CO/CO_2 at 600–800°C. Post-roasting magnetic separation achieves >85% Fe recovery from refractory ores (Kukkala et al., 2024) (Yu et al., 2017).

b) Carbothermic Reduction:

Microwave-assisted reduction of pyrite cinder at 1050°C produced 91.71% Fe recovery, reducing energy use by 30% compared to conventional methods (Long et al., 2016).

I.1.7.3. Modern Beneficiation Techniques: Future Directions and Challenges:

While advancements in beneficiation and processing technologies promise to meet future demand, challenges remain in managing the environmental and economic impacts with putting into consideration that modern iron ore beneficiation techniques previously used and still evolving through advanced technologies aimed at maximizing recovery and minimizing energy and water consumption; for instance. The development of cost-effective and scalable low-carbon iron and steel production methods is imperative.

Moreover, research into integrating carbon capture and storage with steelmaking processes continues to be a critical area of study. Utilizing by-products such as slag in cement production not only addresses waste issues but also contributes to the circular economy (Zeng et al., 2020). Some of these approaches can be presented:

- ***Circuits:***

Closed-loop grinding with hydro-cyclones optimizes particle size for downstream separation. A Qidashan ore achieved 65% Fe grade by reducing overgrinding (Baoyu et al., 2019).

- ***Compound Force Field Separation:***

Combining centrifugal, magnetic, and interfacial forces improved recovery of −10 μm particles by 25% in pilot tests (Tian et al., 2024).

Recent advances in technology involve the use of sensors in sorting ores. For example, X-ray transmission (XRT) or Laser Induced Breakdown Spectroscopy (LIBS) can be exploited to sort by composition in real time. This can significantly reduce the processing cost of coarse ores. HPGRs are better than ball mills at reducing size in a more energy-efficient manner and making microcracks in the rocks that enhance liberation downstream; the latest techniques nowadays are being incorporated with automated control systems using machine learning algorithms for dynamically optimizing process parameters to produce consistent quality of end products with feed variations (Gupta & Yan, 2016).

In conclusion, the beneficiation of iron ores requires tailored approaches based on mineralogical complexity. Advances in hybrid separation and sustainable methods are pivotal for addressing declining ore grades and environmental constraints.

I.1.8 Industrial Applications of Iron Ore:

The primary application of iron ore lies in steel production, which in turn serves as the structural backbone of modern civilization. In construction, steel products ranging from reinforced concrete bars (rebar) to structural sections enable the development of high-rise buildings, long-span bridges, and earthquake-resistant structures, with the average skyscraper containing 15-20 thousand tons of steel. The transportation sector consumes approximately 16% of global steel output, utilizing high-strength low-alloy (HSLA) steels for automotive chassis and advanced rail steels capable of bearing heavier axle loads at higher speeds. Energy infrastructure depends heavily on steel for oil and gas pipelines, wind turbine towers that require 150–200 tons of steel per megawatt of capacity, and nuclear reactor pressure vessels manufactured from specially treated low-carbon steels. The manufacturing sector utilizes precision steel components in machinery, tools, and industrial equipment, while consumer goods ranging from appliances to packaging also incorporate steel in various forms. Beyond conventional applications, specialized iron-based materials find use in medical implants due to their biocompatibility, in electromagnetic shielding for sensitive electronics, and as catalysts in chemical processes like ammonia synthesis. This remarkable diversity of applications stems from the ability to tailor steel's properties through alloying and heat treatment to meet specific mechanical, chemical, and physical requirements across virtually every industrial sector (Jones & Kumar, 2022).

I.1.9 Industrial Advancements in Iron Production:

Because steel is one of the most essential materials in the construction industry, many people are unaware of its importance. The traditional blast furnace route of ironmaking has been supplemented by direct reduction processes using natural gas or hydrogen as reductants, which dramatically reduce CO_2 emissions compared to coke-based reduction. Modern blast furnaces incorporate top gas recycling, pulverized coal injection, and contemporary sensor networks to enhance performance. These furnaces achieve productivity higher than 3 tons/m³/ day and coke rates below 300 kg/ ton of hot metal. Steelmaking has embraced the use of basic oxygen furnaces (BOF) with combined blowing processes that make it possible to control the steel chemistry more accurately. Electric arc furnaces (EAF) now dominate the scrap-based steelmaking, with tap-to-tap times under 40 minutes. Ultra-high-power designs are generally used, as well as chemical energy supplementation. Modern integrated mills achieve a wastewater recycling unitrate of over 98%, slag valorization for cement making and near-100% recovery and reuse of process gases. The digital world is now being used by the sectors in their functioning. For example, Plant-wide sensor network, predictive maintenance algorithms and simulation techniques in which the optimum material production scheduling and energy are used. New technologies such as hydrogen plasma smelting reduction and electrolytic iron production may

offer carbon-neutral ironmaking routes, but scale-up challenges limit their potential commercial viability (World Steel Association, 2023).

I.1.10 Economic Importance of Iron Ores:

The annual production of iron ore is over 2.5 billion metric tons. Furthermore, its annual market value fluctuates between $200 – $300 billion and is an important global commodity. The geography of the business is quite concentrated. For instance, more than 60% of worldwide seaborne market trade comes from Brazil and Australia. Also, China represents almost 70% of the global iron ore market which feeds the steel industry. Price formation is complex. Chinese infrastructure spending is one thing that influences price formation. Global demand trends for steel also matter. Other influences include mine supply disruptions at the major iron ore mines. with the Platts IODEX 62% Fe index serving as the benchmark for pricing negotiations. For producing nations, iron ore exports frequently represent a significant percentage of total export earnings - for instance, comprising 36% of Australia's total goods exports in 2022. Developing countries with substantial iron ore resources face both opportunities and challenges, as seen in Algeria where the Gara Djebilet deposit's development could potentially generate $2-3 billion annually in export revenues but requires massive infrastructure investments estimated at $5-7 billion for rail and port facilities. The industry's economic impact extends beyond direct mining to encompass extensive value chains including shipping, steel production, and manufacturing sectors that consume steel products, making iron ore availability and pricing critical factors in overall industrial competitiveness (USGS, 2023).

I.1.11 World iron ore trade:

In 2013, China took the lead as the country with the largest iron ore imports, accounting for 65% of the world’s seaborne iron ore trade. The countries with the next largest market shares include Japan (11%), Europe (10%), and Korea (6%). These imports clearly show that the Asian nations still drive the growth of the global iron ore industry. Between 2000 and 2012, iron ore imports into China rose from about 50 Mt/a to around 745 Mt/a but in 2013, China imported about 820 Mt/a for which the major contributors include Australian, Brazilian, South African, Canadian and Indian imported ores. Rio Tinto and BHP Billiton and Vale in Brazil are the three largest iron ore producers. Their major operations are mainly in Australia. Together these firms control over 74 percent of the seaborne trade in the world’s iron ore.

In recent years, China’s iron ore imports have continued to grow, reaching nearly 1200 Mt/a in 2023, with further increases expected through 2025 (International Iron Ore Study Group, 2024).

I.1.11.1 World iron ore reserves and resources:

Key iron ore-producing countries do not lack iron ore reserves that can be technically and economically exploited. Australia has the largest reserves of both unprocessed (crude) ore and contained iron, followed quite closely by Brazil which has slightly higher in-situ iron grades. Russia has advantageous iron ore reserves and grades but, not surprisingly, China is at a disadvantage in that regard (See Table I.2 and figure I.1).

Table I.2: World iron ore trade

Iron ore imports	**2013 (Mt)**	**2023 (Mt)**	**2024 (Mt)**
China	820	1180	1240
Japan	136	100	100
The European Union	128	120	120
South Korea	63	60	Not mentioned
Iron ore exports			
Australia	579	855	866
Brazil	330	380	390
India (net exports)	9	44	38
Canada	36	36	36
South Africa	48	59	61
World trade	1225	1590	1600

Sources: *Australian Government Bureau of Resources and Energy Economics (BREE), Bloomberg, United National Conference on Trade and Development (UNCTAD). GMK Center (2024), Lloyd's lyst, Mysteel.net,Bloomberg,UNCTAD.*

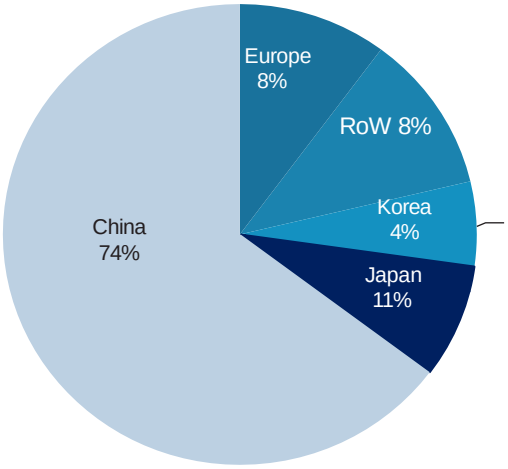


Figure I.1 Distribution of world seaborne iron ore trade by destination in 2023 (RoW: rest of the world) (*Australian Government Bureau of Resources and Energy Economics (BREE))*

Large amounts of unprocessed ore in China are substantial and similar to those of Russia, they are significantly lower in grade, so the contained iron is only about half that of Russia. This is obviously a long-term issue for China given its current iron ore production rate and need for raw materials to feed its steel industry. India will also face long-term supply issues given the scope for economic development and its rapidly rising population. In addition to their reserves, the main iron ore-producing countries also have substantial resources with reasonable prospects for eventual economic extraction. The reserves and resources currently under development and evaluation in a number of countries in West Africa, including Guinea, Sierra Leone, Liberia, Cameroon, and the Democratic Republic of Congo.

Table I.3: Estimated iron ore reserves in 2013 in the main iron ore-producing countries

Rank	Country	Iron ore reserves (Mt)	
		Unprocessed ore	Iron content
1	Australia	35,000	17,000
2	Brazil	31,000	16,000
3	Russia	25,000	14,000
4	China	23,000	7200
5	India	8100	5200
6	Venezuela	4000	2400
7	Canada	6300	2300
8	Ukraine	6500	2300
9	Sweden	3500	2200
10	The United States	6900	2100
11	Iran	2500	1400
12	Kazakhstan	2500	900
13	South Africa	1000	650
	Other countries	14,000	7100

***Source**: US Geological Survey (2014)*

I.1.12 Challenges in Algeria's Iron Ore Sector:

Algeria's iron ore industry faces multiple technical and economic challenges that have hindered the full exploitation of its substantial mineral resources. The Gara Djebilet deposit, containing an estimated 1.7 billion tons of ore at 57% Fe grade, remains largely undeveloped due to its high phosphorus content (0.8-1.2%), which exceeds typical steel industry specifications of <0.05% for most applications. Developing effective beneficiation strategies for this ore requires multi-stage processing combining pre-concentration to remove silica, followed by specialized phosphorus removal techniques such as bioleaching or reverse flotation, (Saidi, M., et al,2022). significantly increasing projected operating costs. Infrastructure deficiencies present another major obstacle, with the remote location of deposits in southwestern Algeria necessitating over 1,000 km of new rail lines to connect mines to potential port facilities, which would require capital investments exceeding $5 billion. The existing El Hadjar steel complex, designed for processing El-Ouenza mine ores, operates with outdated technology and suffers from chronic under capacity, limiting

domestic demand for beneficiated ores. Compounding these technical challenges are regulatory uncertainties and limited private sector participation in Algeria's mining industry, discouraging foreign direct investment needed for large-scale project development. Addressing these barriers will require coordinated policy reforms, investment incentives, and technology partnerships to develop commercially viable processing routes for Algeria's challenging ore types (Boukhanouf, 2021).

I.2 The El-Ouenza Iron Mine: A Comprehensive Study on Geology, Operation, and Sustainable Development:

Iron ore is a basic building block in modern industrial civilization. It is a key raw material used to make steel, which is essential in building infrastructure, manufacturing ecosystems, and transportation networks to drive economic development across the globe. Annually, approximately 2.5 billion tons of iron ore are mined on six continents with the Pilbara region of Australia, the Carajás Province of Brazil, and the Liaoning Basin of China making up much of the volume of production and international trade that affect global commodity markets and industrial policy development. This extremely large extraction quantity shows that vital steel has become the skeleton of urbanization and technology. For example, 1.6 tons of iron ore feedstock is required to produce 1 t of steel in a conventional blast furnace. In Algeria, an industrializing North African country seeking to ensure greater industrial self-sufficiency and lessen dependence on imports—iron ore–is considered a mineral of great national significance as it would permit steel-making in the El Hadjar integrated steel complex in Annaba. It is the largest facility in North Africa in the world. Operationally viable and internationally competitive to rely on domestic ore supply chains. El-Ouenza is the most important iron deposit in Algeria. It is geologically complex and has been mined for over 100 years, and the ore grade issue will be examined in the context of environmental reclamation and technological modernization in an era of sustainable development. The El-Ouenza iron ore deposit is a fascinating site in northeastern Algeria. This review provides a systematic overview of the site stratigraphy, mining processes, processing techniques, and waste reuse possibilities. Socioeconomic implications are important aspects of the deposit, Furthermore, it is a key site for future-oriented resource management strategies capable of balancing economic and environmental goals across the entire mine life cycle that begins at exploration and ends at closure and post-mining land use (Ysbaa, B. Et al. 2021).

I.2.1 Geographic Location in Algeria:

- Precise Coordinates and Physiographic Setting:

The El-Ouenza mine is located on topographically high ground in the Tébessa Mountain range of north-eastern Algeria. Its exact coordinates are 35°56′N 8°08′E. The mining concession is located approximately 12 km west of the international border with Tunisia, and 120 km south of the Mediterranean Sea. This location provides a transboundary context that can promote

binational environmental cooperation as well as proximity to the Mediterranean shipping infrastructure. The deposit occupies a vast area of 15 km² in a semi-arid region in Tébessa Province. The altitude of the site is approximately 900 m above mean sea level. The site's microclimate affects operational logistics and ecological management programs. The mining district is divided into three main operating areas owing to geological and mineralogical differences. The area is Shagoura Sud: the central mining area, comprising steeply dipping hematite lenses. This area extends over an area of 3.2 km² and goes to depths of over 250 m below surface levels. **Shagoura Nord**: The mines cover an extent of 5.7 km² of northern plateaus under a weathered pile of goethite-limonite blanket. The average thickness of the deposits was 30 m. **Douamis**: This area covers 6.1 km² in the southwestern part of the district. It features complex folded hematite-phyllite sequences. This area has a considerable future resource potential. However, there is currently a processing challenge. The Mn content is between 0.8 and 3.2% and varies between layers.

I.2.2 Transportation Infrastructure and Economic Connectivity:

El-Ouenza is industrially important because there is a railway line specially designed to enable the transport of 2.5 million tons of iron ore to the El Hadjar steel complex in Annaba. This 120-kilometre-long railway line with a track gauge of 1,435 mm and a maximum gradient of 1.5% was completed in 1939 during the French era. It is fully functional today and can handle 40-tonne capacity hopper cars. The transported iron ore constitutes 80% of the domestic iron ore supply of Algeria. This is the material basis for the steel production capacity of 1.2 million tones that occurs in Algeria. RN16 national highway, a two-lane paved road maintained by the National Highway Directorate, connects Tébessa to Annaba. This road provides access to mining districts. However, mine access roads, which are 42 km long, usually require extensive maintenance because of erosion caused by rainfall during the rainy season. The annual rainfall in this area ranges between 400 and 600 mm. Most of these events occurred between October and April. Consequently, plant extraction operations were suspended during the peak weathering period. As the mine is located close to Tunisia, there are opportunities and challenges presented by this proximity. Binational agreements make it easy to jointly manage groundwater in the transboundary Continental Intercalaire aquifer system, which lies at depths of 150-400 m in both countries and has reserves of more than 30,000 km³. In addition, airborne particulate matter must be jointly and carefully measured. As a result, two sets of twelve air quality stations (6 in each country) monitor PM_{10} and $PM_{2.5}$ levels every hour. This helps both countries jointly manage particulates that affect transboundary pollution based on the provisions of the 2002 Algeria-Tunisia Environmental Act .This geographical positioning establishes El-Ouenza as a critical economic asset within Algeria's mineral portfolio while embedding it within a complex matrix of logistical, environmental, and geopolitical considerations that profoundly influence operational decision-making and long-term strategic planning (Evtekhov et al., 2016) (Baala, 2021) (Thèses Algérie, 2020) (Faculté des Sciences, 2019).

I.2.3 Structural Evolution and Stratigraphic Architecture of Geomorphology:

The geological structure of El-Ouenza was developed in a larger structural context corresponding to the Saharan Atlas domain (A.A.) orogeny. A.A. corresponds to the first major orogenic event of the Alpine North African (North African A.) fold belt, which was carried out under conditions of collision between the African and Eurasian plates. These two-part continental movements occurred during the Eocene-Miocene period, generating compressive stress of over 150 Mpa that induced folding and faulting of Proterozoic to Cambrian metasedimentary sequences. This long deformation period of 15 million years permitted the development of complex structural traps, which were particularly favorable for mineralization. Nestled in a rock column with three main rocks, this deposit is part of the Boukhadra region. The most significant is a quartz arenite unit (coarse sediments) present in the Lower Ordovician Tébessa Quartzite Formation, which has a thickness between 150 and 200 m. It consists predominantly of quartz arenites, whose grains are broken and/or fragmented owing to diagenesis (90–95% SiO_2). Next, the dolomite unit (fine rocks) formed in the Middle Cambrian El-Ouenza Dolomite. It had a thickness of 80–120 m. It was composed of dolostone (10–20% MgO). Finally, the main Tébessa rocks were exposed in the Boukhadra region (50–80 m). This is a vertical development in the eastern sector of the Triglia Group of Rocks. Furthermore, polyphase deformation caused by folding and thrusting disturbs these layers. The axial planes of the folds showed dips between 40 °and 60°. In addition, the displacement of the thrusts was between 200 and 500 m. As a result, a series of compartments developed due to folding and thrusting, which made up the Triomphe exploitation land. In this region, we have ENE-WSW trending anticlines and synclines with a wavelength of 2–3 km. These were dissected by a fault set striking N to S and spaced 500 to 800 m apart. Furthermore, the faults compartmentalize mineralization into sectors, namely, Shagoura Sud, Shagoura Nord, and Douamis. Additionally, these sectors have morphologies that influence extraction methods.

In Shagoura Sud, high-grade hematite forms steeply dipping lenses (45-60°) within quartzite host rock bounded by reverse faults that displace ore bodies vertically by 10-50 meters, creating isolated blocks requiring customized extraction sequences to minimize dilution from interbedded quartz veins that constitute 25-35% of the rock volume in certain horizons. Conversely, Shagoura Nord exhibits shallow-dipping (20-30°) blankets of weathered goethite-limonite overlying unoxidized hematite at depths of 30-50 meters, a morphology resulting from supergene alteration processes during the Plio-Pleistocene that reduced iron grades from 55% to 45-50% while concentrating manganese oxides along fracture networks in dendritic formations that complicate beneficiation. The Douamis sector displays intricately folded ore bands interleaved with manganese-rich phyllites, indicating syn-sedimentary mineralization during the Cambrian that was subsequently modified by Atlasic tectonism, with manganese concentrations reaching 3% near fracture surfaces where secondary pyrolusite (MnO_2) and cryptomelane ($K(Mn^{4+}, Mn^{2+})_8O_{16}$) precipitate in botryoidal aggregates.

Stratigraphically, three principal units govern mineralization patterns: the Basal Quartzite Unit (50-100m thick) hosts massive hematite with minor pyrite in concentrations of 2-5% that formed through hydrothermal replacement at temperatures of 200-250°C evidenced by fluid inclusion studies; the Intermediate Dolomite-Phyllite Unit (30-60m thick) contains stratabound hematite-goethite lenses where oxidation fronts advanced along bedding planes at rates of 1-5 cm/century; and the Upper Silicified Limestone Unit (20-40m thick) features disseminated hematite within karstified zones where collapse breccias created porosity exceeding 30% in localized areas. Each unit records different phases of hydrothermal activity and weathering history that collectively create the deposit's renowned heterogeneity, with oxidation depths varying from 30 m in Shagoura Nord's fractured zones to 80 m in Douamis, where phyllite layers inhibit fluid migration, resulting in iron content fluctuations between 40-60% Fe over lateral distances as short as 10 m, a variability that challenges resource estimation accuracy and necessitates advanced geostatistical approaches for effective mine planning (Baala, 2021) (Evtekhov et al., 2016) (Douamis Report, 2014) (MSILA University, 2020) (DSpace-Univ-Annaba, n.d.).

I.2.4 Mineralization and Ore Characteristics: Paragenetic Sequences and Metallurgical Implications:

The mineralogical composition of the El-Ouenza ores reveals a dynamic interplay between primary hydrothermal processes initiated during the Cambrian rifting and subsequent weathering regimes active since the Neogene, with hematite (Fe_2O_3) dominating unweathered zones as coarse-grained specular crystals reaching 5 mm in diameter in the quartzite veins of Shagoura Sud and fine-grained microcrystalline disseminations (10-50μm) in the dolomitic matrices of Douamis, often intergrown with gangue minerals that complicate liberation during beneficiation due to textural complexities along mineral boundaries. In Shagoura Nord's near-surface environment, pseudomorphic replacement of hematite by goethite preserves the original sedimentary banding while reducing iron grades by 10-15% and introducing vuggy porosity of 25-30% that diminishes metallurgical recovery by 15-20% compared to unweathered counterparts, whereas limonite formation in groundwater-saturated zones exhibits botryoidal textures enriched with manganese (2-3% MnO) and arsenic (150-300 ppm), which pose significant environmental and processing challenges through increased reagent consumption.

Gangue mineralogy varies substantially across stratigraphic horizons: quartz appears abundantly (15-25%) as coarse veins exceeding 10 cm width in primary zones and cryptocrystalline masses in oxidized horizons, requiring fine grinding to 75μm for effective liberation; clay minerals, particularly kaolinite and illite (5-12%), dominate weathered zones where they introduce alumina (4-8% Al_2O_3) that compromises pellet quality by reducing compressive strength from 250 kg/pellet to 180 kg/pellet at equivalent binder dosages; manganese oxides such as pyrolusite (MnO_2) and cryptomelane form dendritic coatings in fractures with crystal lengths of 1-5 mm; and carbonates including siderite ($FeCO_2$) occur in deep, unoxidized zones where they contribute

CO_2 emissions during thermal processing at rates of 0.8tons CO_2 per ton of concentrate produced.

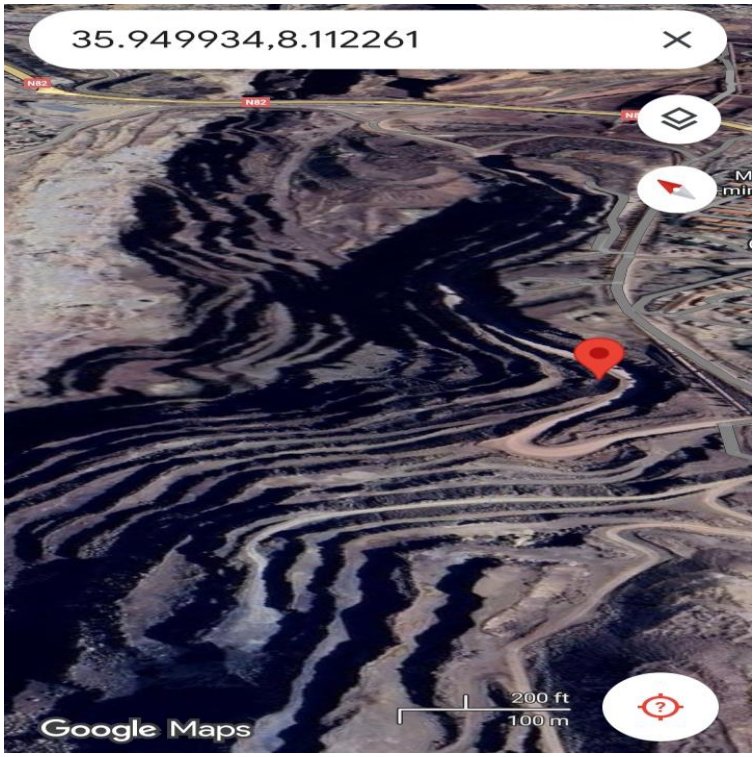
Based on comprehensive borehole assays and petrographic analysis of 2,000 thin sections, ores are classified into four distinct types reflecting geological evolution and spatial distribution: Type 1 (Massive Hematite) occurs in Shagoura Sud's lower strata as banded iron formation relics with specular hematite (>55% Fe, <15% SiO_2, 3-5% Al_2O_3) and minor pyrite (2-4%) that formed under reducing conditions at depths exceeding 500 meters; Type 2 (Hematite-Goethite Blend) characterizes Shagoura Nord's transition zone with boxwork textures from hematite dissolution (48-55% Fe, 15-20% SiO_2, 4-6% Al_2O_3 where oxidation progressed along microfractures; Type 3 (Goethite-Limonite Dominant) prevails in Shagoura Nord's upper levels with high porosity (40-48% Fe, 20-25% SiO_2, 6-8% Al_2O_3, 1-3% MnO) developed under seasonally fluctuating water tables; and Type 4 (Low-Grade Stockpiles) represents historical waste with elevated silica (25-35%) and alumina (8-12%) requiring advanced valorization due to complex mineral associations. This mineralogical diversity originates from Cambrian rifting events that initiated mineralization through basin-bounding fault systems that channeled Fe-rich fluids into porous horizons, followed by Atlasic orogeny that remobilized ores along fractures through pressure solution mechanisms, creating vertical geochemical zoning evident in sulfur isotope signatures ($\delta^{34}S$ values of -3‰ to +5‰ indicating magmatic-hydrothermal sources) and cerium anomalies ($Ce/Ce^* = 1.2$-1.8 suggesting oxidative remobilization) that delineate hypogene, supergene, and lateritic zones with distinctive metallurgical behaviors requiring customized processing approaches for optimal resource recovery (MSILA University, 2020) (Baala, 2021) (DSpace-Univ-Annaba, n.d.) (Enrichissement Report, 2020).

I.2.5 Mining and Processing Methods: Integrated Extraction to Concentration Technologies:

I.2.5.1 Sector-Adapted Extraction Methodologies:

El-Ouenza employs conventional open-pit mining methodologies meticulously adapted to each sector's geological peculiarities; in Shagoura Sud, where high-grade hematite forms steeply dipping lenses (45-60°), operations utilize precision drilling with rotary percussion rigs (Atlas Copco D90KS) producing 150 mm diameter blast holes at 5 m spacing, loaded with ANFO explosives at 0.8 kg/m³ powder factors for controlled fragmentation that minimizes quartz dilution to less than 15%, with GPS-guided hydraulic excavators (Komatsu PC3000) selectively loading material for direct rail transport to Annaba. However, the steep dip angles necessitate high-wall configurations with 70° slopes that increase geotechnical risks, requiring continuous monitoring through 50 prism stations and 12 inclinometers installed along critical sections, with stabilization measures including rock bolting (32 mm diameter, 8m length) at 2m grid spacing and shotcrete application (100 mm thickness) on unstable faces.

Shagoura Nord's shallow-dipping (20-30°) weathered goethite-limonite layers demand fundamentally different strategies: rotary drilling (Sandvik DR460) of moisture-rich ore (8-12% natural moisture content) at wider 7m spacing to prevent hole collapse, followed by reduced-charge blasting (0.5kg/m³) that preserves delicate goethite structures, and dedicated rotary drying systems (8m diameter, 30m length) that reduce moisture to <5% before crushing, preventing clogging in downstream processing equipment while optimizing energy efficiency through waste heat recovery from dryer exhaust gases. The Douamis sector employs sensor-based sorting at active pit faces using STEINERT KSS X-ray transmission technology that identifies Mn-bearing minerals based on atomic density contrasts >2.8 g/cm³, rejecting 30% of low-grade material before processing and significantly reducing volumes entering the concentration circuit while improving concentrate quality. Across all sectors, haulage operations deploy 28 CAT 789D trucks with 180-tonne capacities traveling along 42 km of internal roads that require 15,000 tons/month of laterite gravel for dust suppression and surface stabilization, representing an annual maintenance cost exceeding $1.2 million due to erosional damage during seasonal rains



that deliver 450 mm precipitation between November and March.

Figure I.5 View of El-Ouenza mine Open pit (Google Maps; 2025).

I.2.5.2 Beneficiation Challenges and Titration Dependency Crisis:

Beneficiation strategies confront sector-specific complexities exacerbated by analytical limitations: the Shagoura Sud circuit employs three-stage crushing (primary jaw crusher FL Smidth 1.5m x 2.0m reducing ore from 1000mm to 250mm; secondary cone crusher Metso HP800 at 250mm to 80mm; tertiary impact crusher Sandvik CI732 at 80mm to 25mm) followed by ball milling (5.5m diameter x 7.5m length) to 75µm for mineral liberation, but titration's inability to differentiate Fe^{2+}/Fe^{3+} in blended feeds causes overgrinding of softer goethite components, consuming 25-30 kWh/ton when selective comminution could conserve 15-20% energy. Reverse flotation of Douamis ores suffers from recurrent reagent poisoning because titration cannot detect manganese interference (1-3% MnO), leading to unexplained hematite depression when amine collectors (Armeen T at 300g/ton) adsorb onto MnO_2 surfaces, reducing concentrate grades from 62% Fe to 58% Fe and increasing silica content from 6% to 9%. The absence of real-time silica assays further prevents the dynamic adjustment of hydro-cyclone operations, resulting in alumina-rich clay reports to pellet feeds that diminish agglomerate strength below commercial specifications of 250 kg/pellet to 180 kg/pellet maximum.

laboratory technicians spent 70% of shifts in manual sample preparation (crushing, digestion, titration) rather than process optimization, while 48-hour assay delays forced supervisors to operate grinding circuits using historical averages rather than real-time data, culminating in estimated annual losses exceeding $2 million through energy overconsumption (exceeding 30 GWh/year) and recovery shortfalls (5-7% below theoretical maximum). This analytical deficiency is compounded by Algeria's import restrictions on advanced instrumentation and insufficient technical training programs, creating a self-perpetuating technological gap in which reliance on 19th-century analytical methods impedes 21st-century operational efficiency and environmental compliance.

I.2.5.3 Agglomeration Technologies and Modernization Roadmap:

To valorize fine-grained processing waste, researchers have optimized pelletization using 2-3% bentonite binders (montmorillonite content >85%) in disc pelletizers (9m diameter, 35° inclination) that yield 10–16 mm pellets with 63-65% Fe and compressive strengths exceeding 250 kg/pellet after induration at 1,250°C for 30 min, meeting blast furnace specifications while reducing the return fines generation to <5% through precise moisture control at 9.2% feed humidity. Sintering trials in Dwight-Lloyd machines (4m width, 120m² grate area) at 1,250-1,300°C with 10% coke breeze (5–10 mm size fraction) produce agglomerates suitable for direct furnace charging, although energy consumption remains higher than pelletizing at 25-30 kWh/ton versus 18-22 kWh/ton due to higher exhaust gas volumes requiring treatment.

Modernization initiatives focus on overcoming titration constraints through phased implementation: portable XRF analyzers (Olympus Vanta series, $25,000/unit) enable pit-face Fe/Mn/Si quantification with ±0.5% accuracy in <2 minutes, eliminating assay delays; on-site ICP-OES laboratories (PerkinElmer Avio 500, $180,000) provide hourly trace element monitoring for As, Pb, and Cr; and automated mineralogy systems (MLA-SEM, $500,000) optimize liberation characteristics sector-by-sector, revealing that Shagoura Sud's specular hematite could be liberated at 150µm rather than standard 75µm, potentially reducing grinding energy by 30%. Complementary investments in solar hybridization (20 MW photovoltaic plant with 60 MWh battery storage, $5.2 million) leverage Algeria's 2,500 kWh/m²/year solar insolation to reduce grinding circuit emissions by 15,000 tons CO_2/year while insulating operations from grid instability, representing a convergence of analytical precision and renewable energy integration that defines the future of sustainable mining (Enrichissement Report, 2020; Thèses Algérie, 2020; Tébessa University, 2020; Faculté des Sciences, 2019).

I.2.6 Reuse and recycling of valuables:

I.2.6.1 Legacy Environmental liabilities, and remediation initiatives:

The mining that has occurred for decades at El-Ouenza has created over 100 million tons of tailings that have been deposited over 320 hectares of unlined ponds in the Oued Boukhadra watershed. This has resulted in a highly complex environmental dilemma that occurs via many pathways. Silica-rich wastes (20-25% SiO_2) that contain residual iron and arsenic levels of 150-500ppm leach into water during rainy seasons. Contamination of the transboundary Continental Intercalaire aquifer by these tailings resulted in arsenic levels reaching 300 ppb. This is already over 300% of the World Health Organization (WHO) guidelines, which means that binational remediation will be required under the auspices of the 2002 Environmental Cooperation Accord. The uncovered stockpiles generate 12,000 tons of dust emissions per year, causing particulate matter. PM2.5, analyzed in the village of Bir El Ater, revealed that the levels regularly reach 75 µg/m³ when compared to the World Health Organization standard of 25 µg/m³ and the subsequent asthma levels of 40% in children of long-term residents. This status was validated using pulmonary function tests conducted in 2022. The instability of slopes on the peripheries of waste repositories, whose inclinations vary between 25° and 30°, causes erosion. Freeze-thaw cycles, where temperatures vary between -5° and 25°, create ice lenses in the clay-rich interbeds and lead to a 40% reduction in shear strength. The stability of these slopes leads to the transport of 8,000 tons/year of contaminated sediments into agricultural fields, further worsening the scope of damage. The reclamation liabilities that will make the land and community safer are assessed to be worth $12 million for an overall stabilization project through measures such as terracing, Phyto capping, and drainage control infrastructure. (Soomro, A. Et al,2024).

I.2.6.2 Circular Economy Material Repurposing Pathways:

Strategic repurposing of mining waste transforms environmental liabilities into economic assets through science-driven valorization: silica-dominated tailings substitute 30% of natural sand in C25-grade concrete production, achieving compressive strengths of 32 MPa at 28 days curing while reducing cement consumption by 15% and associated carbon emissions by 0.4 tons CO_2 per cubic meter of concrete produced. Hematite-rich fines (<75μm) undergo low-intensity magnetic separation (1,200 Gauss) and calcination at 800°C to produce iron oxide red pigments of >98% Fe_2O_3 purity for construction coatings, establishing a potential $5 million annual revenue stream from previously discarded materials through partnerships with Algerian paint manufacturers (SIPPEX, COFINA). Geopolymerization represents a revolutionary pathway in which alkali activation (8M NaOH + sodium silicate solution) of phyllosilicate-rich tailings yields structural binders with a compressive strength of 32MPa without Portland cement, simultaneously sequestering heavy metals through incorporation into aluminosilicate matrices, while consuming 60% less energy than conventional cement production.

Manganese recovery from Douamis tailings via bioleaching with “Shewanella oneidensis” at pH 3.5-4.0 and 30°C produces Mn^{2+} solutions that undergo electrolysis to deposit battery-grade MnO_2 on titanium anodes, achieving 95% purity suitable for lithium-ion battery cathodes, positioning El-Ouenza within emerging battery value chains while resolving historical contamination issues. Slope stabilization integrates engineering and ecology through terraced phytocaps of “Atriplex halimus” (saltbush) and “Ficus carica” planted at 1 plant/m² density that reduces erosion by 70% while phytoextracting 15 kg/ha/year of trace metals. Permeable reactive barriers composed of limestone-zeolite blends (50:50 ratio) neutralize acidic seepage in groundwater recharge zones by raising the pH from 3.5 to 6.8 while precipitating heavy metals as hydroxides, demonstrating how circular economy principles can reconcile ecological restoration with resource efficiency at landscape scales.

I.2.6.3 Socioeconomic Integration and Community Health Initiatives:

For El-Ouenza City's 50,000 residents, mine dependencies intertwine with environmental burdens: silicosis prevalence among 800 waste workers reaches 32%, as confirmed by radiographic surveys, demanding mobile clinics equipped with digital radiography units for early detection during biannual occupational health campaigns. Youth unemployment exceeding 45% necessitates vocational training centers in geopolymer manufacturing and solar infrastructure maintenance, with curricula developed in partnership with Tébessa University to certify 200 technicians annually for employment in valorization industries. Revenue-sharing mechanisms—allocating 2% of valorization profits to community health funds—could transform social contracts by financing asthma treatment programs providing free bronchodilators to 1,200 affected children and scholarships for 50 university students annually in mining-affected communities, where historical inequities persist since colonial administration.

Policy frameworks such as Circular Economy Tax Rebates (30% deduction for waste-to-product investments) incentivize private sector participation in silica-based construction material plants, while Community Benefit Agreements legally bind 20% of processing efficiency savings to local infrastructure development, formalizing reciprocity absent in colonial-era extraction paradigms and establishing new standards for resource transitions in developing economies. These integrated approaches position El-Ouenza as a testbed for the UN Sustainable Development Goals, particularly SDG 9 (Industry, Innovation and Infrastructure), SDG 11 (Sustainable Cities), and SDG 12 (Responsible Consumption), through measurable reductions in resource intensity, pollution loading, and health disparities (Faculté des Sciences, 2019; Idres et al., 2017; Mero et al., 2018; Thèses Algérie, 2020).

I.2.7 Previous studies:

By integrating Zerzour's geostatistical precision (3D kriging models reducing reserve estimation errors to <5%), Ramos's material repurposing frameworks (geopolymer binders cutting cement emissions by 60%), and Mero's community engagement models (revenue-sharing mechanisms funding health/education), El-Ouenza can pioneer a Global South template for 21st-century mining—where subterranean wealth funds surface prosperity, geological inheritance becomes a sustainable legacy, and Algeria positions itself at the vanguard of resource-efficient mineral development. This transition demanded courageous policy reforms: revising equipment import regulations to facilitate analytical technology acquisition, establishing a National Mining Waste Valorization Fund capitalized at $50 million, and ratifying enhanced binational water governance protocols with Tunisia. Although requiring investment exceeding $25 million over 2025-2030, the return transcends economics: the redemption of colonial extraction enclaves into a beacon of the regenerative industry that aligns mineral endowment with intergenerational equity and ecological resilience across the Maghreb region. As climate change intensifies water stress and decarbonization reshapes steel technology, El-Ouenza's metamorphosis offers lessons for mining regions worldwide, proving that sustainability emerges not from abandoning extractive industries but from reimagining their purpose within planetary boundaries and social justice imperatives.

I.2.8 Integrating Geological Heritage and Sustainable Futures:

El-Ouenza embodies Algeria's mineral paradox: a century-old deposit of immense geological wealth constrained by technological inheritance and environmental legacy. Breaking titration analytical stranglehold through portable XRF and ICP-OES laboratories represents the critical catalyst for transformation, enabling real-time ore control that optimizes extraction sequencing, reduces energy intensity by 20%, and unlocks 100 million tons of stranded resources within historical waste stockpiles. Beyond technical modernization, El-Ouenza's future hinges on reimagining mining paradigms: waste becomes feedstock for circular manufacturing industries; slopes evolve into stabilized phytoremediation sites that sequester carbon and restore biodiversity; and communities transition from impact-bearers to innovation partners in valorization enterprises that generate dignified employment beyond extraction.

Conclusion:

This study examined iron ore in-depth from multiple perspectives, establishing its essential mineralogical characteristics, beneficiation techniques, and its economic importance.

The analysis reveals that while conventional beneficiation methods remain effective for hematite and magnetite ores, increasingly complex ore types, such as those found in Algeria, require innovative beneficiation solutions combining advanced approaches. Modern advances in sensor sorting, high-pressure grinding, and hydrogen reduction demonstrate the industry's technological adaptability, particularly in response to environmental imperatives. For Algeria to realize its potential in this sector, strategic investments must address the technical challenges associated with system infrastructure limitations, potentially through international partnerships leveraging recent advances in bioleaching and hydrometallurgy.

This study highlights the critical importance of continuing research into sustainable enrichment methods capable of exploiting complex deposits while minimizing environmental impact, particularly in developing countries seeking to develop their mineral resources.

Chapter II: Materials and Experimental Methods

II.1 Introduction:

This chapter outlines the comprehensive methodologies and analytical procedures used to study the samples from the El-Ouenza iron deposit. This study had two main goals: the first goal is: the characterization of El-Ouenza iron ore by defining and identifying the grain size distribution and assessing the liberation state of the minerals according to the normalized process, chemical and mineralogical composition of the samples, and quantifying their mineral phases. The second goal is: to use magnetic separation to separate and valorize the El-Ouenza iron ore to obtain an iron rich in hematite. The influence of magnetic separation parameters on the enrichment of El-Ouenza ore were carried out.

The specific tools employed for this study are described in this chapter.

II.2 Sampling:

Sampling is the operation of collecting samples that represent the entire surface area of the studied zone. With making sure that the samples were well preserved to avoid any possible contamination. (Matías Miguel, Salvarredy Aranguren., 2008).

Following a well-defined sampling protocol aims to obtain representative samples containing all the physical and chemical characteristics of the entire study site (Pineau J. L., 1996). The main steps characterizing a sampling approach are the development of a collection strategy, collection of samples on-site, preservation of samples, and preparation for various analyses and processing methods. The value of the characterization results depends on the adequate execution of all steps. The collection strategy is based on the volume and number of samples, as well as the choice of sampling points (number and positioning). The representativeness of the samples depends largely on the choices made (A. Gosselin et al., 1999).

The samples investigated in this study were collected from the Chagoura zone, located within the larger El-Ouenza iron ore deposit in northeastern Algeria. The Chagoura sector represents a local ore stock of more than 3 million tons, characterized by moderate to low iron grades. It was chosen because of its underutilized potential and the increasing interest in upgrading lower-grade iron ores for industrial use.

The geological context of the sampling area corresponds to the Proterozoic units of the Ouenza deposit, where iron mineralization occurs mainly as hematite, frequently associated with quartz, goethite, and minor amounts of clay minerals.

Representative ore samples were collected from various accessible points within the Chagoura stockpile of the El-Ouenza Mine. The collection was performed manually in collaboration with site engineers to ensure the coverage of geologically distinct zones. These samples were intended to represent the local variability of iron mineralization and were later transferred to the laboratory at El-Ouenza for preparation and analyses.

II.3 Comminution and valorization of iron ore:

Sample preparation followed standard laboratory procedures (**NF EN 933-1)** aimed at comminution (reducing the particle-size and enhancing mineral liberation), and the application of magnetic separation. Each sample for each test was weighted of 30g.

The main steps are illustrated in the following flowsheet processing (figure II.1):

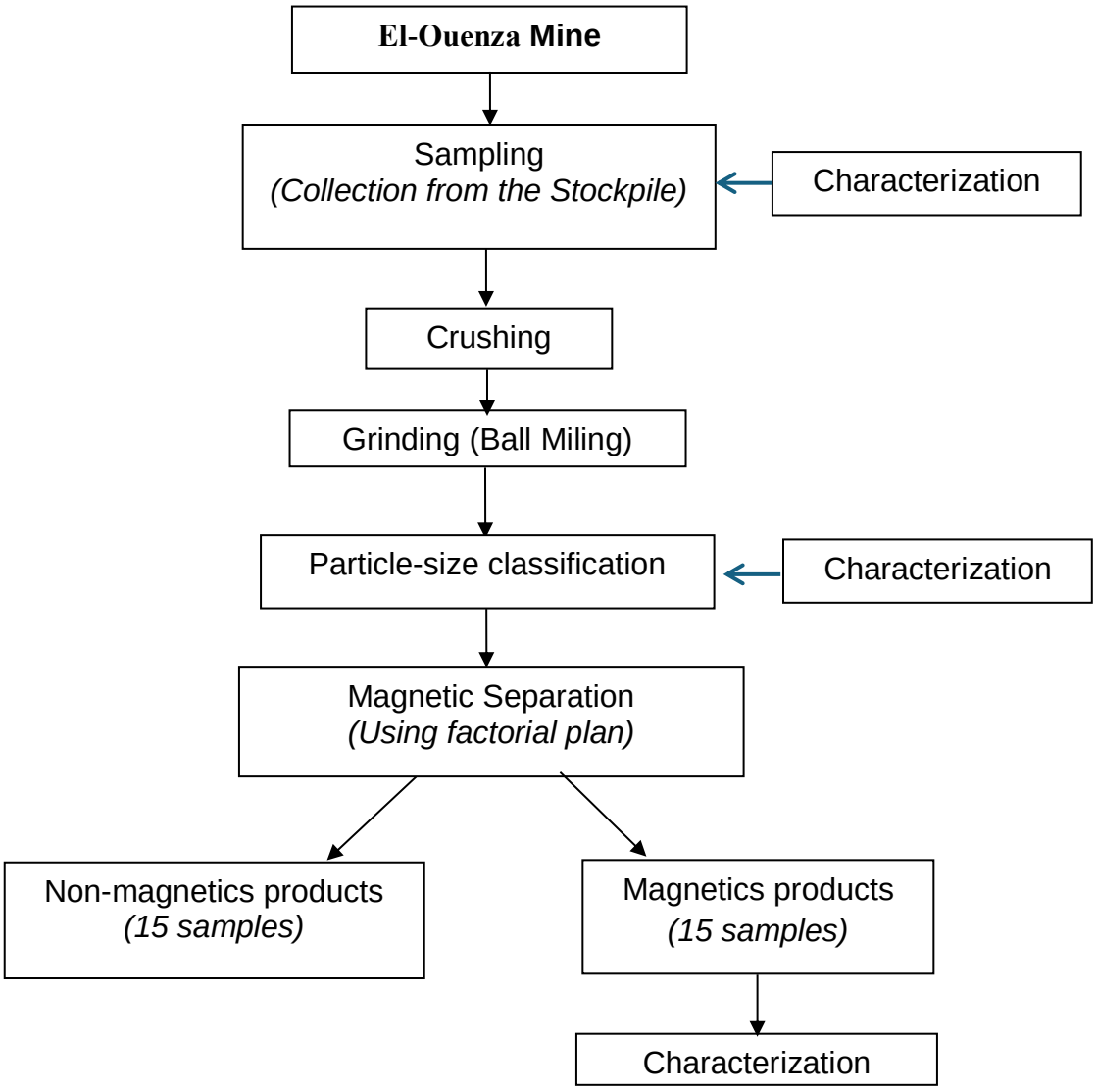


Figure II.1: The proposed flowsheet of El- Ouenza iron ore

II.3.1 Crushing:

The first step in comminution process was dry crushing, which reduced the ore to a particle size of approximately 4 mm. This initial size reduction is essential for handling and further treatment. Crushing does not typically produce tailings or loss of material (European Office for the PRIP, 2004). To reduce the iron ore of the selected sample from El- Ouenza mine, a laboratory Retsch crusher was used, adjusted between 20 and 1mm (Figure II.1).



Figure II.2: Laboratory crusher of El-Ouenza mine.

II.3.2 Grinding:

The crushed material (iron ore) was subjected to the secondary step. For the grinding process, a laboratory grinder was used to achieve a size of less than 1 mm. This size threshold was selected to enhance mineral liberation, which is essential for accurate chemical and mineralogical analyses as well as downstream separation processes. The type of used grinder is Retsch RS100 (Figure II.2).



Figure II.3: El-Ouenza mine laboratory disc grinder.

After collection, the raw samples were subjected to primary crushing followed by grinding using a laboratory grinder to achieve a particle size of less than 1 mm. This particle size threshold was selected to allow optimal liberation of iron minerals prior to the characterization and concentration steps. The ground material was then homogenized and subdivided into test portions for further analysis.

II.3.3 Quartering:

To ensure sample representativity, the ground material was subjected to quartering (also known as coning and quartering). This step involved homogenizing the sample and systematically reducing its volume by dividing it into four equal parts, discarding two diagonally opposite quarters, and recombining the remaining two. The process was repeated as needed to obtain laboratory-scale subsamples while preserving the original mineralogical composition



Figure II.4: Sampling quartering method

(https://blog.wstyler.com/particle-analysis/how-to-prepare-a-sample-for-particle-size-testing)

II.4 Analytical Methods

II.4.1. Particle Size Distribution

Particle size analysis was conducted to evaluate the grain-size distribution of particles in the ore sample and identify the distinct size classes within a material. This analysis is fundamental to understanding the texture and structure of the ore and provides essential data for interpreting mineral liberation and the distribution of mineral species across particle size fractions. Chemical analysis can subsequently be applied to each fraction to assess the selective mineral concentrations.

The particle size distribution was determined on a dried sample of 3070 g of iron ore using a Control dry sieving machine (Figure III.5) equipped with sieves of dimensions 200 mm × 50 m. This analysis was carried out at the Mining Institution laboratory, Larbi Tebessi University.

Sieving was performed for 30 min at an amplitude setting of 60, in accordance with the European standard **NF EN 933-1 (see the Annexes section)**. This standard defines the method for determining the particle size distribution of aggregates by dry or wet sieving through a set of test sieves of defined aperture sizes.

The sieve stack included mesh openings of: (2 mm, 1 mm, 0.5 mm, 0.25 mm, 0.125 mm, 0.063 mm)



Figure II.5 The samples and the laboratory sieve stack

After sieving, the retained fractions on each sieve were weighed using a precision balance with an accuracy of 0.01 g. The relative weight of each fraction was calculated to determine the percentage distribution of particles.

This analysis revealed that the majority of the sample mass was distributed between 0.125 and 0.5 mm, suggesting an overall fine texture and good liberation potential for iron-bearing minerals. The data obtained also support the decision to proceed with magnetic separation of fine fractions, especially those below 1 mm.

II.5 Chemical Composition (Determination of Fe_2O_3 Content by Volumetric Titration)

To determine the iron content of the ore samples, a volumetric redox titration method was employed. The same procedure employed by the El-Ouenza mine for routine evaluation. This classic wet chemistry technique allows for the accurate quantification of iron oxides, particularly Fe_2O_3, by reducing ferric ions (Fe^{3+}) to ferrous ions (Fe^{2+}) and titrating with a standardized oxidizing agent. The procedure was performed at the El-Ouenza mine laboratory under supervision using standard protocols.

- ***Sample Dissolution***

From each particle size fraction (−1 mm and −0.063 mm), 0.1 g of the sample was weighed into a clean beaker. To each beaker, 25 mL of hydrochloric acid (HCl) was added. The mixture was gently heated to dissolve the iron oxides, as indicated by the disappearance of reddish-brown particles. Once fully dissolved, the solution was removed from the heat, and distilled water was added to rinse the walls of the beaker, adjusting the total volume to 100 mL.



Figure II.6: Measuring and heating procedure

- ***Reduction and Stabilization of Fe^{2+}:***

To reduce Fe^{3+} to Fe^{2}, stannous chloride ($SnCl_2$) was added dropwise until the solution changed from orange to colorless, indicating complete reduction. Then, 10 mL of mercuric chloride ($HgCl_2$) was added to eliminate any excess Sn^{2+} by precipitating the $HgCl_2$. This step is critical for preventing interference during titration.

- ***Acid* Complexation:**

A previously prepared acidic mixture was added to each sample. The mixture was composed of the following:

150 mL sulfuric acid (H_2SO_4)

150 mL phosphoric acid (H_3PO_4)

Diluted with distilled water to 1000 mL

This acidic environment enhances the titration endpoint visibility and stabilizes the Fe^{2+} complex.

- ***Titration Procedure:***

After adding 10 drops of a color indicator, each solution was placed on a mechanical stirrer. Standardized potassium dichromate solution ($K_2Cr_2O_7$) as added dropwise from the burette

The titrant, originally prepared from crystalline potassium dichromate, had a titer factor of 2.93, as provided by a laboratory engineer.

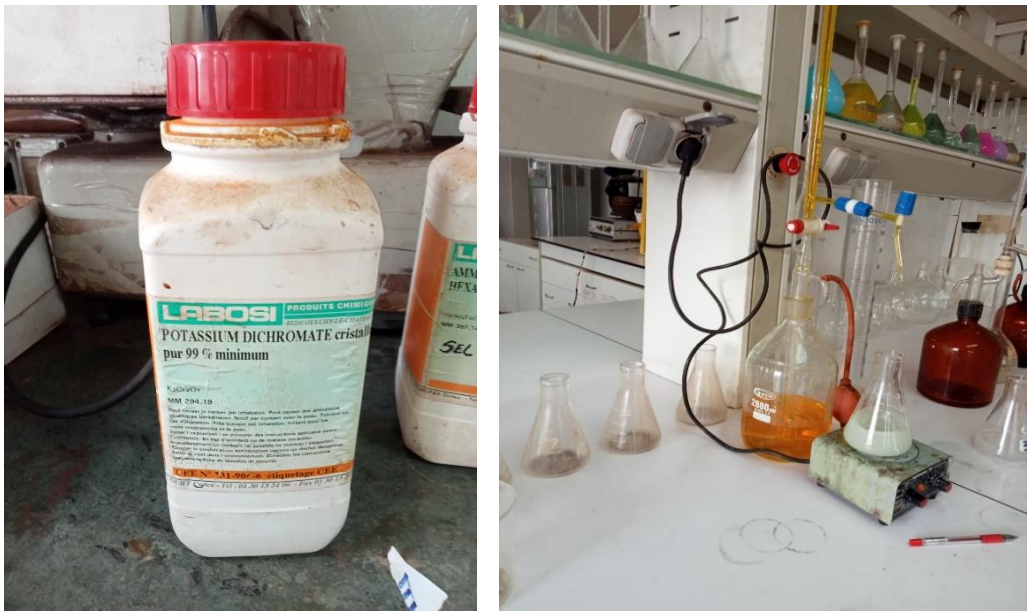


Figure II.7 Titration procedure

The endpoint was marked by a color change from colorless to purple, indicating the complete oxidation of Fe^{2+} back to Fe^{3+} by $K_2Cr_2O_7$.

Fe (%) = 2.93 * Volume of $K_2Cr_2O_7$used (mL).

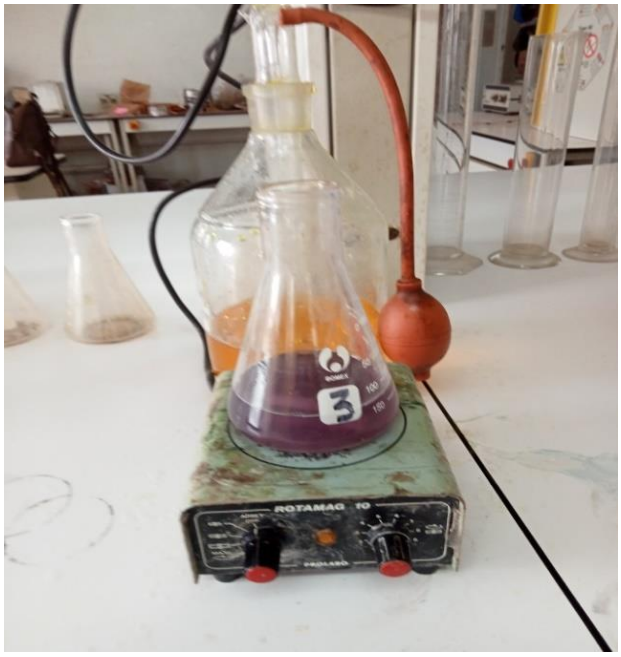


Figure II.8 The endpoint of the titration

The titration results showed high reproducibility between the different particle-size fractions. The average iron content was calculated by taking the mean of all titration values, resulting in an overall Fe_2O_3 content of approximately 43–44 %. These values are consistent with the known characteristics of moderate-grade ores from the Chagoura zone.

II.6 Complementary Analyses:

In addition to the basic testing, representative samples were submitted for advanced analysis.

II.6.1 X-Ray Fluorescence (XRF):

a non-destructive technique used to determine the chemical composition of a material by measuring the characteristic X-rays emitted by elements when excited by a primary X-ray source.

It enables both qualitative and quantitative elementals analysis of major, minor, and trace elements in solid, powdered, or fused samples.

This method is widely used for analyzing ores, rocks, soils, and industrial products due to its precision, speed, and reliability. In our study all the chemicals analyses were carried out using a **S8 Tiger, Bruker** (figure II.8) at the cement (JICA) company laboratory of *Hadjar-Soud, Spa*. SCHS. Bekouche Lakhder located in Azzaba city.

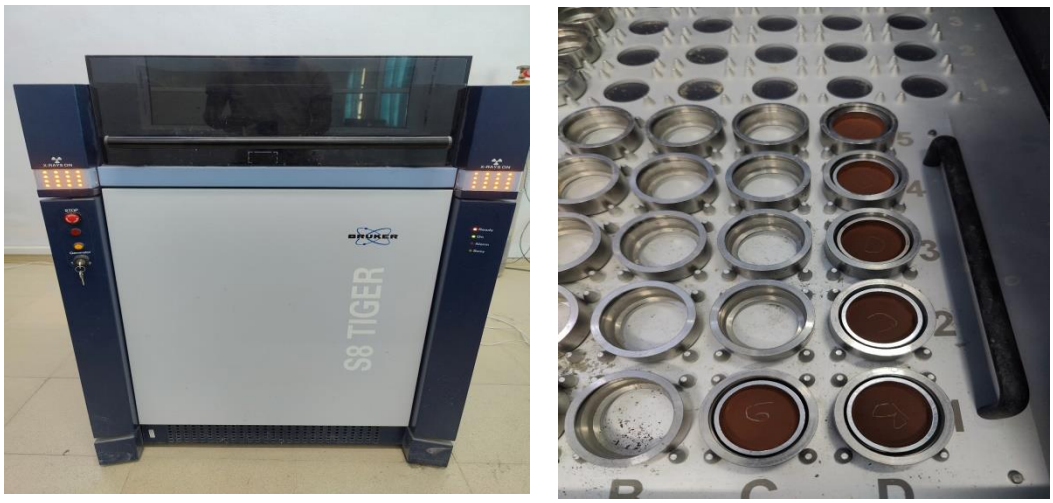


Figure II.9: The used XRF machine (laboratory of GICA, Skikda, 2025)

II.6.2 X-Ray Diffraction (XRD):

In materials research, scientists ask many analytical questions related to the chemical composition and crystalline makeup of materials. X-ray diffraction (XRD) is the only laboratory technique that accurately and non-destructively obtains structural information such as chemical composition, crystalline structure, crystallite size, lattice strain, preferred orientation, and layer thickness. These researchers therefore use XRD to analyze a wide range of materials, from powders to solids, thin films, and nanomaterials (Malvent Panalytical, 2025). In this study; all the mineralogical analyses were carried out using a **D2 Phaser invented by Bruker** (figure II. 9) at the cement (JICA) company laboratory of *Hadjar-Soud, Spa*. SCHS. Bekouche Lakhder located in Azzaba city.



Figure II.10: The used XRD machine (laboratory of GICA, Skikda, 2025)

II.6.3 Scanning Electron Microscopy (SEM-EDS):

Scanning Electron Microscopy (SEM) provides a high resolution, high magnification image of a sample material by emitting a finely focused beam of electrons onto a sample. This beam interacts with the molecular composition of the sample. These interactions produce a series of measurable electron energies that are analyzed by the scanning electron microscope to create a three-dimensional image (Gossman Forensics)

The sample of iron ore collected from El- Ouenza mine was analyzed using PHILIPS / FEI QUANTA 250, Figure II.10 at the National Higher School of Technology and Engineering, Sidi Amar, Annaba

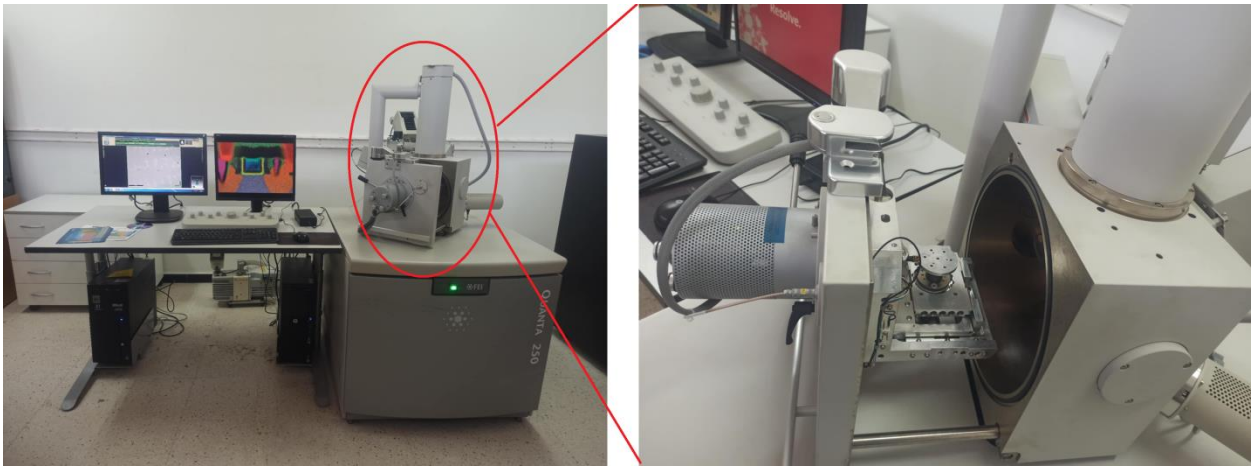


Figure II.11: The used SEM-EDS (Laboratory of NHSTE, Annaba)

II.7 Magnetic Separation Testing:

Magnetic separation is a physical method of separating components of mixtures based on differences in their magnetic susceptibility. It is commonly used to extract or concentrate magnetic materials from non-magnetic ones, particularly in the mining industry and environmental applications.

It is especially effective for separating ferromagnetic and paramagnetic minerals (like magnetite or hematite) from diamagnetic or non-magnetic ones (such as quartz, kaolinite, or calcite).

II.7.1 Principal of operation:

The magnetic separation of solid waste is a method of separating ferromagnetic substances using the magnetic field generated by the magnetic separation equipment. Magnetic separation is primarily used in solid waste treatment systems to recover or enrich ferrous metals, or in certain processes to remove ferrous materials from solid waste. Overhead magnetic separation equipment is used in some large-scale equipment to recover iron metal prior to crushing. For

example, the Fe could be recovered before the waste is incinerated. Magnetic separation and recovery devices have also been used in landfill treatment sites to separate ferrous metals from waste before disposal (Zhou Tao et al., 2023)

II.7.2. Used Equipment Description:

Magnetic separation experiments were conducted using a custom-built dry magnetic separator designed by Dr. M. Laraba (figure II.11). This experimental was specifically developed to test the magnetic behavior of fine and medium iron ore fractions from the El-Ouenza mine under various conditions. The hematite is classed as a paramagnetic material, with χ =500 ~ 760.10^{-6} cm^3/g at room temperature respectively (Jan Drzymala, 2007).

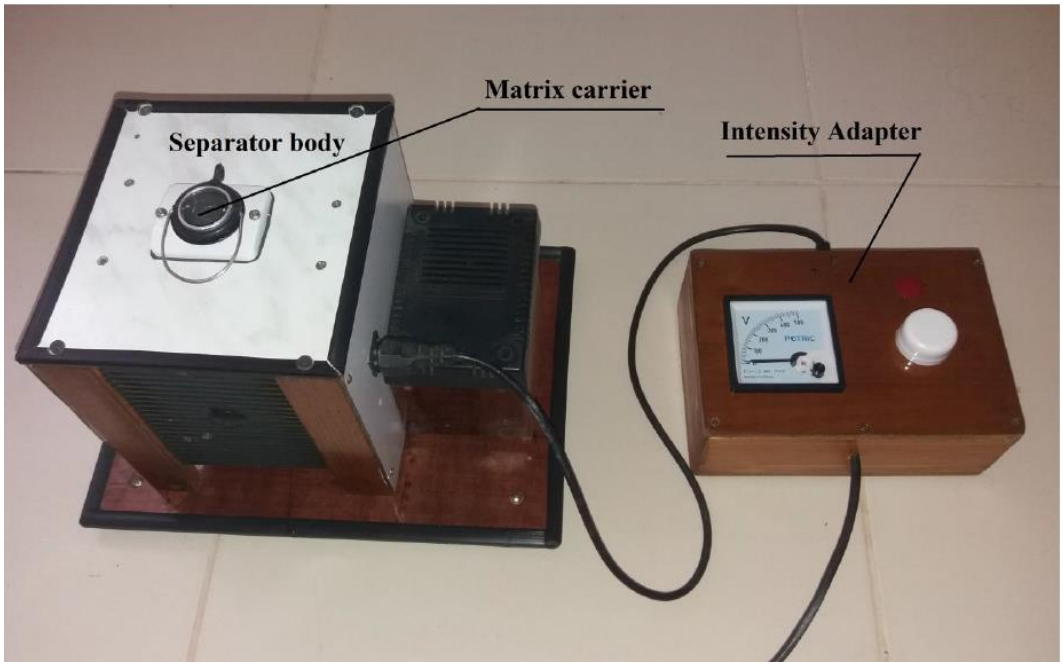


Figure II.12: Used magnetic separator (Manufactured by Dr. Laraba M.)

II.7.3. Operating principle of the magnetic separator:

The machine operates on the principle of generating a magnetic field using an adjustable electromagnet. This machine is equipped by a coil that containing a canister (a box filled with an extraction matrix (figure II.12).

When the magnetic field is applied, the material is passed through the matrix; the particles with a sufficiently high magnetic susceptibility are attracted to the balls matrix, and the non-magnetic particles (tailings) leave the system (Figure II.12, step 1). When the matrix retention capacity is reached, the feed is stopped, a water wash is carried out under field to clean the matrix of

mechanically trapped particles (magnetic particles), then the magnetic field is brought back to near zero, in order to expel, by pressurized water, the magnetic particles (Figure II-12, step 2). The feed can then resume. These different operations constitute the operating cycle of this separator.

In this magnetic separator, the matrix is constituted by steel balls (figure II.13).

This matrix has three main goals:

- To produce collection sites for paramagnetic particles and thus enable the separation of non-magnetic particles;

- To obtain high magnetic field gradient values in the separation zone, thereby generating strong attractive forces;

- To amplify the applied external magnetic field, with a more uniform distribution of field lines throughout the separation zone (Jan Drzymala, 2007).

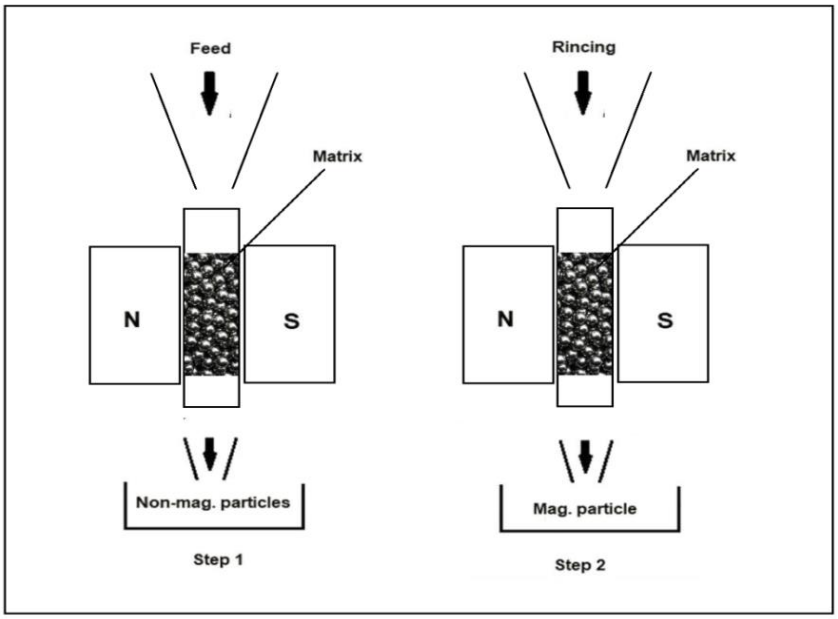


Figure II.12: Principle of the laboratory magnetic separator (Modified from Laraba M. 2022)

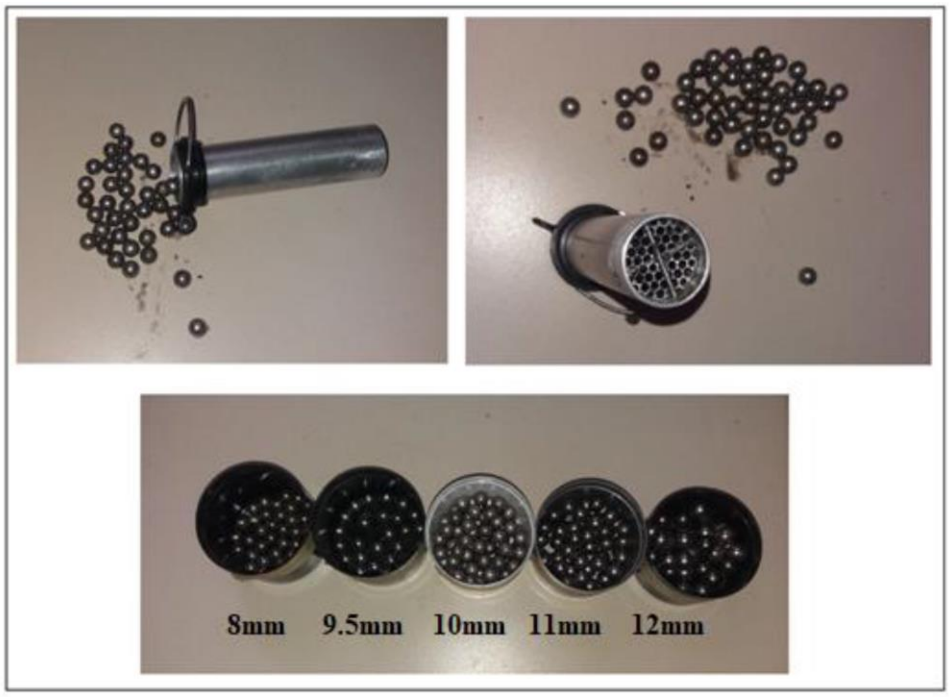


Figure II.13: The used Matrix Balls with different sizes

A matrix must indeed offer maximum collection efficiency, minimum magnetic reluctance, good fluid permeability, but also good ease of cleaning. Table II.1 gives the filling factors of the main types of matrices. The height of the matrix is also an important parameter as it can contribute to an increase in the mechanical retention power, but above all as it will determine the retention time of the particles in the field (Jan Drzymala, 2007).

Table II.1: Filling factors of different matrices (Jan Drzymala, 2007).

Matrix	**Filling factor *F***	**Element diameter (mm)**
Balls	**0,50 à 0,64**	**2 à 6**
Iron foam	0,01 à 0,05	0,008 à 0,35
Expanded metal	0,12 à 0,27	0,030 à 4
Wire mesh (metal weaving)	0,15 à 0,25	0,50 à 3
Metallic knit	0,05 à 0,10	0,02 à 0,4
Toothed platesa	0,50 à 0,80	4 à 8 cannelures par 2,5 cm

For a ball matrix diameter of 2 to 6 mm, the filling factor is 0.5 to 0.64, (50% to 64%).

For a higher filling factor means more surface area for magnetic particles to be captured, this can improve separation efficiency, as well as increases pressure drop and the risk of clogging.

For a lower filling factor means reduce capture efficiency but allows better flow and lower energy consumption.

II.8 Statistical approach:

II.8.1 Design of Experiment (DOE):

Design of experiments (DOE) is a branch of applied statistics that deals with planning, conducting, analyzing, and interpreting controlled tests to evaluate the factors that control the value of a parameter or group of parameters. DOE is a powerful data collection and analysis tool that can be used in a variety of experimental situations. Before doing any experiment using common sense evaluating a procedure is called DOE. (K. Soundaranayaki, 2022).

Design of experiments is a statistical methodology for systematically investigating input (X) independent- output (y) (dependent) relationship.

- To identify important design variables:
  - Planning the experiments;
  - To optimize process and product design;
  - Achieve robust performance.
- Key technology in product and process design (lab scale to field scale)
- Used in Chemical Engineering, Bio Process Engineering, Environmental Engineering, Industrial Engineering and Manufacturing unit (K. Soundaranayaki, 2022).

In our study, the **Box-Behnken** factorial design was selected to establish the relation between the variables parameters of magnetic separator (magnetic field intensity (I), particle size of iron ore (SP) and dimension of matrix balls DB) and response functions of grade and recovery. All the experiments were conducted on laboratory model of magnetic separator that cited in the previous paragraphs. The experimental data was analyzed using Minitab-19 software.

The 3 variables factors with each at 3 different levels have been listed in Table II.2.

Table II.2: Variables factors and their levels

Variables factors	Symbol	Coded variables level		
		Low (-1)	Center (0)	High (+1)
Grain size (GS) mm	X1	0.063	0.53	1
Intensity (I) T	X2	0.5	1.25	2
Dimension of Ball matrix (DB) mm	X3	8	10	12

II.8.2 Response surface methodology (RSM):

Response surface methodology (RSM) is a collection of statistical and mechanical methods that are useful for modeling and analyzing problems. In this technique, the main objective is to optimize the response surface that is influenced by various process parameters. The RSM also quantifies the relationship between the controllable input parameters and the response surface. The design procedure of RSM is:

- Designing of experiments for adequate and reliable measurement of the response,
- Developing a mathematical model of the second-order response surface with the best fitting,
- Finding the optimal set of parameters that produce a maximum or minimum value of response,
- Representing the direct and interactive effects of process parameters through two or three dimensional plots.

If all variables were assumed to be measurable then the response surface can be expressed as:

$$\boldsymbol{y} = f\,(\mathrm{X1}, \mathrm{X2}, \mathrm{X3}, \ldots \mathrm{Xk}) \qquad \textbf{(1)}$$

Where:

y is the output variables (response) and Xi the input variables of action called factor.

For the three-level three-factorial Box-Behnken experimental design, a total of 15 experimental runs are required table II.3 (Aslan, N. 2008, Ozgen, S. et al. 2009). The objective is to optimize the response *y* with an assumption that the independent variables are continuous and controllable through the experimentation. It is also required to find a suitable approximation for the true functional relationship between independent variables and the response surface, typically a second-order model is utilized in response surface methodology (Gunaraj, V. & Murgan, N. (1999), Kwak, J.S. (2005), Aslan, N. (2007a) and Aslan, N. (2007b).

In Design of Experiments (DOE) and particularly in Response Surface Methodology (RSM), the general form of multiple quadratic regression model is used using the general following mathematic relation:

$$\boldsymbol{y = \beta_0 + \sum_{i=1}^{k} \beta_i x_i + \sum_{i=1}^{k} \beta_{ii} x_i^2 + \sum_{i=1}^{k-1} \sum_{i=2}^{k} \beta_{ij} x_i x_j + \varepsilon} \qquad \textbf{(2)}$$

Where:

x_1, x_2, x_3 : are the input variables that exert influence on the response variable y*;*
$\beta_0, \beta ii, \ldots\ldots \beta ij$: in which i=1, 2, …,k and j=1,2, …, k are the unknown parameters
ε: represents a random error (negligible).

Table II.3: Encoded and coded variables of each test.

Test	Encoded variables			Coded variables		
	X_1	X_2	X_3	DB (mm)	GS(mm)	I (T)
1	**0**	**0**	**0**	10	0,53	1,25
2	0	1	-1	10	1,00	0,50
3	**0**	**0**	**0**	10	0,53	1,25
4	-1	1	0	8	1,00	1,25
5	1	-1	0	12	0,063	1,25
6	1	1	0	12	1,00	1,25
7	0	-1	-1	10	0,063	0,50
8	**0**	**0**	**0**	10	0,53	1,25
9	0	1	1	10	1,00	2,00
10	1	0	1	12	0,53	2,00
11	-1	0	1	8	0,53	2,00
12	0	-1	1	10	0,063	2,00
13	-1	-1	0	8	0,063	1,25
14	1	0	-1	12	0,53	0,50
15	-1	0	-1	8	0,53	0,50

Following separation under the selected conditions, the magnetic (concentrate) and non-magnetic (tailing) fractions were collected and prepared for the complementary Analyses (See chapter III).

II.8.3 Calculation of technological indicators

Each separation product can be characterized by qualitative and quantitative indices. For this reason, several equations were used (P.I. Pilov & O.V. Petrova, 2013).

Material balance equation for separation products

$$Q_F = Q_C + Q_T \qquad \textbf{(3)}$$

- ***Balance equation for yields***

$$\gamma_F = \gamma_C + \gamma_T, \quad \% \qquad \textbf{(4)}$$

- ***Yield of concentrate***

$$\gamma_C = Q_C / Q_F \,.\, 100, \quad \% \qquad \textbf{(5)}$$

- ***Yield of tails***

$$\gamma_T = Q_T / Q_F \,.\, 100, \quad \% \qquad \textbf{(6)}$$

Conclusion

This chapter presents in detail the materials used and experimental methods implemented to study the characterization and enrichment of iron ore of the El-Ouenza mine; samples were carefully collected, prepared, and subjected to a series of methods in order to determine particle size distribution, chemical and mineralogical compositions.

The magnetic separation protocol was defined taking into consideration the ore characteristics and the optimization objective set.

These procedures created a reliable database that will serve as a basis for interpreting the results presented in the following chapter.

Chapter III
Results and Discussion

III.1 Introduction:

In the first part of this chapter, we will present the various results of the characterization carried out on the El-Ouneza iron ore and the analyses of the magnetic products issued from high-intensity magnetic separation (HIMS) included grain-size chemical analysis, scanning electron microscopy coupled with energy-dispersive spectroscopy (SEM-EDS), X-ray fluorescence (XRF), and X-ray diffraction (XRD).

In the second part of this chapter, we will present the results of statistical analyses using Minita-19 software to study the effects of magnetic separation parameters on the recovery of El-Ouneza iron ore, as well as an optimization of these parameters.

III.2 Results of Iron ore characterization

III.2.1 Grain-size Analysis:

Grain-size (particle size) analysis is a method used to determine the particle size distribution in a material such as ores. It is a crucial step in several scientific and industrial fields, particularly in mineral processing.

The Grain-size study was performed using a series of standard sieves following NE-NF 933-2 specifications. A total of 3070 g of iron ore was processed, from which 3063.05 g remained post-sieving, indicating minimal loss and reliable handling. The results of the grain-size analysis are reported in table III.1.

Table III.1: Grain-size analysis of El-Ouneza iron ore

Fraction, mm	Wight, (g)	Cumulative weight (%)	Retained (%)	Passing through sieve (%)
> 1	31.6	1.03	1.03	98.97
-1 + 0,5	168.7	5.49	6.52	93.48
-0.5 + 0.250	255.2	8.33	14.85	85.15
-0.250 + 0.125	1237.2	40.39	55.24	44.76
-0.125 + 0.063	1162.2	37.94	93.18	6.82
-0.063	208.15	6.80	99.98	0.02
Total	3063.05	99.98	--	--

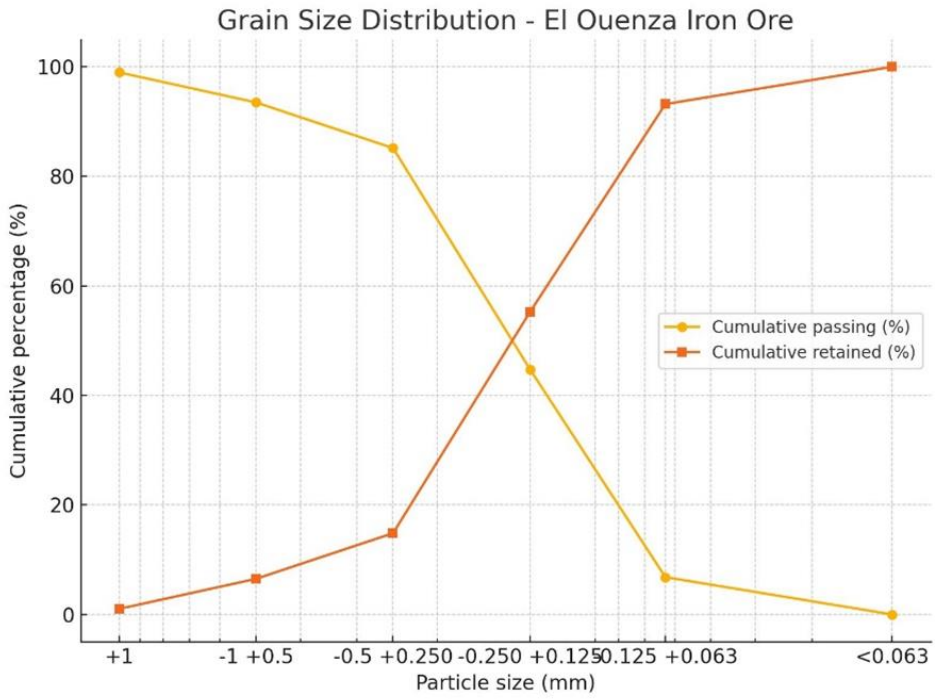


Figure III.1: Grain-size curve of the iron ore from El-Ouneza mine

According to the grain-size distribution curve, it can be seen that all particles measuring +1 mm passed through the sieve, indicating that the El-Ouneza iron ore contains very few coarse particles.

Regarding the fineness of the ore, the cumulative past curve drops and changes direction from +0.250 mm, indicating that the iron ore is composed mainly of fine particles <0.250 mm.

From the cumulative past curve, the D10, D50, and D80 can be determined, including:

- D10: dimensions in which 10% of the ore passes, indicating the fine fraction (D10 = 0.08 mm);

- D50: dimensions in which 50% of the ore passes, indicating the medium fraction (D50 = 0.25 mm);

- D80: dimensions in which 80% of the ore passes, indicating the coarse fraction (D = 0.35 mm).

III.2.2 Gain-size chemical Analysis:

Grain-size chemical analysis is a method that combines conventional grain-size analysis with chemical analysis of different fractions to determine the distribution of chemical elements and/or minerals based on grain-size. It also identifies the fractions richest or poorest in useful minerals, thus optimizing recovery processes by selecting the most suitable fractions.

Table III.1: Results of Gain-size chemical analysis of low-grade iron ore from El-Ouenza mine (%)

Fraction, mm	Wight, g	**SiO_2**	Al_2O_3	**Fe_2O_3**	**CaO**	MgO	SO_3	K_2O	**MnO**	LOI
> 1	31,6	**17,30**	1,40	**41,09**	**16,75**	1,63	0,07	0,05	**1,13**	19,49
-1 + 0,5	168,7	**16,47**	1,58	**43,82**	**17,04**	1,75	0,08	0,08	**1,22**	19,82
-0.5 + 0.250	255,2	**16,63**	2,01	**40,89**	**18,34**	2,17	0,20	0,09	**1,30**	20,21
-0.250 + 0.125	1237,2	**21,13**	2,74	**41,56**	**14,67**	1,79	0,22	0,15	**1,29**	17,57
-0.125 + 0.063	1162,2	**24,91**	3,11	**43,28**	**11,69**	1,69	0,20	0,18	**1,26**	15,39
-0.063	208,15	**26,89**	4,15	**42,18**	**11,34**	1,58	0,20	0,21	**1,24**	13,93
Average	--	**21,69**	2,83	**42,47**	**15,29**	1,70	0,16	0,15	**1,35**	17,40

The results of gain-size chemical analysis of low-grade iron ore from El-Ouenza mine are represented in table III.1. According to the results its can be conclude that the Fe_2O_3 is the dominant oxide in all fractions of the iron ore samples (with an average of 42, 47% of Fe_2O_3). The presence of CaO with a relatively high content (15, 29%) is beneficial, because the CaO is used as a fluxing agent in the blast furnace (S. BENSAADA, 2010).

The presence of LOI with high proportion indicates the existing of:

- Hydrated minerals such as clays, goethite and gibbsite, etc.
- Carbonates such as calcite ($CaCO_3$) and dolomite
- Organic matter.

III.2.3 Mineralogical analysis (XRD)

The mineralogical analysis was conducted on the selected sample iron ore and on the magnetic products issued from the high intensity magnetic separation using X-ray diffraction (XRD) method at. The XRD patterns were identified with the HighScore-Plus software. The obtained results of XRD are represented in figure III.2 and III.4.

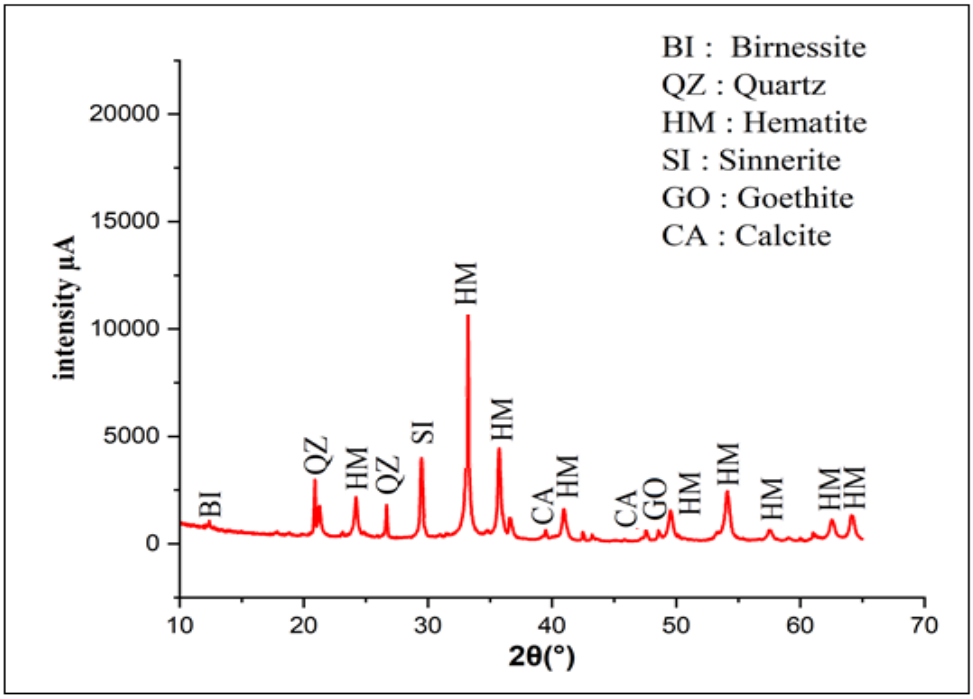


Figure III.2: The XRD pattern of the El-Ouneza iron ore

The XRD analysis confirmed the dominance of hematite in d'El-Ouneza iron ore, with the presence of quartz, sinnerite (with formula: Cu6As4S9), birnnesite calcite quartz and goethite (FeO(OH)). These findings are consistent with the SEM results, reinforcing the presence of iron-rich and silicate/carbonate-bearing phases. The identification of quartz and calcite supports the observation of high SiO_2 and CaO contents respectively.

Birnessite (with wake peak): This mineral (nominally $MnO_2 \cdot nH_2O$), also known as δ-MnO_2, is a hydrous manganese dioxide mineral with a chemical formula of $Na_{0.7}Ca_{0.3}Mn_7O_{14} \cdot 2.8H_2O$ (Jones, L. H. P.; et al., 1956). These mineralogical analyses are in agreement with the chemical analyses.

III.2.4 SEM-EDS Microanalysis:

SEM imaging and associated EDS microanalysis provided detailed insight into the ore's microstructure and chemical distribution. The analyzed zone was representative of the whole sample, analyzed at 25 kV acceleration and 1202x magnification.

The results of the scanning electron microscope (SEM) analysis of the low-grade iron ore sample are illustrated in Figure III.2 and Table III.3 Different phases are distinguished based on their density differences, such that high-density phases appear brighter. Some minerals appear dark, while others are white or gray in color. The mineral crystals vary in size, shape, and orientation angles. Based on the mineralogical composition of the sample and the corresponding densities, it

can be said that the iron-bearing minerals (hematite and goethite) are observed in the SEM images with greater brightness. The presence of quartz, appearing dark gray to black, is also noted as a dominant compound associated with iron oxides, as well as calcite, which appears also in gray color.

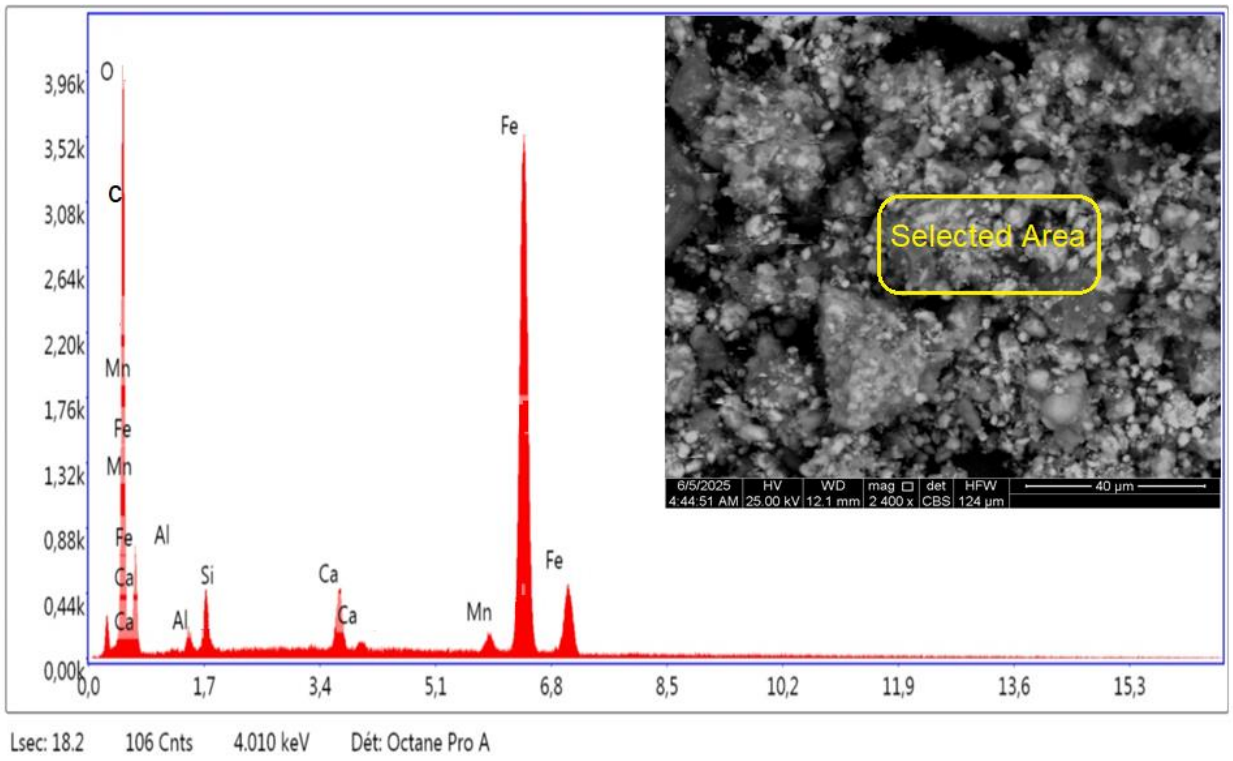


Figure III. 3: SEM-EDS analysis of El-Ouenza iron ore.

TableIII.3: Elemental analysis of iron ore according to EDS pattern

Element	Wt. (%)	Intensity
C	12.95	95.03
O	59.45	1349.75
Al	2.13	103.51
Si	3.09	233.41
Ca	1.37	252.74
Mn	0.69	110.55
Fe	**20.32**	2783.53

According to the EDS pattern of the low iron ore sample taken from the El-Ouenza mine, a main peak is observed, mainly composed of iron oxides (hematite and/or goethite), unlike the other elements in the sample, which show weaker peaks, such as Ca and Si, which could indicate the

presence of calcite and quartz respectively. These finding results are in good agreement with the chemical analysis of iron ore cited previously.

III.2.5 Technological indices results

The result of technological indices are represented in table III.5

Table III.5: Technological indices of magnetic separation tests

Test N°	Material balance (g) $Q_F = Q_{c+} Q_t$ **(30g)**		Yields (%)	
	Q_c	Q_t	γ_c	γ_t
1	24,75	5,25	82,50	17,50
2	23.70	6,30	76,70	23,30
3	24.81	5,19	82,73	17,27
4	24.65	5,35	82,17	17,83
5	25.32	4,68	84,40	15,60
6	24.87	5,13	82,90	17,10
7	24.84	5,16	82,83	17,17
8	23.79	6,21	79,30	20,70
9	26.28	3,72	87,62	12,38
10	27.14	2,86	90,47	9,53
11	23,95	6,05	79,83	20,17
12	25,26	4,74	84,20	15,80
13	24,22	5,78	80,73	19,27
14	23,38	6,62	77,93	22,07
15	23,03	6,97	76,75	23,25

III.3 Results of the statically approach

III.3.1 Experimental design for the magnetic separation tests

The results from factorial designed experiments are given in Table III.3. The second order response function (Equation 2) representing grade and yield (using equation 6) of magnetic product (concentrate) could be expressed as functions of grain-size iron ore, dimension of ball matrix and field intensity. The regressions equations for the grade and yield are given in equation (8) and (9) respectively.

- **For the grade :**

Fe_2O_3 Grade (%) = 41,50 + 1,831 DB (mm) + 5,15 GS (mm) + 7,42 I (T)
- 0,936 DB (mm)*GS (mm) - 0,625 DB (mm)*I (T)
+ 2,100 GS (mm)*I (T) **(8)**

- **For the Yield :**

$$\textbf{Fe}_2\textbf{O}_3\textbf{ Yield (\%)} = 86{,}54 - 0{,}539\ DB\ (mm) - 1{,}35\ GS\ (mm) - 14{,}72\ I\ (T) - 0{,}788\ DB\ (mm)*GS\ (mm) + 1{,}577\ DB\ (mm)*I\ (T) + 6{,}79\ GS\ (mm)*I\ (T) \quad \textbf{(9)}$$

Table III.4: Results of factorial designed of experiments (DOE)

Test N.	Coded variables			Results (Responses)	
	DB (mm)	GS (mm)	I (T)	Grade (%)	Yield (%)
1	10	0,53	1,25	61,23	82,50
2	10	1,00	0,50	57,36	76,70
3	10	0,53	1,25	60,12	82,73
4	8	1,00	1,25	59,15	82,17
5	12	0,063	1,25	62,78	84,40
6	12	1,00	1,25	59,85	82,90
7	10	0,063	0,50	60,64	82,83
8	10	0,53	1,25	60,34	79,30
9	10	1,00	2,00	62,52	87,62
10	12	0,53	2,00	61,87	**90,47**
11	8	0,53	2,00	61,78	79,83
12	10	0,063	2,00	**62,85**	84,20
13	8	0,063	1,25	58,57	80,73
14	12	0,53	0,50	60,58	77,93
15	8	0,53	0,50	56,74	76,75

According to table III.4; its can be seen that the value of Fe_2O_3 grade is higher (62, 85%) in the test **number: 12** (with DB=10mm, GS=0.063mm and I=2T). The high value of Fe_2O_3 yield (90.47%) is also was attained in the **test number 10.** The magnetic product of the test number 12 was also analyzed with XRD (figure III.4).

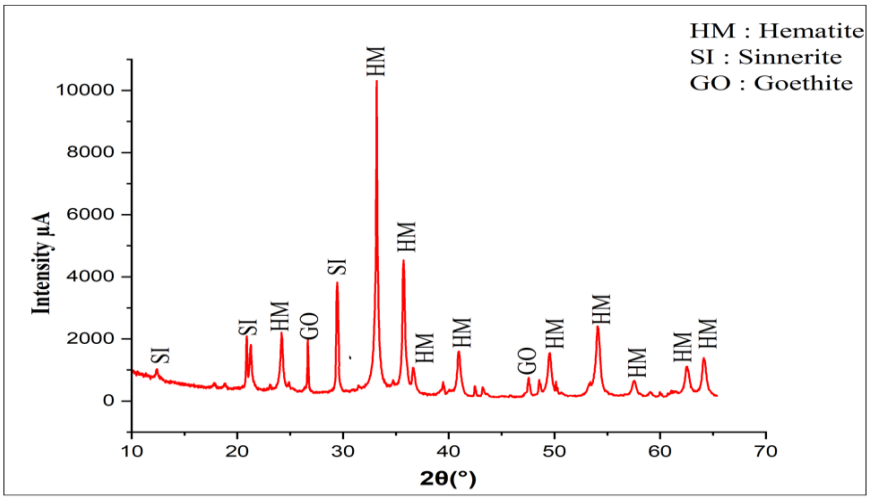


Figure III.4: XRD pattern of the magnetic product (Test 12)

The dominant mineral in this XRD pattern is hematite with minor proportion of goethite and sinnerite. This XRD confirm that the high intensity magnetic separation is an efficiency process to improve the grade of hematite from El-Ouneza iron ore.

III.3.2 ANOVA and Pareto Diagram

ANOVA is an abbreviation for analysis of variance. Developed by British statistician Sir Ronald Aylmer Fisher in the early 20th century, ANOVA combines statistical models, including the F-test (**Fisher's test)**, and P-value. The ANOVA method is used to study the relationship between a quantitative variable and one or two qualitative variables (Anaïs Annereau, 2023).

The ANOVA table is the final result of a series of complex calculation formulas. It presents three types of usable numerical data:

- The degrees of freedom or DF.
- The result, denoted by F.
- The significance, denoted by p.

The p-value is obtained using the DF and F data and is the variance ratio that confirms or refutes the hypothesis being tested. If the p-value is less than $\alpha=0.05$ (significance threshold which is the same in our case), that is to say that the qualitative variables (variable factors) have a significant effect on the quantitative variable (responses), (Anaïs Annereau, 2023).

Typically, a Pareto chart shows the absolute values of the normalized (standardized) effects, ranked from highest to lowest. The chart also plots a reference line to indicate which effects are statistically significant. The reference line indicating statistical significance depends on the significance level (denoted by α or alpha) (Minitab-19). One-way ANOVA was applied to estimate the significance of the model ($p < 0.05$) (Nayak and Pal 2011, Ahmad et al. 2019b, Patel et al. 2017).

- **For the grade :**

The ANOVA results Fe_2O_3 grade is illustrated in Table III.5.

Table III.5: Table of grade ANOVA

Source	DF	F-Value	P-Value	Effect
Model	6	24,87	**0,000**	Very significant
Linear	3	40,21	**0,000**	All significant
DB (mm)	1	25,80	**0,001**	Highly significant
GS (mm)	1	14,26	**0,005**	Significant
I (T)	1	**80,58**	**0,000**	**Extremely significant**
2-Way Interaction	3	9,39	0,005	Significant
DB (mm)*GS (mm)	1	9,89	**0,014**	Significant
DB (mm)*I (T)	1	11,30	**0,010**	Significant
GS (mm)*I (T)	1	7,00	**0,029**	Significant

According to the Table III.5; it can conclude that all main factors and interactions are statistically significant ($p < 0.05$), presenting that they have an effect on the variation of Fe_2O_3 grade.

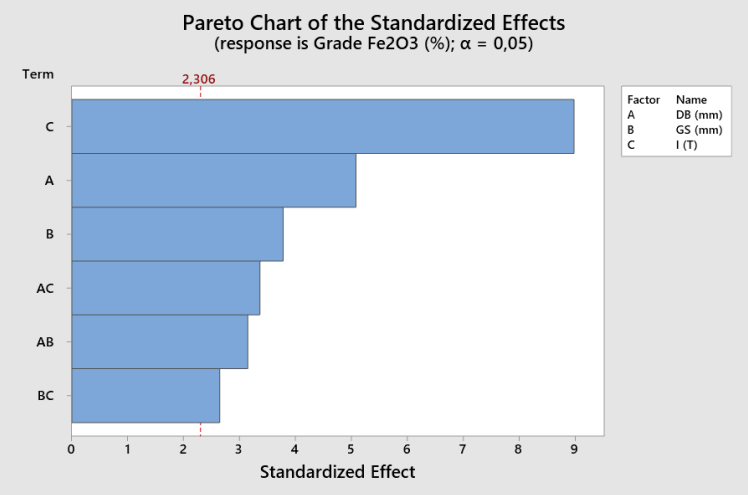


Figure III.5: Pareto diagram of Fe_2O_3 grade

According to Figure III.5, all effects exceed this threshold of the red vertical line (significance threshold α=0.05 which equals 2.306, this indicates that all effects are significant.

The results of ANOVA and Pareto diagram confirm that all factors (DB, GS, I), as well as their interactions, exert a statistically significant effect on the Fe_2O_3 grade. From this diagram; it can be seen also that the most important effect is magnetic field intensity (I), followed by ball matrix dimension (DB) and finally the grain-size (GS). All interactions (DB*I, DB*GS, and GS*I are also significant.

- **For the yield :**

The ANOVA of Fe_2O_3 yield is shown in yield Table III.6.

Table III.6: Table of yield ANOVA

Source	DF	F-Value	P-Value	Effect
Model	6	10,15	**0.002**	Very Significant
Linear	3	15,93	**0,001**	Significant
DB (mm)	1	10,15	**0,013**	Significant
GS (mm)	1	0,32	**0,585**	No Significant
I (T)	1	**37,33**	**0,000**	**Extremely Significant**
2-Way Interaction	3	5,38	0,025	Significant
DB (mm)*GS (mm)	1	0,74	**0,414**	No Significant
DB (mm)*I (T)	1	7,63	**0,025**	Significant
GS (mm)*I (T)	1	7,77	**0,024**	Significant

According to Table III.6; it can be concluded that all main factors and interactions are statistically significant ($p < 0.05$), presenting that they have an effect on the variation of Fe_2O_3 yield. The overall model is generally significant ($p = 0.002$), this is explained by the variations in yields. The high value ($F= 37.33$) for intensity (I) indicates that there is a dominant influence on the yield of Fe_2O_3.

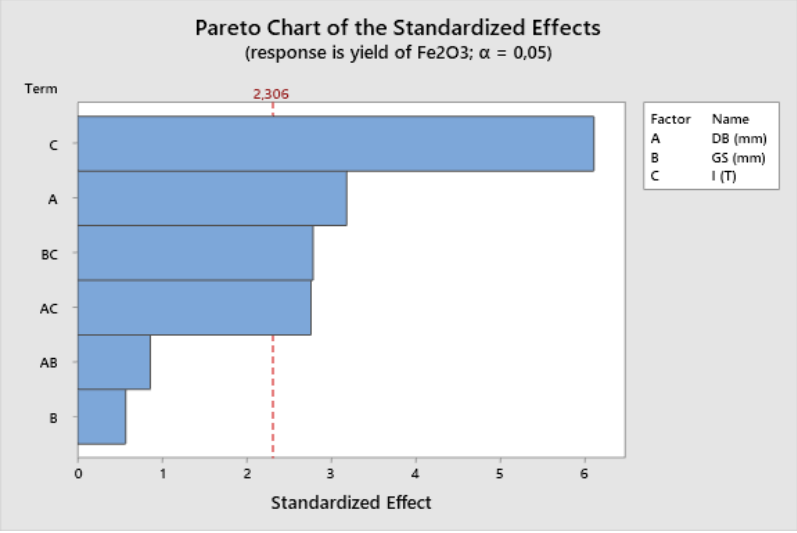


Figure III.6: Pareto diagram of Fe_2O_3 yield

The Pereto diagram (Figure III.6) presents the standardized effects of the factors and their interactions. It shows that the intensity (I) has a very strong effect on the yield of Fe_2O_3 followed by DB and we notice that GS has a weak effect. For the interactions between the factors; we

notice that there is a significant interaction between GS*I and DB*I, while for DB*GS, we notice a weak significance.

III.3.3 Observed and predicted responses of Fe_2O_3 in magnetic products (concentrates)

The observed and the predicted results obtained using the equation 8 and 9 are listed in Table III.7.

Table III.7: Observed and predicted values of grade, recovery and yield.

Test N.	Grade (%)		Yield (%)	
	Observed	Predicted	Observed	Predicted
1	61,23	60,43	82,50	80,06
2	57,36	57,24	76,70	75,84
3	60,12	60,43	82,73	80,06
4	59,15	59,46	82,17	80,43
5	62,78	63,15	84,40	85,18
6	59,85	59,92	82,90	83,00
7	60,64	60,20	82,83	81,31
8	60,34	60,43	79,30	80,06
9	62,52	62,14	87,62	87,60
10	61,87	62,31	90,47	**89,95**
11	61,78	61,97	79,83	81,16
12	62,85	62,15	84,20	83,52
13	58,57	59,19	80,73	79,65
14	60,58	60,77	77,93	78,25
15	56,74	56,68	76,75	78,91

- ***For the grade:***

The linear regression graph scatter plot (figure III.5) presents the relationship between the observed and predicted values of Fe_2O_3 grades in magnetic products.

The regression line shows the ideal prediction, where the observed values match the predicted values perfectly with a coefficient of determination R^2 is 94, 9%. This value indicate that the model used to predict the grade of Fe_2O_3 grades in magnetic products is correct, signifying that the model explains most of the variability in the observed data. This also means that a 1% increase in observed Fe_2O_3 results in a 0.95% increase in predicted grade. The value of the standard deviation of the residuals is low (S=0.424), this confirms the precision.

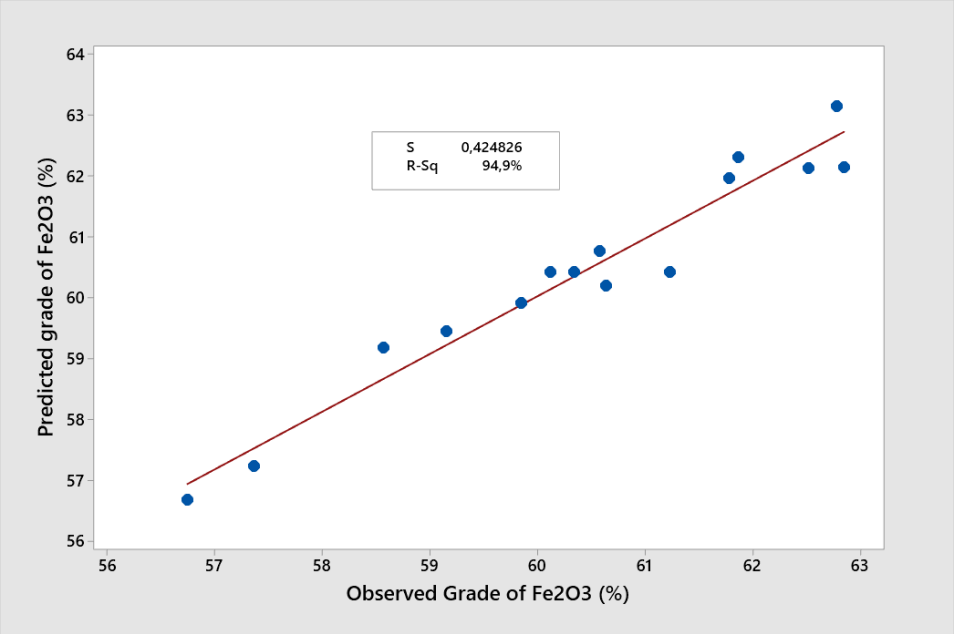


Figure III.5: Relation between observed and predicted values of Fe_2O_3 grade

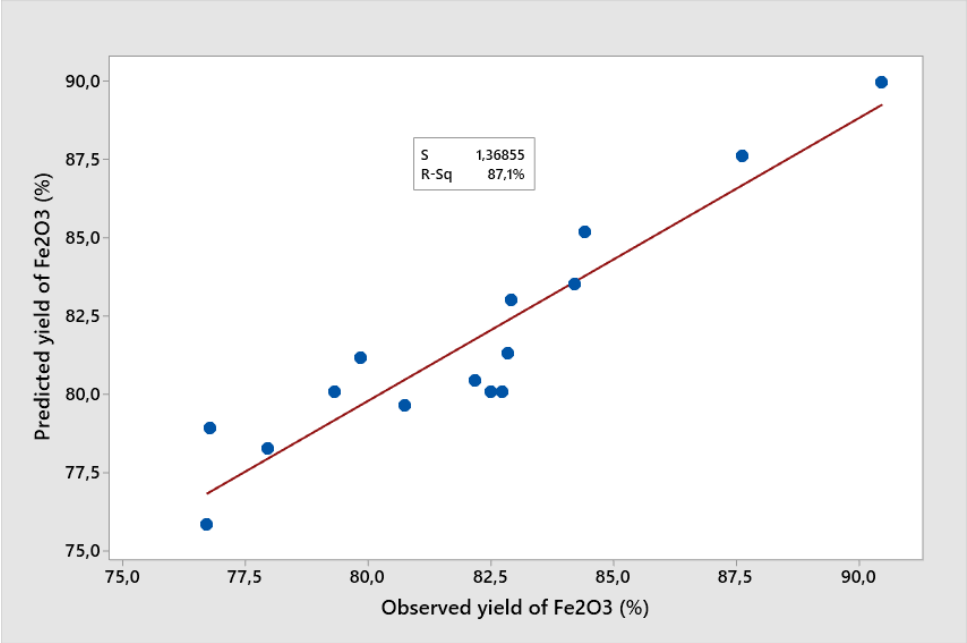


Figure III.6: Relation between observed and predicted values of Fe_2O_3 yield

- ***For the* yield*:***

In Figure III.6, its can be seen that the coefficient of determination R^2 = 87.1%; this means that 87.1% of the variance in the predicted yield is explained by the observed yield. This is a very good fit (often, R^2 >80% is considered excellent in experimental systems).

Regarding the standard error of estimation or the standard deviation of the residuals (S) is approximately 1.37. This shows that the average dispersion of the points around the regression line is approximately ±1.37%, which indicates good predictive accuracy. (A lower value of S indicates a more accurate and reliable model. (A lower value of S indicates a more accurate model).

These results indicate that the regression model can be used reliably to estimate Fe_2O_3 yields from experimental values in the optimization domain of recovery processes.

The observed and predicted data point's relation (Figure III.5 and III.6) demonstrating a very good agreement (R^2 of 94.9 and 87, 1) for grade and yield respectively of the response equations. The high value of R^2 indicates that the quadratic equation is capable of representing the system under the given experimental domain. (Sunita Routray, R. Bhima Rao, 2013).

III.3.4 Effect of process variables on grade of the concentrate (Magnetic Product)

The three-dimensional (3D) response surface plots are very useful in learning about the main effects and interaction effects of the independent variables (factors) and the two-dimensional contour plots give a visual representation of values of the response (Nayak et al. 2014).

In this study, the 3D response surface plot represents the effect of different variables (DB, GS, and I) of HIMS on the Fe_2O_3 grade of the magnetic product and they are represented in Figure III.7.

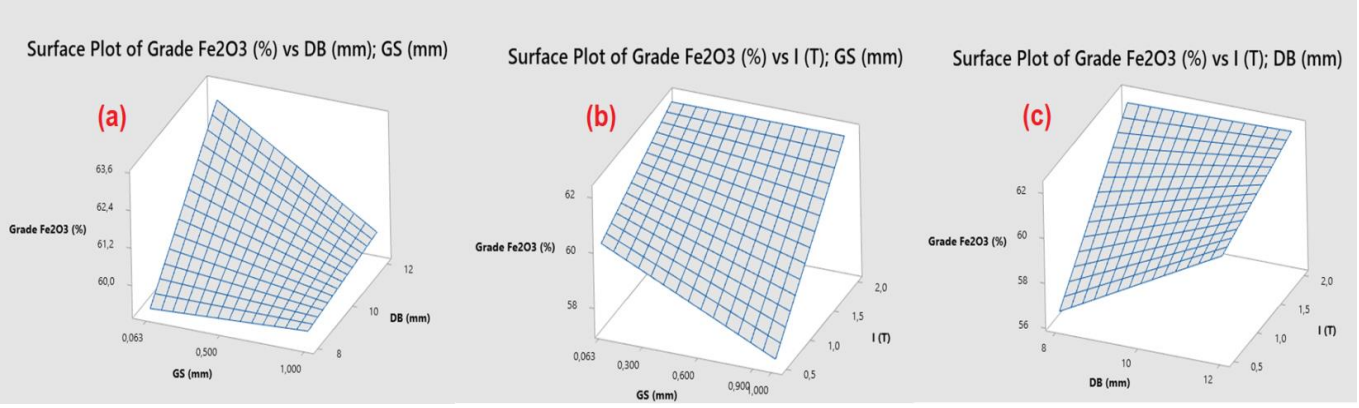


Figure III.7: 3D plots showing the effect of parameters on the Fe_2O_3 grade: a) GS and DB, b) GS and I, c) DB and I

Figure III.7 (a) represents the effect (influence) of GS and DB on the grade on Fe_2O_3. It can be seen that an increase of DB from 8 to 12 mm gives a significant increasing in Fe_2O_3 grade (from ~60% to ~63.6%). A decreasing in particle size (GS from 1.0 to 0.063 mm) leads to a moderate increasing in grade (1.5-2%), this may be due to an increased liberation of hematite particles (A. M. Gaudin, 1939) in addition to an increased specific surface area promoting physical and/or chemical separation (Fuerstenau, 2003).

At constant GS, the larger balls, the higher the Fe_2O_3 content (quality of the concentrate increases). Conversely; when the GS increases; the Fe_2O_3 content decreases slightly. This means that the small particles and large balls of matrix promote better separation of hematite.
In Figure III.7 (b); the 3D surface plot shows how the grade of Fe_2O_3 can be varies with the changes in GS and I. The 3D graph present peaks and troughs, this means that the proportion of Fe_2O_3 strongly depends on GS and DB. The Fe_2O_3 grade increases with increasing I (magnetic field), while an increase in GS decreases the Fe_2O_3 content. This means that finer grains are better separated in a high magnetic field. The best grade can be obtained for GS between 0.063 and 1.0 mm, however, beyond 1mm, the Fe_2O_3 grade could be significantly decreased (to be confirmed).

According to Figure III.7 (c) it can be noted from the nature of the plot that the higher level of the intensity (I) is in good condition to obtain a higher grade of Fe_2O_3. (Expected phenomenon in magnetic separation, where more intense fields attract paramagnetic particles better). A high (I) and (DB) improve the Fe_2O_3 grade in magnetic product. Both variables have a positive and simultaneous effect.

III.3.5 Effect of process variables on yield of concentrate

For the understanding of the results, the predicted model was described in 3D response surface plots (figure III.8), which show the effect of HIMS process variables on the Fe_2O_3 yield.

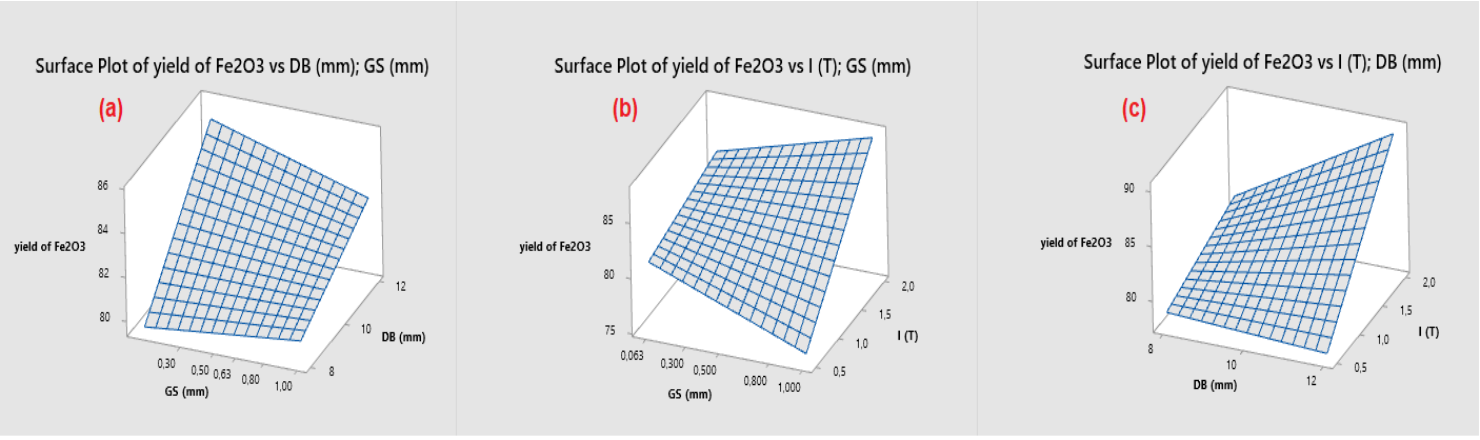


Figure III.8: 3D plots showing the effect of parameters on the Fe_2O_3 yield: a) GS and DB, b) GS and I, c) DB and I

In Figure III.8 (a), the 3D plot present the effect of parameters (GS and DB) on the Fe_2O_3 yield, the plot shows that as the dimensions of matrix balls (DB) increases, the efficiency increases. While an increase in grain-size (GS) causes the efficiency to decrease slightly. A finer GS promotes passage between the matrix balls and better magnetic separation.

Figure III.8 (b) presents the effects of (I) and (GS) on the yield of Fe_2O_3, it is clear that as the yield increases with the magnetic field intensity (I). However; a weaker (GS) also improves the yield. This means that a strong magnetic field (I) attracts fine particles better. For good yield, an arrangement of a strong (I) and fine (GS) is desirable.

The effect of (I) and (DB) on recovery yield of magnetic product is shown in Figure III.8 (c). With increase in the intensity of magnetic field (I) and dimension of balls matrix, there is an increasing of the yield of product.

III.3.6 Main effects of parameters on Fe_2O_3

The Main effects analyses shown in Figure III.9 illustrate the individual influence of each experimental parameter on Fe_2O_3 grade and yield, independent of interactions.

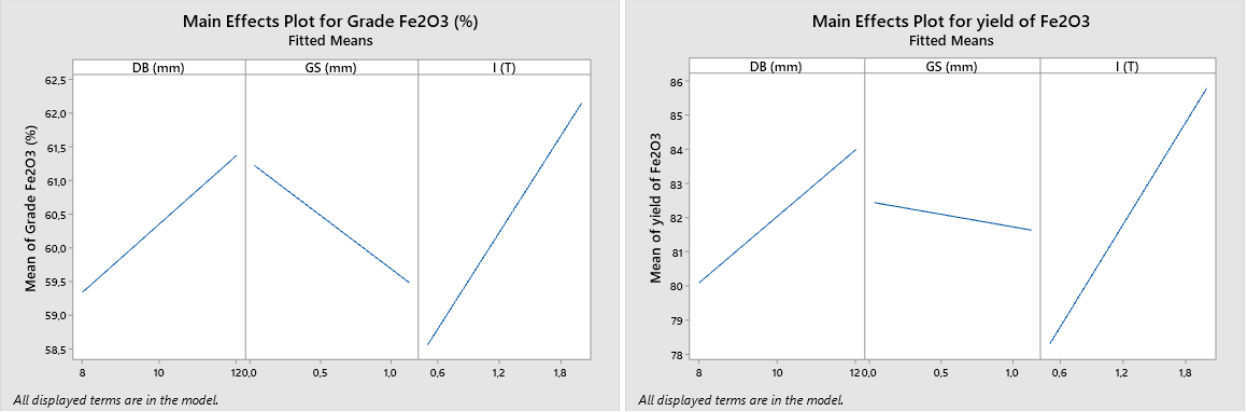


Figure III.9: Main effect plots on the Grade and yield of Fe_2O_3 in the magnetic products

The (DB) exhibits a significant and positive effect on responses (both grade and yield). The increasing in (DB) leads to an improvement in Fe_2O_3 simultaneously of grade and yield.

Concerning grain-size (GS), an opposite tendency was observed; increasing GS results in a slight decrease in grade and a very moderate effect on yield.

Magnetic field intensity (I) is the factor with the important significant effect. Its increase improves significantly both Fe_2O_3 grade and yield. This tendency confirms the effectiveness of the magnetic separation in valorizing iron.

III.3.7 Optimization of magnetic separation variables on responses

In mineral processing, both grade and yield are the widely used parameters for evaluating the performance of any valorization operation. The model equations were optimized for HIMS factors using Minitab-19 software to maximize the grade of the product.

- **For the grade**

The Maximum Fe_2O_3 grade (63.18%) of product can be attained by optimizing the variables factors at:

- **Dimension of ball matrix (DB) = 12mm,**
- **Grain-Size (GS) = 0.063mm**
- **Intensity (I) = 2 T**

- **For the yield**

The Maximum Fe_2O_3 yield (91.25%) of product can be attained by optimizing the variables factors at:

- **Dimension of ball matrix (DB)=12mm,**
- **Grain-Size (GS) = 1mm**
- **Intensity (I) = 2 T**

- **For the both grade and yield**

The Maximum Fe_2O_3 grade and yield (63.18% and 91.25% respectively) of product can be achieved by optimizing the variables factors at:

- **Dimension of ball matrix (DB)=12mm,**
- **Grain-Size (GS) = 0.24mm**
- **Intensity (I) = 2 T**

Conclusion

In this part, a characterization iron ore from the El-Ouneza mine and an evaluation of the performances of the high-intensity magnetic separation process were carried out.

The Gain-size analysis revealed a fine particle distribution, with 80% being less than 0.25mm, representing good liberation of the useful mineral. Grain-size chemical analyses revealed a predominance of F_2O_3, averaging 42.47%, with a high CaO content. The loss on ignition is significant, indicating the presence of organic matter and carbonates, as well as hydrated minerals.

According to SEM-EDS and XRD analyses, hematite is predominant in the ore, accompanied by goethite, quartz, calcite, etc. The statistical study conducted using Minitab-19 software and Box-Behnken design allowed us to study the influence of each parameter applied in the separation (intensity, particle size, and matrix bead size) on the efficiency of iron ore beneficiation operations.

The statistical results obtained showed a very good correlation between the observed (experimental) and predicted values. The magnetic field intensity was found to be the important and significant factor in all tests, followed by Dimension of balls matrix, while the grain-size had a moderate influence.

Response surface Methodology (RSM) and Pareto curves presented the optimal conditions to maximize both iron grade and yield. The maximum grade and yield (63.18% and 91.18% respectively) were achieved at DB of 12mm, grain-size of 0.24mm and an intensity of 2T.

General Conclusion

This thesis present the characterization and valorization of iron ore from the Chagoura site, El-Ouenza mine, located in east of Algeria.

Through a series of chemical and mineralogical (XRF, DRX, SEM-EDS), it can be conclude that the ore is mainly composed of hematite and goethite, with the presence of quartz and calcite as gangue. Grain-size analysis revealed that the majority of the fractions constituting the iron ore are fine dimensions, which indicate the liberation of the useful mineral (hematite) from its gangue.

Grain-size chemical analyses revealed a predominance of F_2O_3 in all fractions, averaging 42.47%, with a high CaO content. The loss on ignition (LOI) is significant, indicating the presence of organic matter and carbonates, as well as hydrated minerals.

The statistical approach conducted using Minitab-19 software and Box-Behnken design allowed us to study the influence of each parameter applied in the magnetic separation (intensity, particle size, and matrix bead size) on the efficiency of iron ore beneficiation operations.

The magnetic field intensity (I) was found to be the important and significant factor in all tests, followed by dimension of balls matrix, while the grain-size had a moderate influence. The obtained regression model has high reliability in predicting the F_2O_3 content from the observed values, and it can be used for analyses and/or simulations in the beneficiation of El-Ouneza iron ore.

Response surface Methodology (RSM) and Pareto curves presented the optimal conditions to maximize both iron grade and yield. The maximum grade and yield (63.18% and 91.18% respectively) were achieved at DB of 12mm, grain-size of 0.24mm and an intensity of 2T.

Overall; this study determines the effectiveness of the HIMS method for upgrading iron ore form El-Ouneza mine and confirm that an optimization of process parameters can improve significantly the quality of concentrate using HIMS.

References:

A. M. Gaudin, 1939, Principles of Mineral Dressing (book)

Ahmad, N., et al., 2019b. Preparation of a novel curcumin nanoemulsion by ultrasonication and its comparative effects in wound healing and the treatment of inflammation. RSC advances, 9 (35), 20192–20206.

Anaïs Annereau, 2023, https://blog.hubspot.fr/marketing/anova-test

Annaba University. (2019). PV CSF – Valorisation des déchets miniers de l'Ouenza. Faculté des Sciences. (https://facsct.univ-annaba.dz/wp-content/uploads/2020/06/le-PV-CSF-du-17042019-.pdf)

Aslan, N. (2007a): Application of response surface methodology and central composite rotatable design for modeling the influence of some operating variables of a Multi-Gravity Separator for coal cleaning. – Fuel, **86**: 769-776. *(https://www.sciencedirect.com/science/article/pii/S0016236106004406)*

Aslan, N. (2007b): Modeling and optimization of Multi- Gravity Separator to produce celestite concentrate. – Powder Technology, **174**: 127-133. (https://www.sciencedirect.com/science/article/pii/S0032591007000046)

Aslan, N. (2008): Application of response surface methodology and central composite rotatable design for modeling and optimization of a multi-gravity separator for chromite concentration. – Powder Technology **185**: 80-86. (https://www.sciencedirect.com/science/article/pii/S0032591007005098)

Ayari, J. Et al.(2023). Alkaline Tailings Management in Semi-Arid Regions. Environmental Science and Pollution Research.

(https://www.sciencedirect.com/science/article/pii/S0375674223000274)

Baala, D. (2021). Caractérisation des stériles de la mine de l'Ouenza [Doctoral Thesis]. Université Badji Mokhtar Annaba.(https://biblio.univ-annaba.dz/wp-content/uploads/2021/06/These-Baala-Dirar.pdf)

Bolonin, A. V. (2019). Oxygen and carbon isotope composition in primary carbonatites of the world: data summary and linear trends. *Open Journal of Geology*, *9*(08), 424. (https://www.scirp.org/html/3-1211237_94561.htm)

Boukhanouf, R. (2021). Algeria's Iron Ore Resources: Challenges and Opportunities.

Bouzenoune, A. & Lécolle, P. (1997). Aptian Host Rocks and Siderite Oxidation Processes at El-Ouenza. Economic Geology. (https://doi.org/10.2113/gsecongeo.92.4.511)

Chokin, K., Yedilbayev, A., Yugai, V., & Medvedev, A. (2022). Beneficiation of magnetically separated iron-containing ore waste. Processes, 10(11), 2212.

Chun, T., Zhu, D., & Pan, J. (2015). Simultaneously Roasting and Magnetic Separation to Treat Low Grade Siderite and Hematite Ores. Mineral Processing and Extractive Metallurgy Review, *36*(4), 223–226. https://doi.org/10.1080/08827508.2014.928620

Clout, J. M. F., & Manuel, J. R. (2015). Iron Ore Mineralogy and Processing. Elsevier.

Clout, J. M. F., & Manuel, J. R. (2022). Mineralogical, chemical, and physical metallurgical characteristics of iron ore. In *Iron Ore* (pp. 59-108). Woodhead Publishing.

Cullity, B. D., & Graham, C. D. (2008). Introduction to Magnetic Materials. Wiley.

Douamis Report. (2014). Caractérisation et choix d'un schéma de traitement du minerai de Douamis (Ouenza). Université d'Annaba. (https://biblio.univ-annaba.dz/wp-content/uploads/2014/05/caracterisation-et-choix-dun-schema-de-traitement-du-minerai-de-Douamis.pdf)

DSpace-Univ-Annaba. (n.d.).Geochemical and environmental analysis of El-Ouenza iron ores. (https://dspace.univ-annaba.dz/items/b3228f8c-06e2-4fd2-a2a4-37b0306ec2c1)

Enrichissement Report. (2020). Mémoire de Master: Enrichissement et agglomération du minerai de fer pauvre de l'Ouenza. Université de Tébessa. (https://theses-algerie.com/1476055008091639/memoire-de-master/universite-larbi-tebessi---tebessa/enrichissement-et-agglom%C3%A9ration-du-minerai-de-fer-pauvre-de-l-ouenza)

Evtekhov, V. D., Khoudour, D., & Meddahi, R. (2016). Mineralogy of Iron Ores of Ouenza Deposit. REM: International Engineering Journal. (https://doi.org/10.1590/0370-44672016700051)

Faculté des Sciences, Univ-Annaba. (2019). Rapport du Comité Scientifique sur les impacts environnementaux de la mine d'El-Ouenza. (https://facsct.univ-annaba.dz/wp-content/uploads/2020/06/le-PV-CSF-du-17042019-.pdf)

Frausto da Silva, J. J. R., & Williams, R. J. P. (2001). The Biological Chemistry of the Elements. Oxford University Press.

Frietsch, R. (1978). On the magmatic origin of iron ores of the Kiruna type. *Economic geology*, *73*(4), 478-485.

Fuerstenau, M. C., & Han, K. N., 2003, Principles of mineral processing. *Society for Mining, Metallurgy & Exploration (SME).*

Gatsé Ebotehouna, C., Xie, Y., Adomako-Ansah, K., & Pei, L. (2019). Fluid inclusion and oxygen isotope characteristics of vein quartz associated with the nabeba iron deposit, Republic of Congo: Implications for the enrichment of hypogene ores. *Minerals*, *9*(11), 677.

Gitau, F., Alabi, O.O., Aramide, F.O. *et al.* Towards a Sustainable and Enhanced Iron Ore Recovery: Bio-beneficiation Review. *Mining, Metallurgy & Exploration* **41**, 1069–1078 (2024). https://doi.org/10.1007/s42461-024-00950-2

Gunaraj, V. & MuruGan, N. (1999): Application of response surface methodologies for redicting weld base quality in submerged arc welding of pipes. – Journal of Materials Processing Technology, **88**: 266-275.
Gupta, A., & Yan, D. (2016). Mineral Processing Design and Operations. Elsevier.

Hassanzadeh, F., Atapour, H., & Ranjbar, H. (2023). The Ediacaran metamorphosed banded iron formation (BIF) at Gohar Zamin mine (Gol-e-Gohar# 3 anomaly), Sirjan (southeastern Iran): Perspective from ore structures, bulk ore-rock geochemistry and OS-Pb isotopic signatures. *Precambrian Research*, *394*, 107124.

Idres, Y. Et al. (2017). Valorization Pathways for Hematite-Poor Ores in Algerian Mining Districts. Minerals Engineering. (https://doi.org/10.1016/j.mineng.2017.02.008)

Integrated Hydrogeological Modeling of Mine Impacts on Transboundary Aquifers. Water Resources Research. (https://doi.org/10.1029/2023WR035876)

International Iron Ore Study Group, 2024.

Jan Drzymala (2007) Mineral Processing, Foundations of theory and practice of minerallurgy 1st edition, Wroclaw University of Technology, 245.
(https://www.dbc.wroc.pl/Content/2070/Drzymala_mineral.pdf)

Jones, L. H. P.; et al. (1956). "Birnessite, a new manganese oxide mineral from Aberdeenshire, Scotland". *Mineralogical Magazine and Journal of the Mineralogical Society*. **31** (235): 283–288. Bibcode:1956MinM...31..283J. https://doi.org/10.1180/minmag.1956.031.235.01
Jones, R., & Kumar, S. (2022). Advances in Steel Manufacturing Using Iron Ore. Steel Technology Journal, 39(2), 177-195.
(https://link.springer.com/article/10.3103/s0967091215090077)

K. Soundaranayaki, 2022, Introduction to Design of Experiments (DOE). Centre for Research , Anna university ,Chennai -25
(https://www.indianjournals.com/ijor.aspx?target=ijor:wei&volume=64r&issue=12&article=004)

KwaK, J.S. (2005): Application of Taguchi and response surface methodologies for geometric error in surface grinding process. – International Journal of Machine Tools and Manufacture, **45**: 327-334.
(https://www.sciencedirect.com/science/article/pii/S0890695504001907)

Laraba, M., Abdelmalek, R., Menendez-Aguado, J.M. *et al.* Wet High Intensity Magnetic Separation (WHIMS) of Algerian Kaolin: a Potential Application. *Mining, Metallurgy & Exploration* **39**, 1693–1703 (2022). (https://doi.org/10.1007/s42461-022-00617-w)

Legemza, J., Findorák, R., Fröhlichová, M., & Džupková, M. (2020). Advances in Sintering of Iron Ores and Concentrates. In *Iron Ores*. IntechOpen. (https://books.google.com/books?hl=ar&lr=&id=lVE2EAAAQBAJ&oi=fnd&pg=PA55&dq=Legemza,+J.,+Findor%C3%A1k,+R.,+Fr%C3%B6hlichov%C3%A1,+M.,+%26+D%C5%BEupkov%C3%A1,+M.+(2020).+Advances+in+Sintering+of+Iron+Ores+and+Concentrates.+In+Iron+Ores.+IntechOpen.%E2%80%8F%E2%80%8F&ots=s6P4MPCth5&sig=HtXHk05jnWI3OeNi2Z68EIs2p2I)

Li, G. Et al. (2024). Estimation-of-Distribution Algorithms for Optimizing Mining Truck Dispatching. International Journal of Mining Science and Technology. (https://doi.org/10.1016/j.ijmst.2023.12.004)

Liu, Baoyu, et al. "Development of iron encapsulated hollow beta zeolites for ammonia selective catalytic reduction." *Industrial & Engineering Chemistry Research* 58.8 (2019): 2914-2923. (https://pubs.acs.org/doi/abs/10.1021/acs.iecr.8b04623)

LOUIS, H. *The Iron Ores of Scotland* . *Nature* **105**, 419–420 (1920). (https://doi.org/10.1038/105419a0)

Malvent Panalytical, 2025 (https://www.malvernpanalytical.com/en/products/technology/xray-analysis/x-ray-diffraction)

Mao, X. M., You, Z. X., Zhang, Y. B., Fan, Z. Y., Li, G. H., & Jiang, T. (2014). Calcium ferrite formation characteristic during iron ore sintering with different oxygen atmospheres. *Journal of Central South University*, *21*, 3043-3048. (https://link.springer.com/article/10.1007/s11771-014-2274-z)

Matías Migueland, Salvarredy Aranguren. (2008). Contamination en métaux lourds des eaux de surface et des sédiments du Val de Milluni (Andes Boliviennes) par des déchets miniers. Approches géochimique, minéralogique et hydrochimique, en vue de l'obtention du Doctorat de l'université de TOULOUSE, pp 489. (https://theses.hal.science/tel-00277431/)

Mero, P. Et al. (2018). Stakeholder Engagement Frameworks for Mine Rehabilitation Planning. Resources Policy. (https://doi.org/10.1016/j.resourpol.2018.07.006)

MSILA University. (2020). *Mineralogy of Iron Ores of El-Ouenza Deposit. (https://num.univ-msila.dz/DWE/public/attachements/2020/02/29/mineralogy-of-iron-ores-of-ouenza-deposit-algeria-1pdf-qkz5ggkx1582934742.pdf)

National Mining Agency of Algeria. (2022). Annual Report on Iron Ore Production.

Nayak, A.K. and Pal, D., 2011. Development of pH-sensitive tamarind seed polysaccharide-alginate composite beads for controlled diclofenac sodium delivery using response surface methodology. International journal of biological macromolecules, 49 (4), 784–793.

Olías, M. Et al. (2015). Controls on Heavy Metal Leaching from Mine Wastes. Applied Geochemistry. (https://doi.org/10.1016/j.apgeochem.2015.03.009)

Oshchepkova, Anastasiya & Chubarov, Victor & Bychinsky, Valery & Kaneva, Ekaterina. (2020). Physicochemical Simulation of the Qualitative and Quantitative Phase Composition of Iron Ores. Journal of Siberian Federal University. Chemistry. 65-77. 10.17516/1998-2836-0169.

Ozgen, S. et al. (2009): Modeling and optimization of hydrocyclone processing of low-grade bentonites. – Applied Clay Science **46**: 305- 313.

Parak, T. (1985). Phosphorus in different types of ore, sulfides in the iron deposits, and the type and origin of ores at Kiruna. *Economic Geology*, *80*(3), 646-665. (https://pubs.geoscienceworld.org/segweb/economicgeology/article-abstract/80/3/646/20027)

Patel, G.M., Shelat, P.K., and Lalwani, A.N., 2017. QbD based development of proliposome of lopinavir for improved oral bioavailability. European journal of pharmaceutical sciences: official journal of the European Federation for Pharmaceutical Sciences, 108, 50–61

P.I. Pilov, O.V. Petrova, (2013), Procédés et machines de traitement des minéraux utiles: le manuel/.: Université Nationale des Mines.

Quast, K. (2018). A review on the characterisation and processing of oolitic iron ores. *Minerals Engineering*, *126*, 89-100. (https://www.sciencedirect.com/science/article/pii/S0892687518302887)

Ramos, V. Et al.(2024). Iron Ore Tailings in Construction Materials: Technical and Environmental Performance. Journal of Cleaner Production. (https://doi.org/10.1016/j.jclepro.2024.142102)

Rezaei, M. & Mousavi, S. (2024). Slope Degradation Mechanisms in Freeze-Thaw Climates. Rock Mechanics and Rock Engineering. (https://doi.org/10.1007/s00603-023-03740-4)

S. BENSAADA, 2010, ELABORATION DES METAUX FERREUX (FONTES ET ACIERS), (https://www.univ-biskra.dz/enseignant/bensaada/elaboration%20acier%20fontes_1_.pdf)

Saidi, M., et al. (2022). Beneficiation of High-Phosphorus Iron Ores in North Africa. Minerals Engineering, 178. (https://pubs.acs.org/doi/abs/10.1021/acsengineeringau.3c00046)

S. J. G. Krishna, M. R. Patil, C. Rudrappa, S. P. Kumar & B. P. Ravi. (https://www.researchgate.net/profile/Sharath-Kumar

16/publication/263417041_Characterisation_and_Processing_of_Some_Iron_Ores_of_India/links/5620aac008aed8dd19404dfd/Characterisation-and-Processing-of-Some-Iron-Ores-of-India.pdf?origin=journalDetail&_tp=eyJwYWdlIjoiam91cm5hbERldGFpbCJ9)

Smith, J., Patel, R., & Thomas, B. (2021). Iron Ore Processing Technologies and Innovations. Materials Science Journal, 56(3), 145-167 .(https://www.tandfonline.com/doi/abs/10.1080/08827500802498215)

SOLID STATE PHYSICS, MINERAL PROCESSING https://doi.org/10.33271/nvngu/2025-1/028

Soomro, A. Et al. (2024). Integrated Hydrogeological Modeling of Mine Impacts on Transboundary Aquifers. Water Resources Research. (https://doi.org/10.1029/2023WR035876)

Sun, X., Bao, J., Li, K., Argyle, M. D., Tan, G., Adidharma, H., ... & Ning, P. (2021). Advance in using plasma technology for modification or fabrication of carbon-based materials and their applications in environmental, material, and energy fields. Advanced Functional Materials, 31(7), 2006287.(https://advanced.onlinelibrary.wiley.com/doi/abs/10.1002/adfm.202006287)

Sunita Routray, R. Bhima Rao, 2013, Optimization of Some Parameters of Rougher Spiral Concentrator for Preconcentration of Total Heavy Minerals from Beach Sand, World of Metallurgy – ERZMETALL **66** (2013) No. 1 (https://www.researchgate.net/profile/Sunita-Routray/publication/287304806_Optimization_of_some_parameters_of_rougher_spiral_concentrator_for_preconcentration_of_total_heavy_minerals_from_beach_sand/links/5e3a9c6a92851c7f7f1d4964/Optimization-of-some-parameters-of-rougher-spiral-concentrator-for-preconcentration-of-total-heavy-minerals-from-beach-sand.pdf)

Tébessa University. (2020). Traitement des rejets de fer – cas de la mine d'Ouenza. (http://oldspace.univ-tebessa.dz:8080/xmlui/handle/123456789/3658)

Teutsong, T., Temga, J.P., Enyegue, A.A. *et al.* Petrographic and geochemical characterization of weathered materials developed on BIF from the Mamelles iron ore deposit in the Nyong unit, South-West Cameroon. *Acta Geochim* **40**, 163–175 (2021). (https://doi.org/10.1007/s11631-020-00421-7) (https://link.springer.com/article/10.1007/s11631-020-00421-7)

Thèses Algérie. (2020).Étude d'impact environnemental du gisement ferrifère de l'Ouenza. Université Larbi Tébessi.
(https://theses-algerie.com/1476055008091639/memoire-de-master/universite-larbi-tebessi---tebessa/enrichissement-et-agglom%C3%A9ration-du-minerai-de-fer-pauvre-de-l-ouenza)

Tian, L., Fan, M., Fan, P., & Yang, H. (2024). Research progress on compound force field separation equipment of fine particles. *Separation Science and Technology*, *59*(6–9), 1037–1067. https://doi.org/10.1080/01496395.2024.2362735

Tserenkhand, B., Sanjaasuren, R., & Solongo, P. (2014). Composition of iron ores from Mongolian western region and its applicability for cement production. *Mongolian Journal of Chemistry*, *14*, 75–79.(https://mongoliajol.info/index.php/MJC/article/view/204)

USGS. (2023). Mineral Commodity Summaries: Iron Ore. United States Geological Survey. (https://books.google.com/books?hl=ar&lr=&id=jE3wAAAAMAAJ&oi=fnd&pg=PA291&dq=related:v7iEkXZDfwJ:scholar.google.com/&ots=ZrmWVCLCsl&sig=13gJfmq9XpupO5EymSew2AcZhQI)

Wallace, C., Fatur, S., Braun, T., & Frey, S. (2024, November). Electrochemical Ironmaking for Green Steel: Turning Low-Grade Ore into High-Purity Iron. In Electrochemical Society Meeting Abstracts prime2024 (No. 25, pp. 2013-2013). The Electrochemical Society, Inc. (https://iopscience.iop.org/article/10.1149/MA2024-02252013mtgabs/meta)

Wang, X., Li, B., Xiang, Z. *et al.* Chemical compositions of sulfides in the porphyry Cu ores,Yangla Cu deposit, Yunnan, China: implication for ore genesis. *Acta Geochim* **39**, 947–972 (2020). (https://link.springer.com/article/10.1007/s11631-020-00433-3)

World Steel Association. (2023). Steel Statistical Yearbook 2023. (https://hej.hyperion.ro/articles/HEJ%20nr2(10)_2023.pdf#page=20)

Ysbaa, S., Haddouche, O., Boutaleb, A., Sami, L., & Kolli, O. (2021). Mineralization and fluid inclusion characteristics of Pb-Zn-Fe-Ba (Cu, F, Sr) ore-deposits in northern east of Algeria. *Arabian Journal of Geosciences*, *14*, 1-13.. (https://link.springer.com/article/10.1007/s12517-021-07281-2)

Zerzour, O. Et al. (2021). Geostatistical Modeling of Iron Grade Distribution in Complex Deposits: Case of El-Ouenza. Natural Resources Research. (https://www.researchgate.net/publication/348940562_Geostatistics-Based_Method_for_Irregular_Mineral_Resource_Estimation_in_Ouenza_Iron_Mine_Northeastern_Algeria)

Zhou Tao, Zhao Youcai, Eugene Atta Nyankson 2023, Chapter 6 - Integrated mechanical separation for municipal solid waste, Resource Recovery Technology for Municipal and Rural Solid Waste, Classification, Mechanical Separation, Recycling, and Transfer, Pages 77-83 (https://www.sciencedirect.com/book/9780323989787/resource-recovery-technology-for-municipal-and-rural-solid-waste)

Annexes

FA163900 ISSN 0335-3931

norme européenne
norme française

NF EN 933-1
Mai 2012

Indice de classement : **P 18-622-1**

ICS : 91.100.15

Essais pour déterminer les caractéristiques géométriques des granulats

Partie 1 : Détermination de la granularité — Analyse granulométrique par tamisage

E : Tests for geometrical properties of aggregates — Part 1: Determination of particle size distribution — Sieving method
D : Prüfverfahren für geometrische Eigenschaften von Gesteinskörnungen — Teil 1: Bestimmung der Korngrößenverteilung — Siebverfahren

© AFNOR 2012 — Tous droits réservés

Norme française homologuée

par décision du Directeur Général d'AFNOR le 18 avril 2012 pour prendre effet le 18 mai 2012.

Remplace la norme homologuée NF EN 933-1, de décembre 1997 et son amendement A1, de février 2006.

Correspondance

La Norme européenne EN 933-1:2012 a le statut d'une norme française.

Analyse

Le présent document décrit la méthode de référence servant au tamisage par voie sèche et au lavage utilisée pour les essais de type initiaux et, en cas de désaccord, à la détermination de la granularité des granulats. Pour les besoins du contrôle de la production en usine en particulier, d'autres méthodes peuvent être utilisées sous réserve qu'une corrélation appropriée avec la méthode de référence ait été établie. Il s'applique à tous les granulats, dont les granulats légers, jusqu'à une taille nominale de 90 mm, mais en excluant les fillers.

Descripteurs

Thésaurus International Technique : granulat, essai, caractéristique géométrique, granularité, analyse granulométrique, analyse au tamis, préparation de spécimen d'essai, calcul.

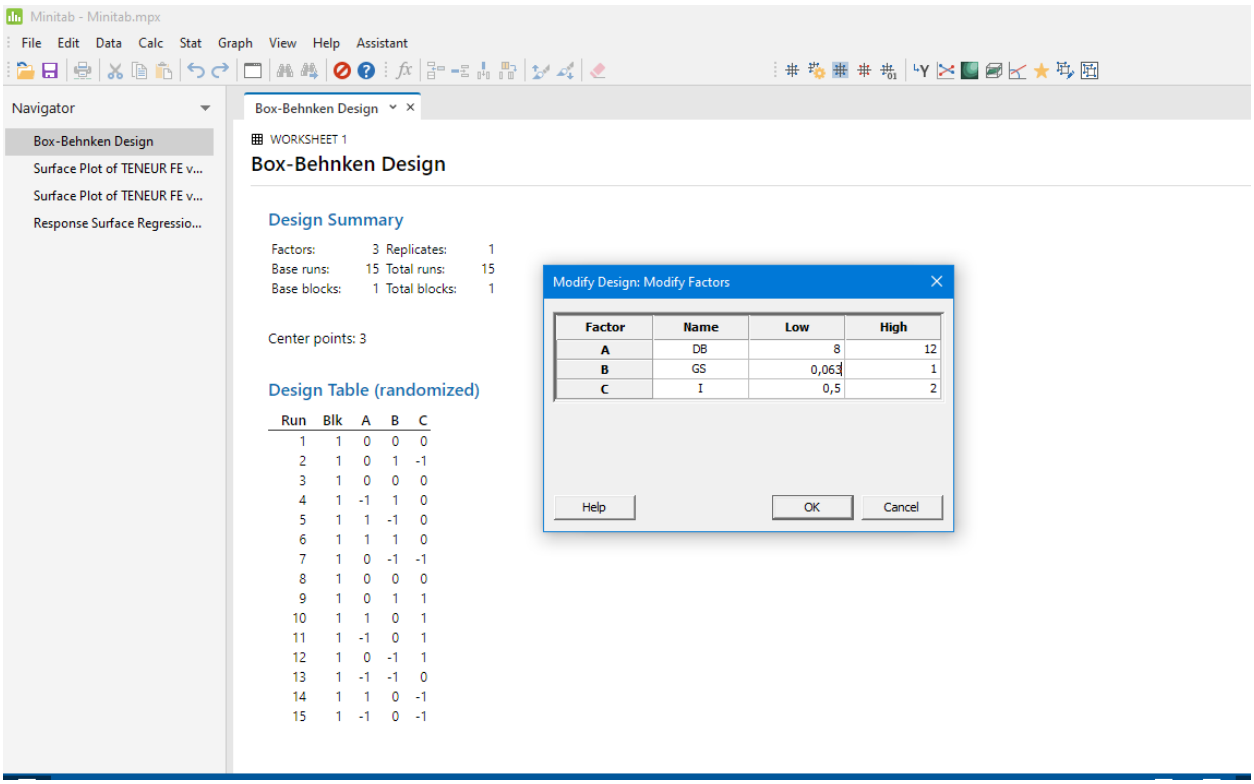
Modifications

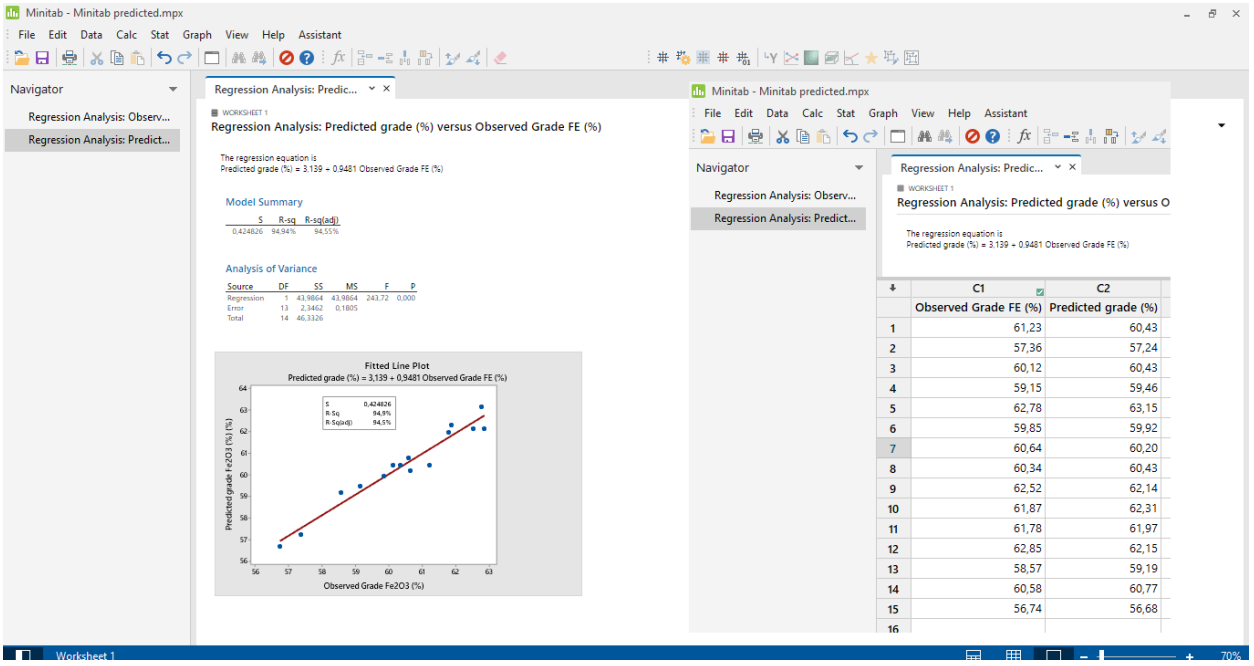
Par rapport aux documents remplacés, révision de la norme.

Corrections

Éditée et diffusée par l'Association Française de Normalisation (AFNOR) — 11, rue Francis de Pressensé — 93571 La Plaine Saint-Denis Cedex
Tél. : + 33 (0)1 41 62 80 00 — Fax : + 33 (0)1 49 17 90 00 — www.afnor.org

© AFNOR 2012 AFNOR 2012 1er tirage 2012-05-F


Minitab - Minitab.mpx
File Edit Data Calc Stat Graph View Help Assistant
Navigator
Box-Behnken Design
Surface Plot of TENEUR FE v...
Surface Plot of TENEUR FE v...
Response Surface Regressio...
Box-Behnken Design
WORKSHEET 1
Box-Behnken Design
Design Summary
Factors: 3 Replicates: 1
Base runs: 15 Total runs: 15
Base blocks: 1 Total blocks: 1
Center points: 3
Design Table (randomized)
Run Blk A B C
1 1 0 0 0
2 1 0 1 -1
3 1 0 0 0
4 1 -1 1 0
5 1 1 -1 0
6 1 1 1 0
7 1 0 -1 -1
8 1 0 0 0
9 1 0 1 1
10 1 1 0 1
11 1 -1 0 1
12 1 0 -1 1
13 1 -1 -1 0
14 1 1 0 -1
15 1 -1 0 -1
Modify Design: Modify Factors
Factor Name Low High
A DB 8 12
B GS 0,063 1
C I 0,5 2
Help
OK
Cancel


Minitab - Minitab predicted.mpx
File Edit Data Calc Stat Graph View Help Assistant
Navigator
Regression Analysis: Observ...
Regression Analysis: Predict...
Regression Analysis: Predic...
WORKSHEET 1
Regression Analysis: Predicted grade (%) versus Observed Grade FE (%)
The regression equation is
Predicted grade (%) = 3.139 + 0.9481 Observed Grade FE (%)
Model Summary
S R-sq R-sq(adj)
0.424826 94.94% 94.55%
Analysis of Variance
Source DF SS MS F P
Regression 1 43.9864 43.9864 243.72 0.000
Error 13 2.3462 0.1805
Total 14 46.3326
Fitted Line Plot
Predicted grade (%) = 3.139 + 0.9481 Observed Grade FE (%)
S 0.424826
R-Sq 94.9%
R-Sq(adj) 94.5%
Predicted grade Fe2O3 (%)
Observed Grade Fe2O3 (%)
Minitab - Minitab predicted.mpx
File Edit Data Calc Stat Graph View Help Assistant
Navigator
Regression Analysis: Observ...
Regression Analysis: Predict...
Regression Analysis: Predic...
WORKSHEET 1
Regression Analysis: Predicted grade (%) versus O
The regression equation is
Predicted grade (%) = 3.139 + 0.9481 Observed Grade FE (%)
C1 C2
Observed Grade FE (%) Predicted grade (%)
1 61,23 60,43
2 57,36 57,24
3 60,12 60,43
4 59,15 59,46
5 62,78 63,15
6 59,85 59,92
7 60,64 60,20
8 60,34 60,43
9 62,52 62,14
10 61,87 62,31
11 61,78 61,97
12 62,85 62,15
13 58,57 59,19
14 60,58 60,77
15 56,74 56,68
16
Worksheet 1
70%

Minitab - Minitab yield.mpx

File Edit Data Calc Stat Graph View Help Assistant

Navigator

Scatterplot of Predicted vs ...

Regression Analysis: Predict...

Regression Analysis: Predict...

Regression Analysis: Predic... ×

WORKSHEET 1

Regression Analysis: Predicted versus Observed

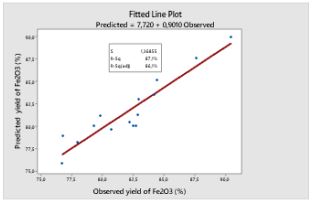
The regression equation is
Predicted = 7,720 + 0,9010 Observed

Model Summary

S	R-sq	R-sq(adj)
1,36855	87,07%	86,08%

Analysis of Variance

Source	DF	SS	MS	F	P
Regression	1	163,973	163,973	87,55	0,000
Error	13	24,348	1,873		
Total	14	188,321			



Minitab - Minitab yield.mpx

File Edit Data Calc Stat Graph View Help Assistant

Navigator

Scatterplot of Predicted vs ...

Regression Analysis: Predict...

Regression Analysis: Predict...

	C1	C2
	Observed	Predicted
1	82,50	80,06
2	76,70	75,84
3	82,73	80,06
4	82,17	80,43
5	84,40	85,18
6	82,90	83,00
7	82,83	81,31
8	79,30	80,06
9	87,62	87,60
10	90,47	89,95
11	79,83	81,16
12	84,20	83,52
13	80,73	79,65
14	77,93	78,25
15	76,75	78,91
16		
17		
18		
19		
20		

Worksheet 1 100%

Minitab - Minitab HAJER 2.m...

File Edit Data Calc Stat Graph View Help Assistant

Navigator

Box-Behnken Design

Response Surface Regression: Grade Fe2O3 (%) versus D...

Response Surface Regressi... ×

WORKSHEET 1

Response Surface Regression: Grade Fe2O3 (%) versus DB (mm); GS (mm); I (T)

Coded Coefficients

Term	Coef	SE Coef	T-Value	P-Value	VIF
Constant	60,347	0,146	414,68	0,000	
DB (mm)	1,013	0,199	5,08	0,001	1,02
GS (mm)	-0,668	0,177	-3,78	0,005	1,00
I (T)	1,790	0,199	8,98	0,000	1,02
DB (mm)*GS (mm)	-0,786	0,250	-3,14	0,014	1,02
DB (mm)*I (T)	-0,938	0,279	-3,36	0,010	1,00
GS (mm)*I (T)	0,662	0,250	2,65	0,029	1,02

Regression Equation in Uncoded Units

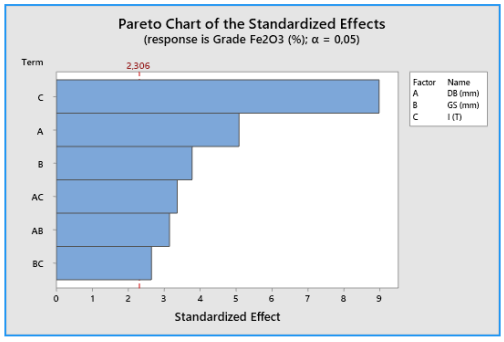
Grade Fe2O3 (%) = 41,50 + 1,831 DB (mm) + 5,15 GS (mm) + 7,42 I (T) - 0,936 DB (mm)*GS (mm) - 0,625 DB (mm)*I (T) + 2,100 GS (mm)*I (T)

Model Summary

S	R-sq	R-sq(adj)	R-sq(pred)
0,557887	94,91%	91,09%	79,33%

Analysis of Variance

Source	DF	Adj SS	Adj MS	F-Value	P-Value
Model	6	46,4391	7,7398	24,87	0,000
Linear	3	37,5478	12,5159	40,21	0,000
DB (mm)	1	8,0286	8,0286	25,80	0,001
GS (mm)	1	4,4387	4,4387	14,26	0,005
I (T)	1	25,0805	25,0805	80,58	0,000
2-Way Interaction	3	8,7710	2,9237	9,39	0,005
DB (mm)*GS (mm)	1	3,0773	3,0773	9,89	0,014
DB (mm)*I (T)	1	3,5156	3,5156	11,30	0,010
GS (mm)*I (T)	1	2,1781	2,1781	7,00	0,029
Error	8	2,4899	0,3112		
Lack-of-Fit	6	1,7990	0,2998	0,87	0,623
Pure Error	2	0,6909	0,3454		
Total	14	48,9290			



Worksheet 1 90%

Minitab - Minitab HAJER 2.m...

File Edit Data Calc Stat Graph View Help Assistant

Navigator

- Box-Behnken Design
- Response Surface Regression: yield of Fe2O3 versus DB (...

Response Surface Regressi...

WORKSHEET 1

Response Surface Regression: yield of Fe2O3 versus DB (mm); GS (mm); I (T)

Coded Coefficients

Term	Coef	SE Coef	T-Value	P-Value	VIF
Constant	82,035	0,447	183,65	0,000	
DB (mm)	1,950	0,612	3,19	0,013	1,02
GS (mm)	-0,309	0,543	-0,57	0,585	1,00
I (T)	3,740	0,612	6,11	0,000	1,02
DB (mm)*GS (mm)	-0,662	0,768	-0,86	0,414	1,02
DB (mm)*I (T)	2,365	0,856	2,76	0,025	1,00
GS (mm)*I (T)	2,139	0,768	2,79	0,024	1,02

Regression Equation in Uncoded Units

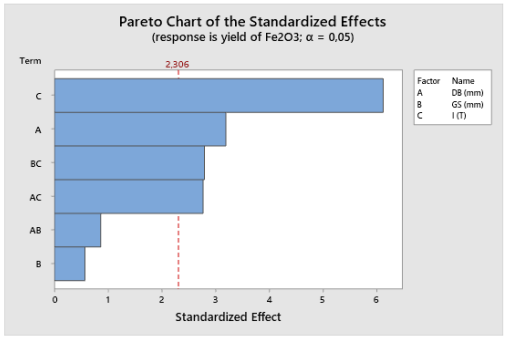
yield of Fe2O3 = 86,54 - 0,539 DB (mm) - 1,35 GS (mm) - 14,72 I (T) - 0,788 DB (mm)*GS (mm) + 1,577 DB (mm)*I (T) + 6,79 GS (mm)*I (T)

Model Summary

S	R-sq	R-sq(adj)	R-sq(pred)
1,71241	88,39%	79,68%	55,32%

Analysis of Variance

Source	DF	Adj SS	Adj MS	F-Value	P-Value
Model	6	178,531	29,755	10,15	0,002
Linear	3	140,165	46,722	15,93	0,001
DB (mm)	1	29,760	29,760	10,15	0,013
GS (mm)	1	0,948	0,948	0,32	0,585
I (T)	1	109,457	109,457	37,33	0,000
2-Way Interaction	3	47,326	15,775	5,38	0,025
DB (mm)*GS (mm)	1	2,178	2,178	0,74	0,414
DB (mm)*I (T)	1	22,373	22,373	7,63	0,025
GS (mm)*I (T)	1	22,775	22,775	7,77	0,024
Error	8	23,459	2,932		
Lack-of-Fit	6	16,106	2,684	0,73	0,676
Pure Error	2	7,353	3,676		
Total	14	201,990			



Worksheet 1

90%

Minitab - Minitab HAJER 2.m...

File Edit Data Calc Stat Graph View Help Assistant

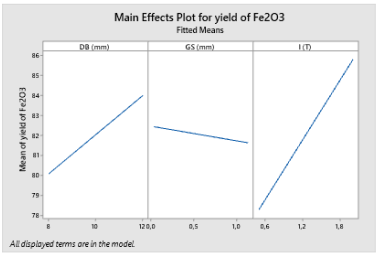
Navigator

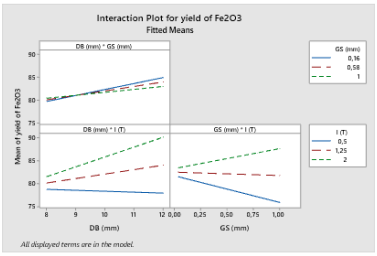
- Box-Behnken Design
- Response Surface Regression: yield of Fe2O3 versus DB (...
- Response Surface Regression: Grade Fe2O3 (%) versus D...
- Surface Plot of Grade Fe2O3 (%) vs DB (mm); GS (mm)
- Surface Plot of Grade Fe2O3 (%) vs I (T); GS (mm)
- Surface Plot of Grade Fe2O3 (%) vs I (T); DB (mm)
- Surface Plot of yield of Fe2O3 vs DB (mm); GS (mm)
- Surface Plot of yield of Fe2O3 vs I (T); GS (mm)
- Surface Plot of yield of Fe2O3 vs I (T); DB (mm)
- Factorial Plots for Grade Fe2O3 (%)
- Factorial Plots for yield of Fe2O3
- Response Optimization: Grade Fe2O3 (%)
- Response Optimization: yield of Fe2O3
- Response Optimization: yield of Fe2O3; Grade Fe2O3 (%)

Factorial Plots for yield of F...

WORKSHEET 1

Factorial Plots for yield of Fe2O3

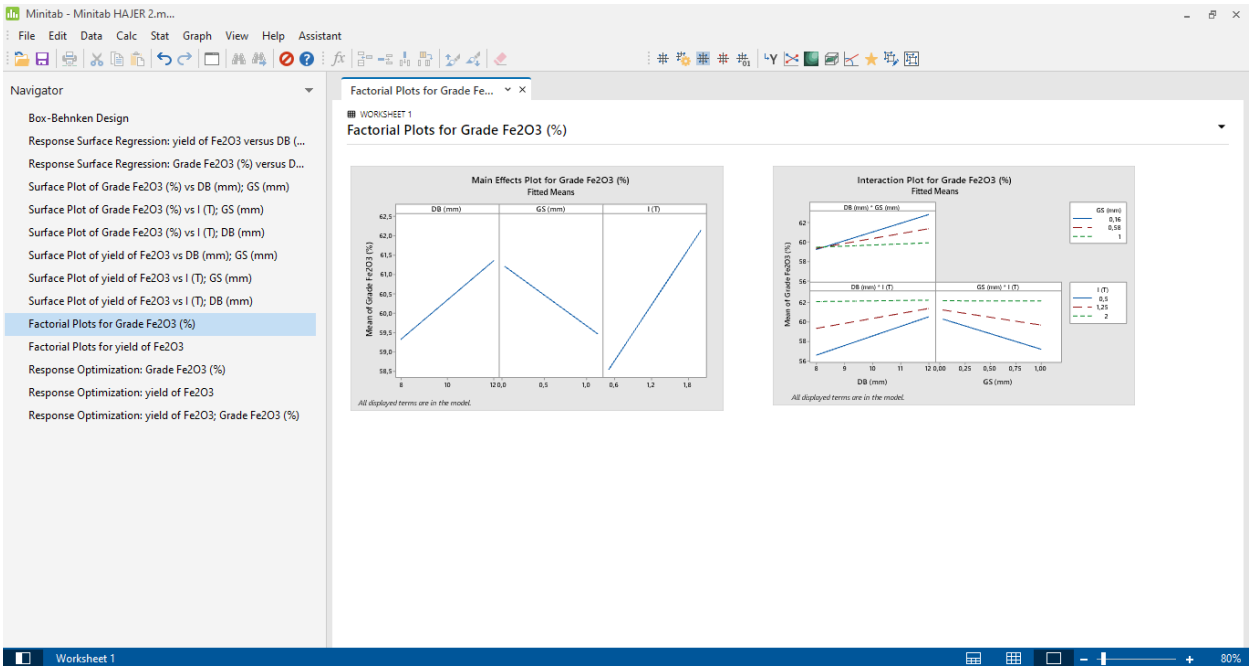


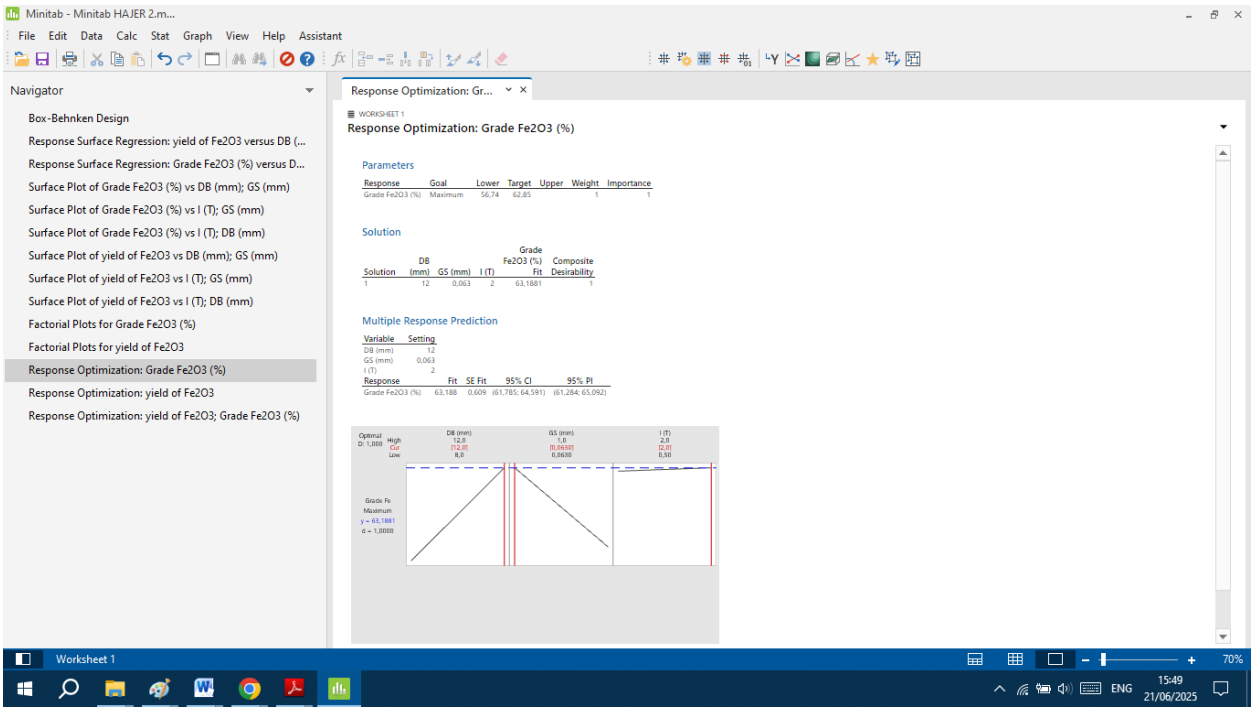


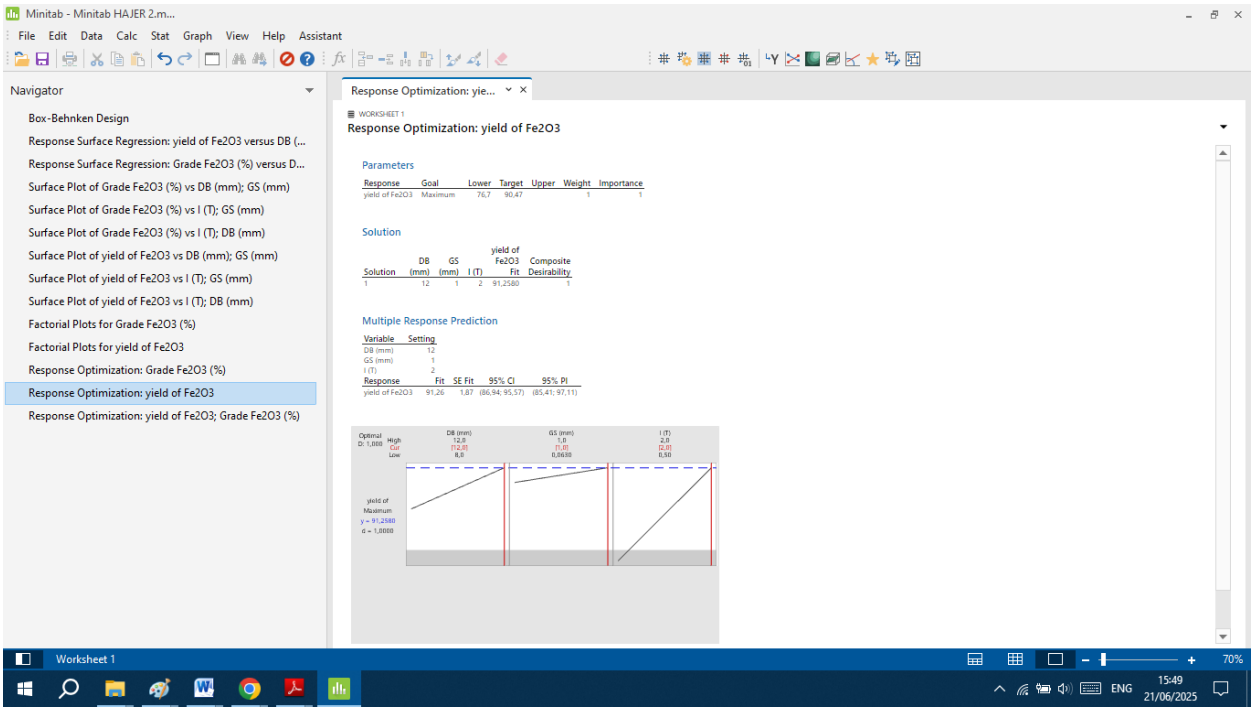
Worksheet 1

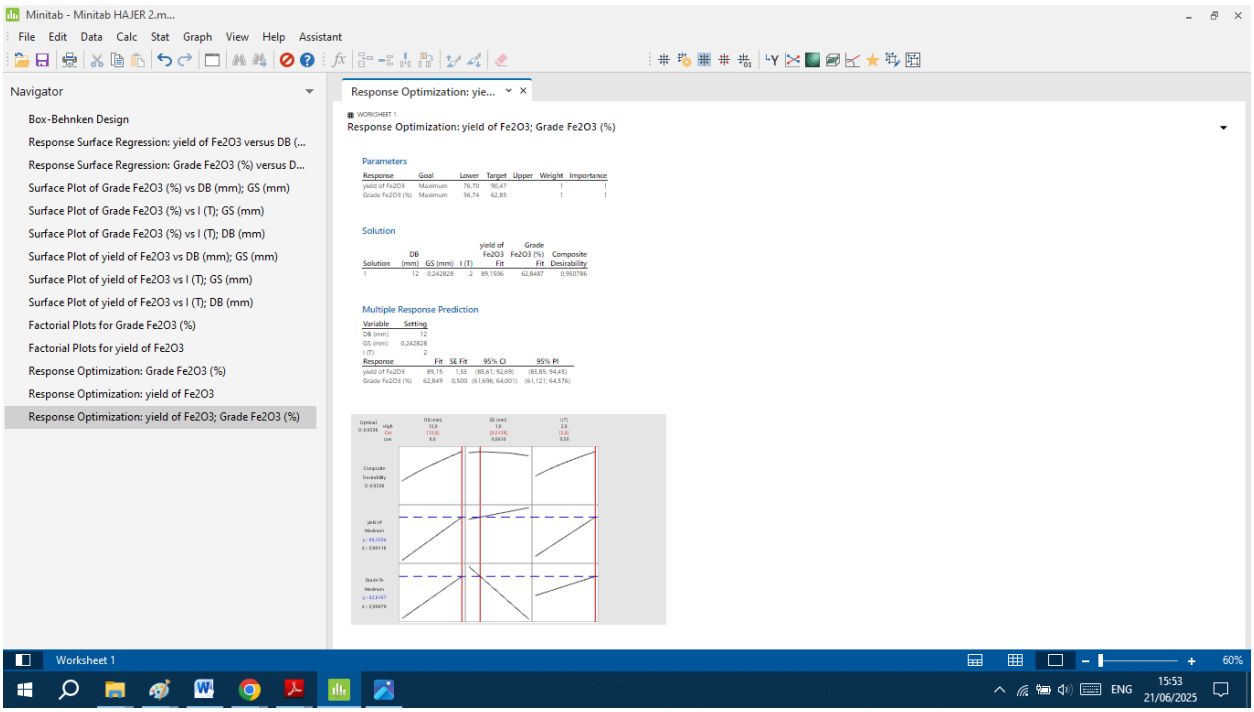
80%

ENG 13:33 23/06/2025


Minitab - Minitab HAJER 2.m...
File Edit Data Calc Stat Graph View Help Assistant
Navigator
Box-Behnken Design
Response Surface Regression: yield of Fe2O3 versus DB (...
Response Surface Regression: Grade Fe2O3 (%) versus D...
Surface Plot of Grade Fe2O3 (%) vs DB (mm); GS (mm)
Surface Plot of Grade Fe2O3 (%) vs I (T); GS (mm)
Surface Plot of Grade Fe2O3 (%) vs I (T); DB (mm)
Surface Plot of yield of Fe2O3 vs DB (mm); GS (mm)
Surface Plot of yield of Fe2O3 vs I (T); GS (mm)
Surface Plot of yield of Fe2O3 vs I (T); DB (mm)
Factorial Plots for Grade Fe2O3 (%)
Factorial Plots for yield of Fe2O3
Response Optimization: Grade Fe2O3 (%)
Response Optimization: yield of Fe2O3
Response Optimization: yield of Fe2O3; Grade Fe2O3 (%)
Factorial Plots for Grade Fe...
WORKSHEET 1
Factorial Plots for Grade Fe2O3 (%)
Main Effects Plot for Grade Fe2O3 (%)
Fitted Means
DB (mm)
GS (mm)
I (T)
Mean of Grade Fe2O3 (%)
All displayed terms are in the model.
Interaction Plot for Grade Fe2O3 (%)
Fitted Means
DB (mm) * GS (mm)
DB (mm) * I (T)
GS (mm) * I (T)
GS (mm)
I (T)
Mean of Grade Fe2O3 (%)
All displayed terms are in the model.
Worksheet 1
80%


Minitab - Minitab HAJER 2.m...
File Edit Data Calc Stat Graph View Help Assistant
Navigator
Box-Behnken Design
Response Surface Regression: yield of Fe2O3 versus DB (...
Response Surface Regression: Grade Fe2O3 (%) versus D...
Surface Plot of Grade Fe2O3 (%) vs DB (mm); GS (mm)
Surface Plot of Grade Fe2O3 (%) vs I (T); GS (mm)
Surface Plot of Grade Fe2O3 (%) vs I (T); DB (mm)
Surface Plot of yield of Fe2O3 vs DB (mm); GS (mm)
Surface Plot of yield of Fe2O3 vs I (T); GS (mm)
Surface Plot of yield of Fe2O3 vs I (T); DB (mm)
Factorial Plots for Grade Fe2O3 (%)
Factorial Plots for yield of Fe2O3
Response Optimization: Grade Fe2O3 (%)
Response Optimization: yield of Fe2O3
Response Optimization: yield of Fe2O3; Grade Fe2O3 (%)
Response Optimization: Gr...
WORKSHEET 1
Response Optimization: Grade Fe2O3 (%)
Parameters
Response Goal Lower Target Upper Weight Importance
Grade Fe2O3 (%) Maximum 56,74 62,85 1 1
Solution
Solution DB (mm) GS (mm) I (T) Grade Fe2O3 (%) Fit Composite Desirability
1 12 0,063 2 63,1881 1
Multiple Response Prediction
Variable Setting
DB (mm) 12
GS (mm) 0,063
I (T) 2
Response Fit SE Fit 95% CI 95% PI
Grade Fe2O3 (%) 63,188 0,609 (61,785; 64,591) (61,284; 65,092)
Worksheet 1
70%
ENG
15:49
21/06/2025


Minitab - Minitab HAJER 2.m...
File Edit Data Calc Stat Graph View Help Assistant
Navigator
Box-Behnken Design
Response Surface Regression: yield of Fe2O3 versus DB (...
Response Surface Regression: Grade Fe2O3 (%) versus D...
Surface Plot of Grade Fe2O3 (%) vs DB (mm); GS (mm)
Surface Plot of Grade Fe2O3 (%) vs I (T); GS (mm)
Surface Plot of Grade Fe2O3 (%) vs I (T); DB (mm)
Surface Plot of yield of Fe2O3 vs DB (mm); GS (mm)
Surface Plot of yield of Fe2O3 vs I (T); GS (mm)
Surface Plot of yield of Fe2O3 vs I (T); DB (mm)
Factorial Plots for Grade Fe2O3 (%)
Factorial Plots for yield of Fe2O3
Response Optimization: Grade Fe2O3 (%)
Response Optimization: yield of Fe2O3
Response Optimization: yield of Fe2O3; Grade Fe2O3 (%)
Response Optimization: yie...
WORKSHEET 1
Response Optimization: yield of Fe2O3
Parameters
Response Goal Lower Target Upper Weight Importance
yield of Fe2O3 Maximum 76,7 90,47 1 1
Solution
Solution DB (mm) GS (mm) I (T) yield of Fe2O3 Fit Composite Desirability
1 12 1 2 91,2580 1
Multiple Response Prediction
Variable Setting
DB (mm) 12
GS (mm) 1
I (T) 2
Response Fit SE Fit 95% CI 95% PI
yield of Fe2O3 91,26 1,87 (86,94; 95,57) (85,41; 97,11)
Worksheet 1
70%
ENG
15:49
21/06/2025


Minitab - Minitab HAJER 2.m...
File Edit Data Calc Stat Graph View Help Assistant
Navigator
Box-Behnken Design
Response Surface Regression: yield of Fe2O3 versus DB (...
Response Surface Regression: Grade Fe2O3 (%) versus D...
Surface Plot of Grade Fe2O3 (%) vs DB (mm); GS (mm)
Surface Plot of Grade Fe2O3 (%) vs I (T); GS (mm)
Surface Plot of Grade Fe2O3 (%) vs I (T); DB (mm)
Surface Plot of yield of Fe2O3 vs DB (mm); GS (mm)
Surface Plot of yield of Fe2O3 vs I (T); GS (mm)
Surface Plot of yield of Fe2O3 vs I (T); DB (mm)
Factorial Plots for Grade Fe2O3 (%)
Factorial Plots for yield of Fe2O3
Response Optimization: Grade Fe2O3 (%)
Response Optimization: yield of Fe2O3
Response Optimization: yield of Fe2O3; Grade Fe2O3 (%)
Response Optimization: yie...
WORKSHEET 1
Response Optimization: yield of Fe2O3; Grade Fe2O3 (%)
Parameters
Response Goal Lower Target Upper Weight Importance
yield of Fe2O3 Maximum 76,70 90,47 1 1
Grade Fe2O3 (%) Maximum 56,74 62,85 1 1
Solution
Solution DB (mm) GS (mm) I (T) yield of Fe2O3 Fit Grade Fe2O3 (%) Fit Composite Desirability
1 12 0,242828 2 89,1506 62,8487 0,950786
Multiple Response Prediction
Variable Setting
DB (mm) 12
GS (mm) 0,242828
I (T) 2
Response Fit SE Fit 95% CI 95% PI
yield of Fe2O3 89,15 1,53 (85,61; 92,69) (83,85; 94,45)
Grade Fe2O3 (%) 62,849 0,500 (61,696; 64,001) (61,121; 64,576)
Worksheet 1
60%
ENG
15:53
21/06/2025

الجمهورية الجزائرية الديمقراطية الشعبية
République Algérienne Démocratique et Populaire

Ministère de l'Enseignement Supérieur
et de la Recherche Scientifique
Université Larbi Tebessi – Tébessa
Institut des Mines
Département mines et géotechnologie

وزارة التعليم العالي و البحث العلمي
جامعة العربي التبسي – تبسة
معهد المناجم
قسم المناجم و الجيوتكنولوجيا

Année universitaire : 2024/2025 Tébessa le : 28/06/2025

Lettre de soutenabilité

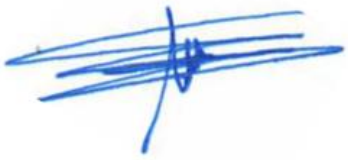
Noms et prénoms de l'étudiante :

Ayad Hadjer

Niveau : **Master** Option : **Valorisation des Ressources Minérales**

Thème **Characterization and Optimization of Iron Ore Beneficiation Parameters: Ouenza Mine Case**

Nom et prénom de l'encadreur : **Laraba Mohammed**

Chapitres réalisés	Signature de l'encadreur
Chapitre I : Bibliographic Review	
Chapitre II : Materials and Experimental Methods	
Chapitre III : Results and Discussion	



الجمهورية الجزائرية الديمقراطية الشعبية
وزارة التعليم العالي والبحث العلمي

مؤسسة التعليم العالي : جامعة العربي التبسي – تبسة

تصريح شرفي
خاص بالالتزام بقواعد النزاهة العلمية لانجاز بحث

انا الممضي أدناه،

السيد (ة).....عياد.....جاجيل.....الصفة : طالب، أستاذ باحث، باحث دائم : .طالبة.....

الحامل لبطاقة التعريف الوطنية رقم : 110000364054340006 و الصادرة بتاريخ ....2023....04....04.... و
المسجل بمعهد .....المناجم..... قسم المناجم والجيوتكنولوجيا
و المكلف بانجاز أعمال بحث (مذكرة التخرج، مذكرة ماستر، مذكرة ماجستير، أطروحة دكتوراه)، عنوانها :
Characterization and Optimization of Iron ore beneficiation parameters - El-OUENZA mine Case

أصرح بشرفي أني ألتزم بمراعاة المعايير العلمية و المنهجية و معايير الأخلاقيات المهنية و النزاهة الأكاديمية المطلوبة في انجاز البحث المذكور أعلاه.

التاريخ: 25 ماي 2025

إمضاء المعني (ة)